Order Number 9130303

NMR spectroscopic studies of two 7Fe ferredoxins

Cheng, Hong, Ph.D.

City University of New York, 1991

U·M·I
300 N. Zeeb Rd.
Ann Arbor, MI 48106

NMR Spectroscopic Studies of Two 7Fe Ferredoxins

by

HONG CHENG

A dissertation submitted to the Graduate Faculty in Chemistry in partial fulfillment of the requirements for the degree of Doctor of Philosophy, The City University of New York

1991

This manuscript has been read and accepted for the Graduate Faculty in Chemistry in satisfaction of the dissertation requirement for the degree of Doctor of Philosophy.

3/25/91
Date

William Sweeney
Chair of Examining Committee

3/26/91
Date

Executive Officer

Prof. William Sweeney

Prof. Fred Naider

Prof. Dixie Goss

Prof. Max Diem

Supervisory Committee

The City University of New York

ABSTRACT

NMR Spectroscopic Studies of Two 7Fe Ferredoxins

by

Hong Cheng

Advisor: Dr. William V. Sweeney

Azotobacter vinelandii ferredoxin I and *Pseudomonas putida* ferredoxin each contains one [3Fe-4S] cluster and one [4Fe-4S] cluster. They have homologous amino acid sequences. The structures of these two 7Fe ferredoxins are considered to be essentially the same.

The ^1H NMR spectra of these two 7Fe ferredoxins look very similar. Six peaks are well resolved in the region downfield of 10 ppm. T_1 relaxation time measurements, temperature dependence studies, pH titrations and deuterium labeling experiments have been performed. Peaks A-E are pH titratable and they are from β-protons on iron-bound cysteines. Peak F is pH independent, and it resolves into two resonances with approximately equal intensity at temperatures below 15 °C or above 25 °C. Neither of the resolved resonances arises from an α- or β-cysteinyl proton. In addition, a partial assignment of the ring system protons of the two 7Fe ferredoxins has been made.

Nuclear Overhauser effects are observed between paramagnetically shifted resonances. 1D steady state NOE experiments show that peaks A and B are from a geminal pair of β-protons. These single proton resonances arise from a cysteine bound to the 3Fe center. Similarly, it is

shown that peak C is from one of the β-protons of Cys16 and peak E is from one of the β-protons of Cys45. Other cysteinyl protons are correlated to peaks A-E based on the results from a NOESY experiment with a short mixing time of 5 ms.

P. putida ferredoxin was ^{13}C enriched at the β-cysteinyl carbon atoms through direct incorporation of labeled cysteine. Eight peaks, 1-8, are observed in the ^{13}C NMR spectrum of this ^{13}C enriched ferredoxin. The correlation between β-cysteinyl carbon and proton resonances have been studied by heteronuclear correlated experiments. The chemical shifts and temperature dependencies of carbon peaks 7 and 8 and their correlated proton resonances indicate that peaks 7 and 8 are from two cysteines with free sulfhydryl groups. Thus, only seven cysteines in these two 7Fe ferredoxins are iron-bound. This result support the view that the correct structure of the 3Fe center is $Fe_3S_4(S^{Cys})_3$, as reported in the revised X-ray structure of *Azotobacter vinelandii* ferredoxin I.

ACKNOWLEDGEMENT

I especially wish to express my sincere thanks to Prof. William V. Sweeney, my thesis advisor, for his guidance and considerable help through my Ph.D study. I would also like to acknowledge his assistance in the preparation of this manuscript and the co-authorship of my first paper which has been published in the Journal of Biological Chemistry (Appendix 5). I would also like to thank the members of my thesis committee, Prof. Fred Naider, Prof. Dixie Goss, and Prof. Max Diem.

I especially want to express my appreciation to Prof. Klaus Grohmann for his help in the synthesis of isotopically labeled cystine and preparation of D,L - β,β'-^{2}H cystine and D,L - β,β'-^{13}C cystine. I would like to thank Dr. Michael Blumenstein for his assistance in NMR instrumentation and very useful discussions. I also like to thank Richard H. Wegener for his critical review of this manuscript.

Finally, I am deeply indebted to my mother not only for bringing us up after lost our dear father and also for her always inspiration and supporting.

I dedicate this work to my parents and to Jane

TABLE OF CONTENTS

LIST OF FIGURES

LIST OF TABLES

LIST OF ABBREVIATIONS

A_c	contact interaction constant
ATCC	American Type Culture Collection
CD	Circular Dichroism
COSY	Correlated Spectroscopy
Cys	Cysteine
DEAE	Diethylaminoethyl
DMSO	dimethyl sulfoxide
DQF-COSY	Double Quantum Filter COSY
DSS	sodium-2,2'-dimethyl-2-silapentane-5-sulphonate
EPR	Electron Paramagnetic Resonance
EXAFS	Extended X-ray Absorption edge Fine Structure
Fd	ferredoxin
FID	Free Induction Decay
h	Planck constant
HIPIP	High Potential Iron-Sulfur Protein
His	Histidine
HMQC	Heteronuclear Multi Quantum Correlated Spectroscopy
HOHAHA	Homonuclear Hartman-Hahn Spectroscopy
HPLC	High Perfomance Liquid Chromatograph
I_j	intensity of the signal from the detected proton H_j with saturating the resonance of the spin H_i
I_j°	intensity of the signal from the detected proton H_j are without saturating the resonance of the spin H_i
k	Boltzmann constant
Leu	Leucine

MMS	methyl methanesulfonate
NMR	nuclear magnetic resonance
NOE	Nuclear Overhauser Effect
NOESY	Nuclear Overhauser Effect Spectroscopy
PITC	Phenylisothiocyanate
Phe	Phenylalanine
r_{AB}	interproton distance between the nucleus A and the nucleus B
R_C	cross relaxation rate constant
R_L	leakage relaxation rate constant
R_S	external relaxation
S	total electronic spin
SM-NOESY	Short Mixing-time NOESY
T	absolute temperature
T_1	longitudinal nuclear spin relaxation time
T_2	transverse nuclear spin relaxation time
T_{1e}	longitudinal electron spin relaxation time
T_{2e}	transverse electron spin relaxation time
T_{1M}	T_1 relaxation time for a paramagnetic system
T_{2M}	T_2 relaxation time for a paramagnetic system
t_m	mixing time
TCA	trichloroacetic acid
TOCSY	Total Correlation Spectroscopy
Trp	Tryptophan
Tyr	Tyrosine
UV-VIS	ultraviolet and visible spectroscopy
Val	Valine

W_0	zero quantum probability
W_2	double quantum probability
β	Bohr magneton
χ	magnetic susceptibility
γ_e	gyromagnetic ration for the electron
γ_H	gyromagnetic ratio for the proton
γ_I	gyromagnetic ratio for the nucleus
$\eta_{i\rightarrow j}$	the nuclear Overhauser effect for j upon saturating spin i
ρ_j	the selective relaxation rate
σ_{ij}	the cross-relaxation rate
τ	correlation time for contact coupling
τ_c	effective correlation time
ω_I	Larmor frequence for the nucleus
ω_e	Larmor frequence for the electron

CHAPTER 1

INTRODUCTION

1.1 Ferredoxins

Ferredoxins are one class of proteins which contain non-heme iron and acid-labile sulfur clusters. They display electron carrier activities in many biological electron transfer processes (1, 2). Since Mortenson et al. (3) first isolated a non-heme iron containing protein from *Clostridium pasteurianum* in 1962, highly diverse and versatile types of ferredoxins have been discovered in many species of microorganisms, plants and animals. Studies on these proteins show that they have chemical similarities and can often be functionally interchangeable (1, 2). The content of non-heme iron and labile sulfur in ferredoxins is equivalent (1, 2), and their molecular weights range are from 6 to 14 kDa. In addition, they are highly acidic (1,2).

Ferredoxins can be classified according to the number of iron atoms and acid-labile sulfur atoms contained in the clusters and their reduction potentials. Currently, three types of iron-sulfur clusters are known in ferredoxins. Referring to the numbers of iron and sulfur contained, they are named as [2Fe-2S], [3Fe-4S] and [4Fe-4S]. Their structures are shown in Figure 1.1.

In all three types of clusters the iron is tetrahedrally coordinated to sulfur with an iron-iron separation of approximately 2.7 Å. Their average bond lengths, Fe...Fe distances and bond angles are listed in Table 1.1.

Figure 1.1 Iron-Sulfur Clusters in Ferredoxins

All of them were determined by X-ray crystallography

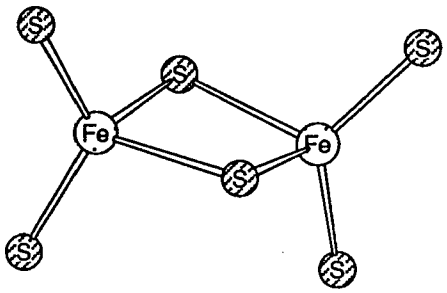

2Fe-2S

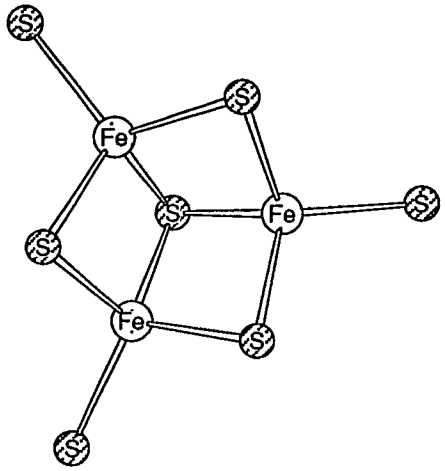

3Fe-4S

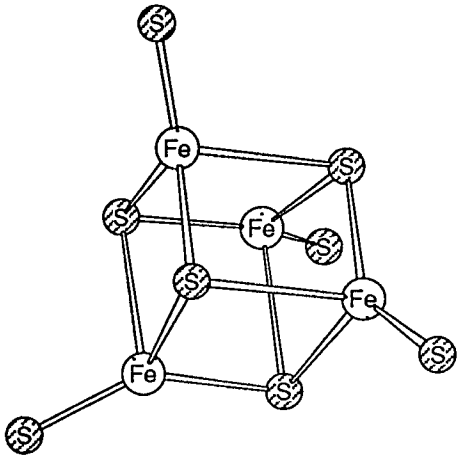

4Fe-4S

Table 1.1 Average Bond Lengths, Fe...Fe Distances, and Bond Angles in Different Iron-Sulfur Clusters

Cluster	[2Fe-2S]	[3Fe-4S]	
	S.platensis	*D.gigas*	*A.vinelandii*
Fe...Fe	2.72 Å	2.76 Å	2.68 Å
Fe-S	2.30 Å	2.27 Å	2.31 Å
Fe-Sγ	2.00 Å	2.24 Å	2.30 Å
S-Fe-S	100.7°	104°	106.9°
S-Fe-Sγ	100°	114.4°	111.9°
Fe-S-Fe	85°	74.7°	71.0°

[4Fe-4S]	HiPIP[a]		2[4Fe-4S] [b]		7Fe[c]
	red	ox	Cplx.I	Cplx.II	
Fe...Fe	2.81 Å	2.73 Å	2.73 Å	2.69 Å	2.71 Å
Fe-S	2.32 Å	2.25 Å	2.23 Å	2.19 Å	2.31 Å
S-Fe-Sγ	2.22 Å	2.21 Å	2.20 Å	2.23 Å	2.32 Å
S-Fe-S	104°	103°	103°	102°	106°
S-Fe-Sγ	114°	115°	115°	115°	113°
Fe-S-Fe	74°	75°	75°	76°	72°

a. *Chromatium Vinosum;* b. *Peptococcus aerogenes;* c. *Azotobacter vinelandii*

1.2 *Azotobacter*-type 7Fe Ferredoxin

Azotobacter-type 7Fe ferredoxins are one group of ferredoxins which contain two different iron-sulfur clusters, [3Fe-4S] and [4Fe-4S], with different reduction potentials. Included in this class are *Azotobacter vinelandii* ferredoxin I (4, 5), *Azotobacter chroococcum* ferredoxin (6), *Pseudomonas putida* (previously: *P. ovals*) ferredoxin (7), *Pseudomonas stutzeri* ferredoxin (8), *Mycobacterium smegmatis* ferredoxin I (9), *Mycobacterium flavum* ferredoxin I (10), *Bacillus acidocaldarius* ferredoxin (11), *Rhodobacter capsulatus* ferredoxin II (12), *Rhodospirillum rubrum* ferredoxin IV (13), *Streptomyces griseus* ferredoxin (14), and *Thermus thermophilus* ferredoxin (15).

The amino acid sequences of eight ferredoxins, *P. putida* ferredoxin (16), *M. smegatis* ferredoxin (17), *T. thermophilus* ferredoxin (15), *A. vinelandii* ferredoxin I (18), *B. acidocaldarius* ferredoxin (11), *P. stutzeri* ferredoxin (7), *R. capsulatus* ferredoxin II (19), and *S. griseus* ferredoxin (14), have been reported (Table 1.2). The ferredoxins from *P. putida* and *P. stutzeri* have homologous amino acid sequences to *A. vinelandii* ferredoxin I. Other than the N-terminal amino acid, the first sixty-one amino acids in these three ferredoxins are identical. Only fifteen amino acids are different between *P. putida* ferredoxin and *A. vinelandii* ferredoxin I from 106 residues overall.

Seven cysteines, Cys8, 16, 20, 39, 42, 45 and 49 are conserved in all of seven 7Fe ferredoxins. Cys11 only exists in *A. vinelandii*, *P. putida* and *P. stutzeri* 7Fe ferredoxins. Cys24 is replaced by Ala24 in *B. acidocaldarius* ferredoxin. The revised X-ray structure of *A. vinelandii* ferredoxin I reveals that Cys8, 16, and 49 are coordinated with [3Fe-4S] cluster, while Cys20, 39, 42 and 45 are coordinated with [4Fe-4S] center (20, 21, 22). The

Table 1.2 Amino Acid Sequences of Eight Different *Azotobacter* -Type 7Fe Ferredoxins

Av:	*Azotobacter vinelandii* (18)
Pp:	*Pseudomonas putida* (16)
Ps:	*Pseudomaonas stutzeri* (7)
Rc:	*Rhodobacter capsulatus* (19)
Ms:	*Mycobacterium smegmatis* (17)
Sg:	*Streptomyces grieus* (14)
Tt:	*Thermus thermophilus* (15)
Ba:	*Bacillus acidocaldarius* (11)

Table 1.3 Amino Acid Sequences of Seven Different Azotobacter-type Ferredoxins

Protein	1				5					10					15					20					25			
Av	A	F	V	V	T	D	N	C	I	K	C	K	Y	T	D	C	V	E	V	C	P	V	D	C	F	Y	E
Pp	T	F	V	V	T	D	N	C	I	K	C	K	Y	T	D	C	V	E	V	C	P	V	D	C	F	Y	E
Ps	T	F	V	V	T	D	N	C	I	K	C	K	Y	T	D	C	V	E	V	C	P	V	D	C	F	Y	E
Rc	T	Y	V	V	T	D	N	C	I	A	C	K	Y	T	D	C	V	E	V	C	P	V	D	C	F	Y	E
Ms	T	Y	V	I	A	E	P	C	V	D	V	K	D	K	A	C	I	E	E	C	P	V	D	C	I	Y	E
Sg	T	Y	V	I	A	Q	P	C	V	D	V	K	D	K	A	C	I	E	E	C	P	V	E	C	I	Y	E
Tt	P	H	V	I	C	Q	P	C	I	G	V	K	D	Q	S	C	V	E	V	C	P	V	E	C	I	Y	D
Ba	P	F	V	I	T	S	P	C	I	G	E	K	A	A	D	C	V	E	T	C	P	V	D	A	I	H	E
			30					35					40					45					50				
Av	G	P	N	F	L	V	I	H	P	D	E	C	I	D	C	A	L	C	E	P	E	C	P	A	Q	A	I
Pp	G	P	N	F	L	V	I	H	P	D	E	C	I	D	C	A	L	C	E	P	E	C	P	A	Q	A	I
Ps	G	P	N	F	L	V	I	H	P	D	E	C	I	D	C	A	L	C	E	P	E	C	P	A	Q	A	I
Rc	G	E	N	T	L	V	I	H	P	D	E	C	I	D	C	G	V	C	E	P	E	C	P	A	D	A	I
Ms	G	A	R	M	L	Y	I	H	P	D	E	C	V	D	C	G	A	C	E	P	V	C	P	V	E	A	I
Sg	G	Q	R	S	L	Y	I	H	P	D	E	C	V	D	C	G	A	C	E	P	V	C	P	V	E	A	I
Tt	G	G	D	Q	F	Y	I	H	P	E	E	C	I	D	C	G	A	C	V	P	A	C	P	V	N	A	I
Ba	G	P	D	Q	Y	Y	I	D	P	D	L	C	I	D	C	A	A	C	E	P	V	C	P	V	N	A	I

Table 1.3 Amino Acid Sequences of Seven Different Azotobacter-type Ferredoxins (continued)

Protein	55					60					65					70					75					80	
Av	F	S	E	D	E	V	P	E	D	M	Q	E	F	I	Q	L	N	A	E	L	A	E	V	W	P	N	I
Pp	F	S	E	D	E	V	P	S	G	M	E	N	F	I	E	L	N	A	E	L	A	E	I	W	P	N	I
Ps	F	S	E	D	E	V	P	E	D	Q	Q	E	F	I	E	L	N	A	D	L	A	E	V	W	P	N	I
Rc	R	P	D	T	E	-	P	-	G	M	E	D	W	V	E	F	N	R	T	Y	A	S	Q	W	P	V	I
Ms	Y	Y	E	D	D	V	P	D	Q	W	S	S	Y	A	Q	A	N	A	D	F	F	A	E	L	G	S	P
Sg	F	Y	E	D	D	T	P	E	E	W	K	D	Y	Y	K	A	N	V	E	F	F	D	D	L	G	S	P
Tt	Y	P	E	E	D	V	P	E	Q	W	K	S	Y	I	E	K	N	R	K	L	A	G	L	E			
Ba	Y	Q	E	E	F	V	P	E	D	E	K	E	F	I	E	K	N	R	N	F	F	R	N	R			
				85					90					95					100					105			
Av	T	E	K	K	D	P	L	P	D	A	E	D	W	D	G	V	K	G	K	L	Q	H	L	E	R		
Pp	T	E	R	K	D	A	L	P	D	A	E	E	W	D	G	K	P	G	K	I	A	D	L	E	R		
Ps	T	E	K	K	D	A	L	A	D	A	E	E	W	D	G	V	K	D	K	L	Q	Y	L	E	R		
Rc	T	I	K	K	D	P	M	P	D	H	K	K	Y	D	G	E	T	G	K	R	E	K	Y	F	S	P	N
Ms	G	G	A	S	K	V	G	Q	T	D	N	D	P	Q	A	I	K	D	L	P	P	Q	G	E	D		
Sg	G	G	A	S	K	L	G	L	I	E	R	D	H	P	F	V	A	G	L	P	P	Q	N	A			
		110																									
Rc	P	G	T	G	D																						

sulfhydryls of Cys11 and 24 are free (20, 21, 22). In site-directed mutation of Cys20 to alanine, the mutant protein still contains one [4Fe-4S] cluster and one [3Fe-4S] cluster (23). The X-ray structure of this mutant protein shows that the ligation of Cys20 is replaced by Cys24 (23).

The calculated molecular weights including seven iron atoms and eight inorganic sulfur atoms are 12,717 for *A. vinelandii* (24) and 12,548 for *P. putida* (16).

1.3 A Novel Three-Iron Cluster

Azotobacter vinelandii ferredoxin I was first isolated independently by Shethna et al. (4) and Yoch and Arnon (5). For a long period, the structure of the 3Fe cluster in *Azotobacter*-type 7Fe ferredoxin was not clear. Primary studies referred to this protein as an 8Fe protein and was similar to *Clostridium*-type ferredoxins which contained two [4Fe-4S] clusters (4, 25). Subsequently, Sweeney et al. (26) reported quantitative EPR experiments and indicated that two clusters had two different redox potentials. Meanwhile, Howard et al. (27) reported their cluster displacement experiments in a 80% dimethyl sulfoxide (DMSO) solution under anaerobic conditions. The results were interpreted that two [4Fe-4S] clusters were present per molecule. However, a similar experiment was performed by Averill et al. (28). Their results showed that there was only one [4Fe-4S] cluster per molecule. They suggested that either the balance of the iron did not give an easily identifiable species or it was in a domain of the protein particularly resistant to solvent-induced unfolding (28).

Two years later, Mössbauer and EPR studies convincingly identified the [4Fe-4S] cluster as the high potential site, whereas, only three iron atoms were contained in the low potential site (29). These result were

consistent with structure information from X-ray crystallography which was reported at the same time by Stout et al. (30). It was the first time that a 3Fe cluster was recognized in a biological organism.

Five X-ray structures have been reported since *Azotobacter vinelandii* ferredoxin I was isolated. The first crystallographic study of ferredoxin I at 4 Å resolution showed that two iron-sulfur clusters were present in each molecule (31, 32). One appeared to be of the [4Fe-4S] type, while the other was smaller. The smaller one was tentatively suggested as an [2Fe-2S] type with uncertainty at that resolution. At 2.5 Å resolution, three peaks of electron density were observed in the smaller cluster site (30). It was explained that the smaller cluster contained three-iron atoms. This result was consistent with the results from the Mössbauer studies (29).

This crystallographic study was subsequently further extended to 1.8 Å resolution and the model extensively refined against the data at that resolution (24). The structure of the three-iron cluster was modeled as a six-membered ring with a slightly puckered twisted-boat conformation and distorted tetrahedral geometry at the irons. The cluster stoichiometry was determined as [3Fe-3S], with ligation of five cysteine residues, and one unknown terminal ligand which was assigned as oxygen (Figure 1.2). In this model, the average iron-iron distance was reported as 4.1 Å which was about 1.4 Å longer than that in two other well known iron-sulfur clusters, i.e., [2Fe-2S] and [4Fe-4S] (Table 1.1). The angles about the three iron atoms, i.e., S-Fe-S, S-Fe-Sγ, and Fe-S-Fe, are scatterred over a range from 35° less to 44° larger than that in [2Fe-2S] and [4Fe-4S] clusters (Table 1.1).

By contrast to the abnormal [3Fe-3S] model in *A. vinelandii* ferredoxin I described by crystallography, an iron-iron separation of 2.7 Å

Figure 1.2 Error Structure of [3Fe-3S] Cluster

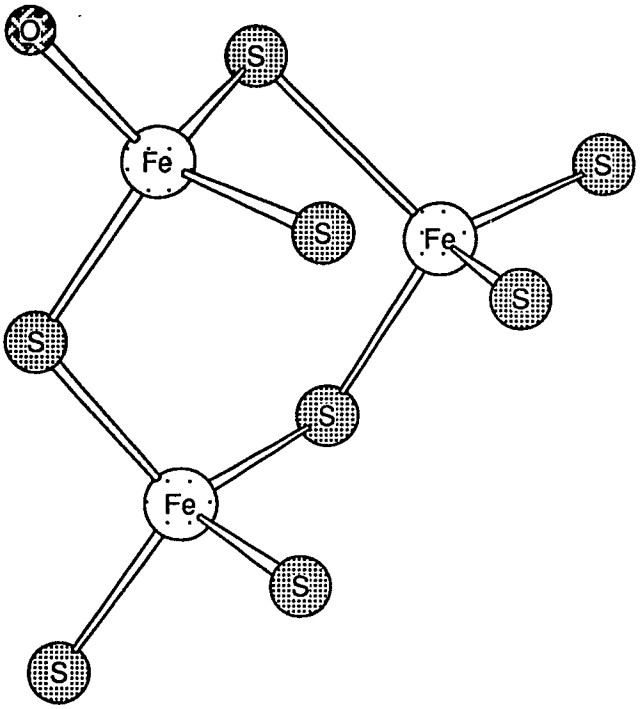

[3Fe-3S] Cluster

was observed in EXAFS (Extended X-ray absorption edge fine structure) studies of other three-iron cluster containing proteins, i.e., *Desulfovibrio gigas* ferredoxin II (33) and beef heart aconitase (34). Further, careful chemical analysis of these three-iron containing proteins showed that their iron:sulfur ratio was 0.75, implying that the cluster was [3Fe-4S] (34). Particularly, an interconversion between the [3Fe-4S] and [4Fe-4S] center in beef heart aconitase was reported (34). This result strongly implied that the 3Fe center in the three-iron containing proteins had a cubane-like structure, which was essentially a [4Fe-4S] cluster with an iron atom plucked out.

Results from other spectroscopic studies of *A. vinelandii* ferredoxin I (except X-ray crystallography) also contradicted this abnormal [3Fe-3S] model. Comparative studies using Mössbauer (35), low temperature magnetic circular dichroism (36), and resonance Raman spectroscopies (37) indicated that the electronic structures of the three-iron clusters in *D. gigas* and beef heart aconitase were very similar to *A. vinelandii* ferredoxin I. Conversions of the 3Fe center to a [4Fe-4S] cluster in *A.vinelandii* ferredoxin I were reported in reconstitution (38) or "super-reduction" (39) of this protein.

Further, optical and EPR studies showed that there was no oxo ligand present in *A.vinelandii* ferredoxin I. All efforts to displace the proposed oxo ligand in *A. vinelandii* ferredoxin I with cyanide were uniformly unsuccessful (40). In addition to that, the electron spin echo envelopes for H_2O- and D_2O- equilibrated samples of ferredoxin I indicated that there were no exchangeable protons on ligands to iron in the 3Fe center of ferredoxin I (40).

Finally, no 4.1 Å iron-iron separation for the 3Fe cluster was detected in EXAFS studies of *A. vinelandii* ferredoxin I. Indeed, an iron-iron distance of 2.7 Å was reported (41, 42). EXAFS data for a ferricyanide treated 3Fe form of *A. vinelandii* indicated that the 3Fe cluster was a cubane-like structure (43).

All the results from above mentioned spectroscopy studies were not consistent with the [3Fe-3S] cluster in *A. vinelandii* ferredoxin I described in the X-ray crystal structure and indicated that the primary X-ray crystal structure of *A. vinelandii* ferredoxin I was in error.

Recently, G. H. Stout et al. (23) and C. D. Stout (20) independently reexamined the X-ray crystallography of *A. vinelandii* ferredoxin I. Both groups concluded that the novel 3Fe cluster presented in Fd I is a cubane-like [3Fe-4S] cluster. The iron-iron distance and cluster angles are similar to [4Fe-4S] cluster (Table 1.1).

The revised X-ray crystal structure indicates that the protein folding in the N-terminal half is similar to the homologous 8Fe ferredoxin structure (21). The structure of Fd I for residues 1 to 57 superposes within 0.85 Å on residues 1 to 53 of the 8Fe ferredoxin for main-chain N, C_α and C atoms, when residues 9, 10, 29 and 30 of FdI are omitted (21). The C terminal residues wrap around this structure (21).

1.4 Spectroscopy Studies

1.4.1 Absorption Spectra

The UV-visible absorption spectra of *A. vinelandii* Fd I and *P. putida* ferredoxin in their isolated forms are presented in Figure 1.3. Two similar

Figure 1.3 UV-VIS Spectra of Isolated Forms of *Azotobacter vinelandii* Ferredoxin I and *Pseudomonus putida* Ferredoxin

(0.01 mM Protein in a 0.1 M Tris-HCl buffer containing 0.1 M NaCl with a pH value of 7.4)

——— *A. vinelandii* ferredoxin I

····· *P. putida* ferredoxin

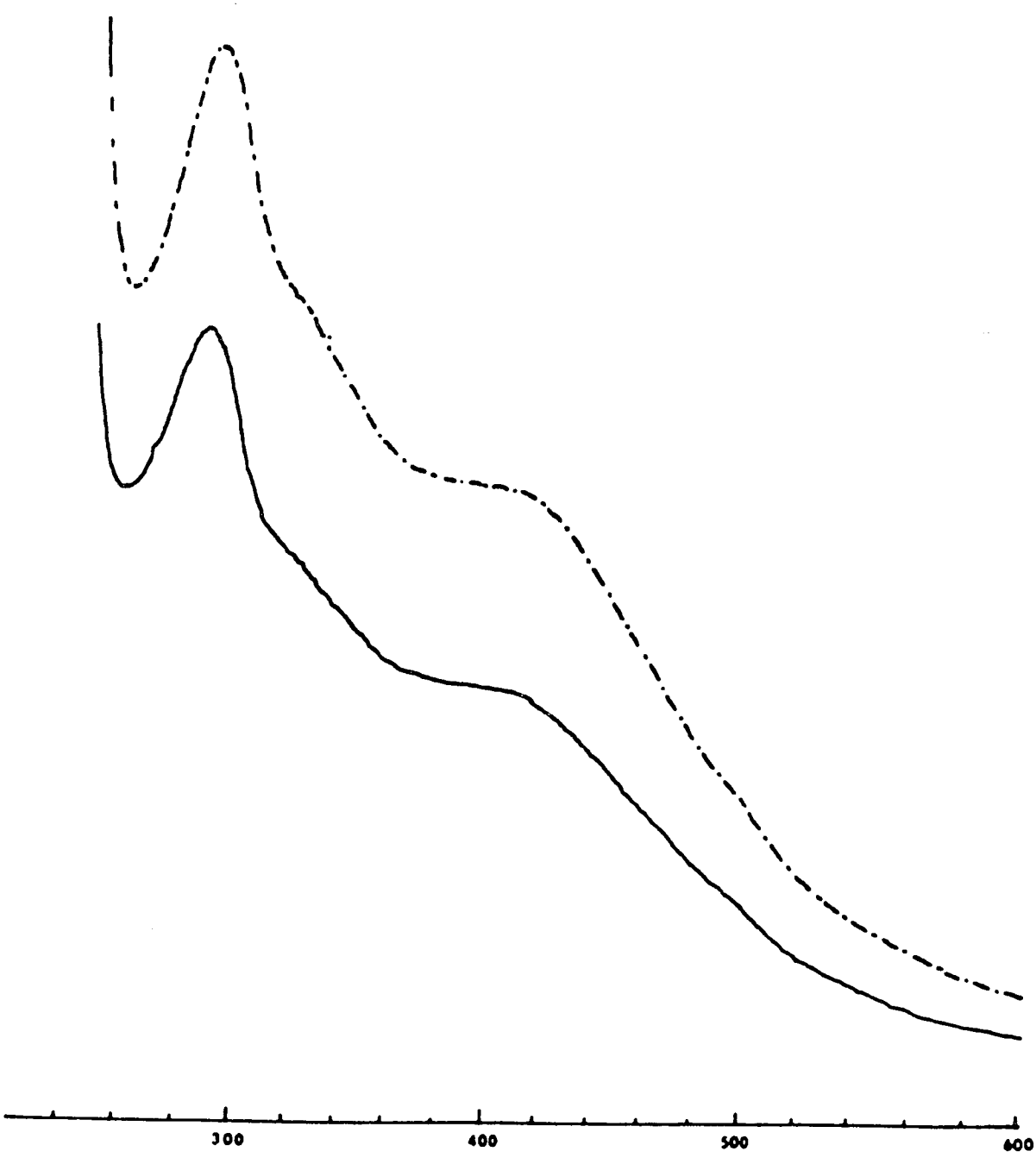
300
400
500
600

spectra exhibit an absorption peak at 283 nm with two shoulders around 400 nm and 320 nm. The shoulder around 400 nm is due to charge transfer between iron and sulfur atoms. A similar absorbance is seen in the UV-visible spectra of 8Fe ferredoxins. The 283 nm peak arises from both the charge transfer and to a smaller extent from aromatic amino acid residues in proteins. The ratio of A_{400} to A_{283} is used to assess the purity of ferredoxin, with 0.59 taken as pure for both ferredoxins (4, 44). Their millimolar extinction coefficients were determined to be 29.8 $mM^{-1}cm^{-1}$ at 400 nm for the isolated form of *A. vinelandii* (45) and 31.7 $mM^{-1}cm^{-1}$ for the isolated form of *P. putida* (46).

Addition of potassium ferricyanide to the ferredoxin caused an increase of absorbance above 480 nm (26, 46), and a slight decrease of absorbance in the visible region was observed with addition of excess amount of solid sodium dithionite to the ferredoxin (5, 46).

1.4.2 CD Spectroscopy

CD spectra for both *A. vinelandii* Fd I (38, 45) and *P. putida* ferredoxin (46) have been published. In the far-ultraviolet region, the isolated form of ferredoxin exhibits a positive peak at 227 nm. It has been suggested that it arose from the charge transfer transitions between iron and sulfur atoms (46). However, no ellipticity band characteristic of secondary structure have been observed.

A CD spectrum of *P. putida* ferredoxin, as isolated, in the near-ultraviolet is presented in figure 1.4. It is relatively complex and a number of positive peaks around 320, 390, 466 and 570 nm are observed. Their positions in the spectrum and the relative intensity of these ellipticity bands are similar to that of *A. vinelandii* Fd I (45).

Figure 1.4 CD Spectra of the Isolated Form of *Pseudomonus putida* 7Fe Ferredoxin in the Near-ultraviolet Region

0.5 mM *P. putida* ferredoxin in a 50 mM phosphate buffer containing 50 mM NaCl

top: pH = 4.8

bottom: pH = 7.4

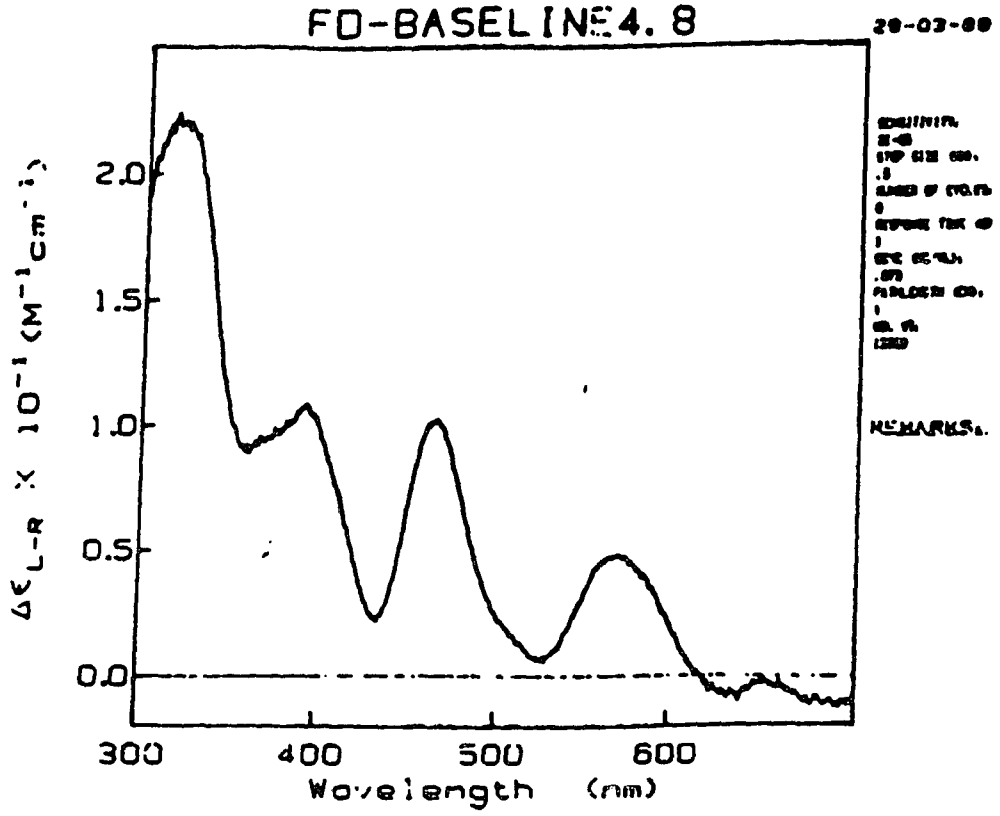
FD-BASELINE4.8
29-03-89
2.0
1.5
1.0
0.5
0.0
300
400
500
600
Wavelength (nm)

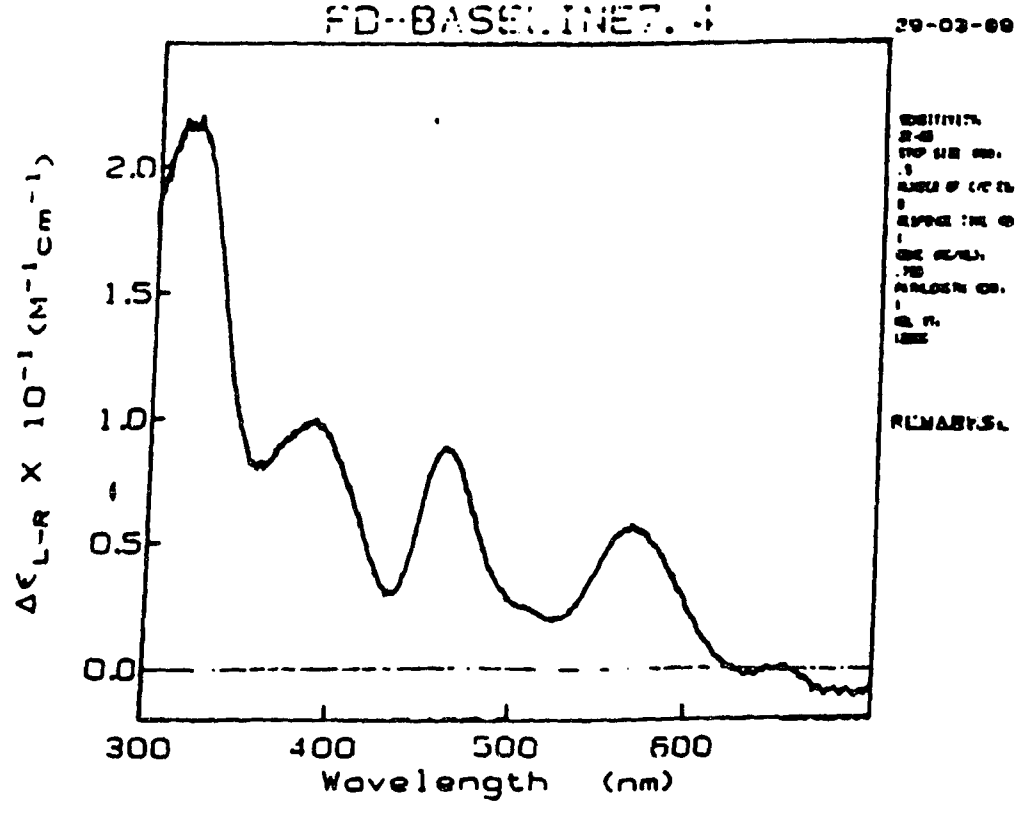
29-03-89
2.0
1.5
1.0
0.5
0.0
300
400
500
600
Wavelength (nm)

When ferricyanide ($Fe(CN)_6^{-3}$) was added into the solution, it was observed that the intensities of these peaks were decreased to zero, and this intensity decrease was titratable with the concentration of ferricyanide (47). Upon reduction with sodium borohydride, the CD spectrum of *P. putida* ferredoxin in this region was remarkably changed (47). No significant pH dependence was encountered in this range (Figure 1.4).

1.4.3 EPR

In their isolated forms, *A. vinelandii* Fd I (4) and *P. putida* ferredoxin (46) each exhibits a nearly isotropic EPR signal around g=2.01 at liquid helium temperature. Broadening of this signal has been observed with increasing temperature. When the temperature is higher than 30K, the signal becomes undetectable. No other signal could be detected in a wide range of magnetic field. Since Mössbauer spectroscopy study has revealed that the [3Fe-4S] cluster is paramagnetic in the isolated form while the [4Fe-4S] cluster is diamagnetic (29), this signal is associated with [3Fe-4S] center.

Although sodium dithionite has been reported to reduce the [3Fe-4S] cluster to a state that remains paramagnetic but EPR-silent, the [4Fe-4S] cluster was unaffected (29). The EPR spectrum showed that the intensity of the g = 2.01 signal was diminished but not zero when sodium dithionite was added (4). This result indicates that sodium dithionite alone can not reduce the 3Fe center completely. In the case of *P. putida* ferredoxin the reduction of the 3Fe center was incomplete, even though the strong reductant, sodium borohydride, was used (47).

1.4.4 Resonance Raman

Resonance Raman spectra of *A. vinelandii* Fd I (48, 37) and *P. putida* ferredoxin (49) have been studied. The low temperature RR spectrum of *A. vinelandii* Fd I in the isolated form is characterized by two prominent peaks at 351 and 397 cm^{-1} and several weaker bands in the 100 to 400 cm^{-1} (i.e., 268, 336, 376 cm^{-1}, etc.). On the other hand, *P. putida* Fd as the isolated form shows two strong bands at 349 and 396 cm^{-1} with several weaker bands (265, 335 and 371 cm^{-1}, etc.). These bands arise from both 3Fe and 4Fe clusters.

When *P. putida* ferredoxin is reduced by excess sodium dithionite, the intensities of bands at 265, 349 and 396 cm^{-1} decreased markedly, which indicated that these bands arose from the 3Fe center (50). The peak at 335 cm^{-1} is a characteristic band of the 4Fe cluster. Their similar RR spectra demonstrated that both *A. vinelandii* Fd I and *P. putida* ferredoxin contain 3Fe and 4Fe clusters.

1.4.5 NMR

Figure 1.5 shows ^1H NMR spectra of *A. vinelandii* ferredoxin I and *P. putida* ferredoxin in their isolated forms. In the region downfield of 10 ppm, each exhibits six resolved resonances (A, B, C, D, E, and F respectively). Early work has indicated that five most downfield resonances, A, B, C, D and E, are single-proton resonances (51).

Based on the results from reduction and oxidation studies, the first three most downfield resonances, A, B and C were assigned to protons near the [3Fe-4S] center, while resonances D and F originated from the protons near the [4Fe-4S] center (51, 52). However, by previous NMR results, the closest cluster to the proton which gave a rise of resonance E cannot be

Figure 1.5 400 MHz ^{1}H NMR Spectra of *Pseudomonus putida* Ferredoxin and *Azotobacter vinelandii* Ferredoxin I as the Isolated Form

top: *P. putida* ferredoxin (0.5 mM)

bottom: *A. vinelandii* ferredoxin I (1 mM)

Recorded in 50 mM phosphate buffer containing 50 mM NaCl and pH was 7.4, temperature was controled at 23 °C

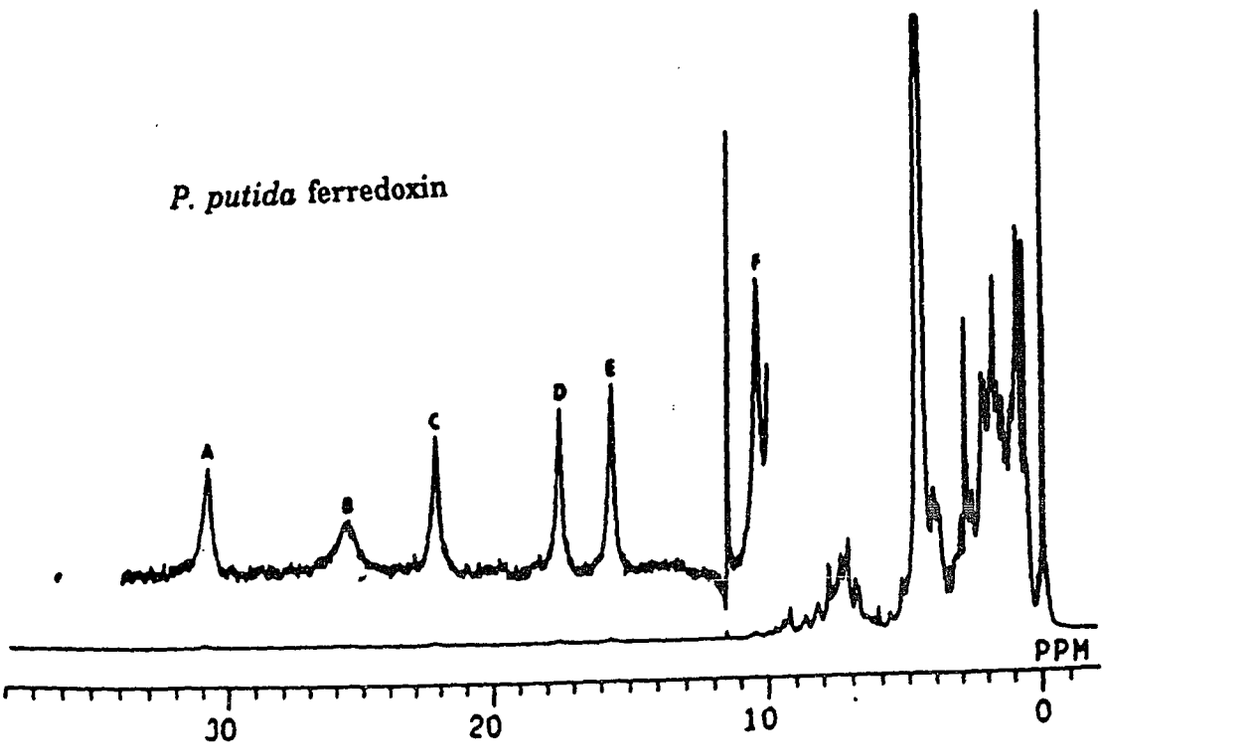
P. putida ferredoxin
A
B
C
D
E
F
PPM
30
20
10
0

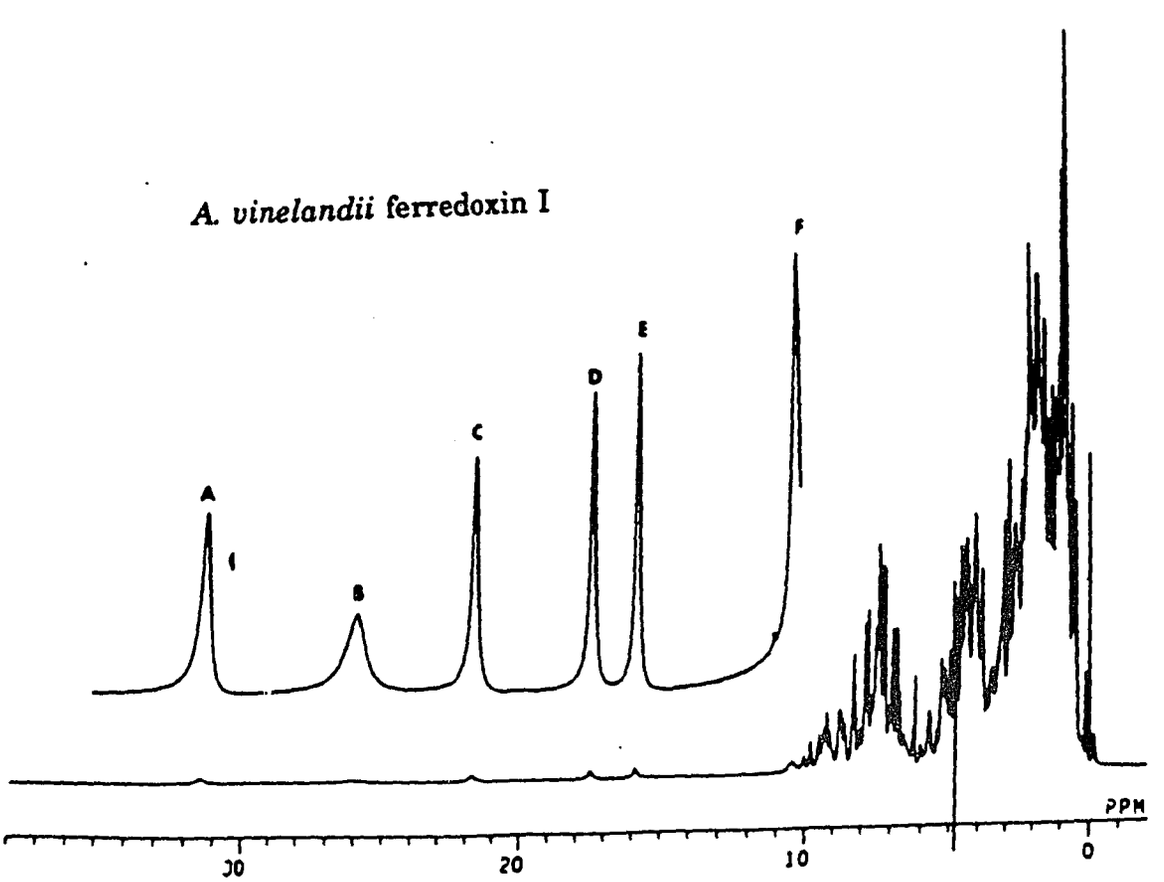
A. vinelandii ferredoxin I
A
B
C
D
E
F
PPM
30
20
10
0

assigned (51, 52).

1.5 Purpose of the Research

NMR spectroscopy has been used in studies of ferredoxins since the 1970s. At the time this research began, and even more recently, 2D-NMR assignment techniques had been successfully applied only to the resonances arising from the nuclei distant from the iron-sulfur centers. The most extensive example is the work done by Oh and Markley (53), where all the resonances except those arising from protons within 7.8 Å of the iron atoms were assigned for the *Anabaena* 2Fe-2S ferredoxin. An important objective of this research has been to develop practical assignment strategies for those resonances arising from nuclei near the iron-sulfur centers.

The iron-sulfur cluster is the active site during the electron transfer. The resonances arising from any nuclei near the iron-sulfur center are inherently the most interesting, as they report events and geometry in the vicinity of the iron-sulfur center. However, unlike the diamagnetic resonances, these resonances are very difficult to assign. Due to the interaction between unpaired electrons and nuclei, the paramagnetically shifted resonances usually have a large chemical shift and are fast relaxing with broad line-widths. Thus, the cross peaks in two-dimentional homonuclear ^1H NMR spectra are usually not observable for any protons close to a iron-sulfur cluster (53).

Another important objective of this research is to confirm the number of the cysteinyl ligands to the 3Fe center using NMR spectroscopy. At the beginning of this research, it was not known if the structure of the

3Fe center was $Fe_3S_3(S^{Cys})_5Oxo$ or $Fe_3S_4(S^{Cys})_4$. Since the number of terminal cysteinyl ligands of the two types of 3Fe clusters are different, a choice between the proposed structure of the 3Fe center can be made after the 7Fe ferredoxin is labeled by β-^{13}C-cysteine.

1.6 References

1. Cammack, R., Krishna, K. K. and Hall, D. O. (1985) Physiol. Vèg. **23** (5)

2. Bruschi, M., and Guerlesquin, F. (1988) *FEMS Microbiol. Rev.* **54**, 155-176

3. Mortenson, L. E., Valentine, R. C. and Carnahan, J. E., (1962) *Biochem. Biophys. Res. Commun.*, **7**, 448-454

4. Shethna, Y. I. (1970) *Biochim. Biophys. Acta 205*, 58-62

5. Yoch, D. C., Benneman, J. R., Valentine R. C., and Arnon, D. I. (1969) *Proc. Natl. Acad. Sci. USA* **64**, 1404-1410

6. Yates, M. G. (1970) *FEBS Lett.* **8**, 281-285

7. Matsumoto, T., Tobari, J., Suzuki, K., Kimura, T., and Tchen, T. T. (1976) *J. Biochem* **79**, 937-943

8. Saeki, K., Wakabayashi, S., Zumft, W. G., and Matsubara, H. (1988) *J. Biochem.* **104**, 242-246

9. Imai, T., Matsumoto, T., Ohta, S., Ohmori, D., Suzuki, K., Tanaka, J., Tsukihara, M., and Tobari, J. (1983) *Biochim. Biophys. Acta 743*, 91-97

10. Yates, M. G., O'Donnell, M. J., Lowe, D. J., and Bothe, H. (1978) *Eur. J. Biochem.* **85**, 291-299

11. Schlatter, D., Waldvogel, S., Zülli, F., Suter, F., Portmann, W. and Zuber, H. (1985) *Biol. Chem. Hoppe-Seyler* **366**, 223-231

12. Jouanneau, Y., Meyer, C., Gaillard, J. and Vignais, P. M. (1990) *Biochem. Biophys. Res. Comm.* **171**, 273-279

13. Yoch, D. C., Carithers, R. P., and Arnon, D. I. (1977) *J. Biol. Chem.* **252**, 7453-7460

14. Trower, M. K., Marshall, J. E., Doleman, M. S., Emptage, M. H., and Sariaslani, F. S. (1990) *Biochim. Biophys. Atca.* **1037**, 290-296

15. Sato, S., Nakazawa, K., Hon-nami, K., and Oshima, T. (1981) *Biochim. Biophys. Acta* **668**, 277-289

16. Hase, T., Wakabayashi, S. Matsubara, H., Ohmori, D., and Suzuki, K. (1977) *FEBS Lett.* **91**, 315-319

17. Hase, T., Wakabayashi, S., Matsubara, H., Imai, T., Matsumoto, T., and Tobari, J. (1979) *FEBS lett.* **103**, 224-228

18. Howard, J. B., Lorsback, T. W., Ghosh, D., Melis, K., and Stout, C. D. (1983) *J. Biol. Chem* **258**, 508-522

19. Duport, C., Jounanequ, Y. and Vignais, P. M. (1990) *Nucleic Acids Research* **18**, 4618

20. Stout, C. D. (1988) *J. Biol. Chem.* **263**, 9256-9260

21. Stout, C. D. (1989) *J. Mol. Biol.* **205**, 545-555

22. Stout, G. H., Turley, S., Sieker, L. C. and Jensen, L. H. (1988) *Proc. Natl Acad. Sci. USA* **85**, 1020-1022

23. Martin, A. E., Burgess, B. K., Stout, C. D., Cash, V. L., Dean, D. R., and Jensen, G. M. (1990) *Proc. Natl. Acad. Sci. USA* **87**, 598-602

24. Ghosh, D., O'Donnell, S., Furey, W.,Jr., Robbins, A. H., and Stout, C. D., (1982) *J. Mol. Biol.*, **158**, 73-109

25. Yoch, D. C. and Arnon, D. I. (1972) *J. Biol. Chem.* **247**, 4514-4520

26. Sweeney, W. V., Rabinowitz, J. C., and Yoch, D. C. (1975) *J. Biol. Chen. 250*, 7842-7847

27. Howard, J. B., Lorsbach, T., and Que, L. (1976) *Biochem. Biophys. Res. Commun.* **70**, 582-588

28. Averill, B. A., Bale, J. R., and Orme-Johnson, W. H. (1978) *J. Amer. Chem. Soc.* **100**, 3034-3043

29. Emptage, M. H., Kent, T. A., Huynh, B. H., Rawlings, J., Orme-Johnson, W. H. and Munck, E. (1980) *J. Biol. Chem.* **255**, 1793-1796

30. Stout, C. D., Ghosh, D., Pattabhi, V. & Robbins, A. H. (1980) *J. Biol. Chem.* **255**, 1797-1800

31. Stout, C. D. (1979) *J. Biol. Chem.* **254**, 3598-3599

32. Stout, C. D. (1979) *Nature* **279**, 83-84

33. Antonio, M. A., Averill, B. A., Moura, I., Moura, J. J. G., Orme-Johnson, W. H., Teo, B. K. and Xavier, A. V. (1982) *J. Biol. Chem.* **257**, 6646-6649

34. Beinert, H., Emptage, M. H., Dreyer, J-L., Scott, R. A., Hahn, J. E., Hodgson, K. O. and Thomson, A. J. (1983) *Proc. Natl Acad. Sci. USA* **80**, 393-396

35. Beinert, H. and Thomson, A. J. (1983) *Arch. Biochem. Biophys.* **222**, 333-361

36. George, S. J., Richards, A. J. M., Thomson, A. J. and Yates, M. G. (1984) *Biochem. J.* **224**, 247-251

37. Johnson, M. K., Czernuszewicz, R. S., Spiro, T. G., Fea, J. A. and Sweeney, W. V. (1983) *J. Am. Chem. Soc.* **105**, 6671-6678

38. Morgan, T. V., Stephens, P. J., Burgess, B. K., and Stout, C. D. (1984) *FEBS* **167**, 137-141

39. Stephens, P. J., Morgan, T. V., Stout, C. D., and Burgess, B. K., (1986) in "Frontiers of Bioinorganic Chemistry" pp. 637-646 (Xlvier, A. V. ed) VCH Publisher, Weisheir

40. Malikayil, J. A., Sweeney, W. V., McCracken, J., and Peisach, J., (1985) *Biochem. Biophys. Research Communication* **133**, 1119-1124

41. Scott, R. A., Kazmi, S. A., Beinert, H., Emptage, M. H., Hahn, J. E., Hodgson, K. O., Stout, C. D. and Thomson, A. J. (1983) *Inorg. Chim. Acta.* **79**, 142

42. Scott, R. A., Penner-Hahn, J. E., Hodgson, K. O., Beinert, H. and Stout, C. D. (1984) in EXAFS and Near Edge Structure III (Hodgson, K. O., Hedmann, B. and Penner-Hann, J. E., eds), pp 105-110, Springer-Verlag, Berlin

43. Stephens, P. J., Morgan, T. V., Devlin, F., Penner-Hahn, J. E., Hodgson, K. O., Scoot, R. A., Stout, C. D. and Burgess, B. K. (1985) *Proc. Natl. Acad. Sci. USA* **82**, 5661-5665

44. Ohmori, D. (1976) *Biochem. Biophys. Res. Commun.*, **72**, 566-574

45. Morgan, T. V., Stephens, P. J., Devlin, F., Stout, C. D., Melis, K. A, and Burgess, B. K. (1984) *Proc. Natl. Acad. Sci. USA* **81**, 1931-1935

46. Ohmori, D. (1984) *Biochim. Biophys. Acta* **790**, 15-21

47. Ohmori, D., Yamakura, F., Suzuki, K., Imai, T., and Nagayama, K., (1986) in "Iron-Sulfur Protein Research", eds. H. Matsubara et al., pp. 116-124. Japan Sci. Soc. Press, Tokyo/Springer-Verlag, Berlin

48. Lutz, M., Moulis, J-L., and Meyer, J.,(1983) *FEBS* **153**, 212-216

49. Imai, T., Saito, H., Tobari, J., Ohmori, D. and Suzuki, K. (1984) *FEBS*, **165**, 227-230

50. Johnson, M. K., Hare, J. W., Spiro, T. G., Moura, J. J. G., Xavier, A.V. and LeGall, J. (1981) *J. Biol. Chem.* **256**, 9806-9808

51. Sweeney, W. V. (1981) *J. Biol. Chem.* **256**, 12222-12227

52. Nagayama, K., Ohmori, D., Imai, T., and Oshima, T., (1986) in "Iron-Sulfur Protein Research", eds. H. Matsubara et al., pp. 125-138. Japan Sci. Soc. Press, Tokyo/Springer-Verlag, Berlin

53. Oh, Byung-Ha and Markley, J. (1990) *Biochemistry* **29**, 3993-4004.

CHAPTER 2

THEORETICAL BACKGROUND

2.1 Chemical Shift

Most ferredoxins are paramagnetic in at least one of their oxidation states. This therefore gives rise to paramagnetically shifted signals in their NMR spectra. The "paramagnetically shifted resonances" implies that shifts of a paramagnetic protein are different from those of diamagnetic compounds. The paramagnetically shifted resonances result from electron-nucleus interactions. Two types of interactions have been described in the literature: Fermi type "contact shift" and dipolar-dipolar "pseudocontact shift".

Fermi type contact shift arises from a through chemical bond scalar interaction between the unpaired electrons and the resonating nuclei. The unpaired electrons present on bound irons of ferredoxin have relatively large magnetic moments. They are capable of delocalizing directly to the nearby atomic nuclei through chemical bonding and building a net electron density on the atomic nuclei. Electron spin density causes large shielding or deshielding of the applied magnetic field at the resonating nuclei. Therefore, the chemical shifts of the resonating nuclei will be changed in NMR spectrum. The contact interaction is proportional to the magnetic susceptibility (χ) of the complex and the contact interaction constant (A_c). The contact interaction is usually expressed by the equation 2.1 (1):

$$\delta_c = \frac{2\pi A_c}{h\gamma_I}\frac{g\beta}{3kT}S(S+1) \qquad (2.1)$$

where A_c is the contact interaction constant, g is the electronic g-factor, β is the Bohr magneton, γ_I is the gyromagnetic ratio for the nucleus, S is the total electronic spin, k is the Boltzmann constant, T is the absolute temperature, and h is the Planck constant.

Poe et al. (2) have proposed a simple mechanism for contact shifts in ferredoxins. The unpaired electron spin density on a bound iron is transferred to a empty p-orbital of a sulfur atom as a result of coordination to the iron. The β-CH_2 protons of cysteine can sense this spin density centered on sulfur by hyperconjugation and manifest the spin density by isotropic hyperfine contact-interaction shifts. Since two β-CH_2 protons of an iron bound cysteinyl residue are nonequivalent with respect to the p-orbital of sulfur, these geminal protons should experience different shifts depending on the different dihedral angles θ between the Fe-Sγ-Cβ and the Sγ-Cβ-H planes by the following relationship (3):

$$A_c = \beta_o + B_2\cos^2\theta \qquad (2.2)$$

where B_2 is related to the spin density on the proton resulting from hyperconjugation, and β_o is related to spin density resulting from other delocalization mechanisms.

In addition to direct delocalization, the unpaired electrons present on bound irons in ferredoxin can also polarize the two paired electrons on the nearby resonating nuclei via dipole-dipole interaction. This mechanism is called "pseudocontact shifts". They can only arise in a system where the magnetic susceptibility of the paramagnetic center is anisotropic, and

hence the electron-nucleus dipole-dipole coupling does not average to zero under the rotational molecular tumbling in solution.

In the case of rhombic symmetry, quantitative expressions describing the pseudocontact shifts can be expressed as (4):

$$\delta_{pc} = \frac{\beta^2 S(S+1)}{9kTr^3} \{[g_z^2 - \frac{1}{2}(g_x^2 + g_y^2)](3\cos^2\Omega - 1) + \frac{3}{2}(g_y^2 - g_x^2)\sin^2\Omega\cos^2\theta\} \quad (2.3)$$

where r is the distance from the electron spin to the nuclear spin, Ω is the polar angle of r made by the vector of r relative to the z axis of the magnetic anisotropy, and θ is the angle between the projection of r in the xy plane and the y axis. For an axially anisotropic system, i.e., $g_z = g_{\parallel}$, $g_x = g_y = g_{\perp}$, this equation (2.3) can be reduced to:

$$\delta_{pc} = \frac{\beta^2 S(S+1)}{9kTr^3} (g_{\parallel}^2 - g_{\perp}^2)(3\cos^2\Omega - 1) \quad (2.4)$$

Therefore, the magnitude and sign of pseudocontact shift can be positive or negative (and even zero when θ equals 54.7 °C). In deriving equations (2.3) and (2.4), it was assumed that the system contained only one thermally populated energy level in the absence of the magnetic field H_o, and that T_{1e} (electron spin-lattice relaxation time) is very short.

The EPR spectrum of 7Fe ferredoxin in the isolated form gives only one isotropic signal at g = 2.01. Hence, the magnetic susceptibility of the iron-sulfur centers is isotropic, and no pseudocontact shifted resonances are expected in the NMR spectra of 7Fe ferredoxins in their isolated oxidation state.

2.2 Antiferromagnetic Coupling

Iron atoms in a paramagnetic complex can be magnetically coupled. The unpaired electrons interact with each other through dipolar and Coulomb (exchange or superexchange) interactions. The magnetic coupling can be described with a spin Hamiltonian. For two iron atoms, it is:

$$\mathbf{H} = -2J\mathbf{S}_1\cdot\mathbf{S}_2 \qquad (2.5)$$

where S_1 and S_2 are the spin vectors for the two iron atoms and J is the magnitude of the interaction. For a system where $S_1 > S_2$, magnetic coupling would lead to a manifold of spin states ($S' = S_1-S_2, S_1-S_2+1, \ldots, S_1+S_2$) at energies of $J[S'(S'+1)]$. For example, for two unpaired electrons each with a spin 1/2, the total spin can be either 0 ($S'= 0$) or 1 ($S'=1$) after magnetic coupling. If magnetic coupling results such that the singlet state ($S'= 0$) is lower than the triplet state ($S'= 1$) in energy, it is called antiferromagnetic coupling. The manifold of spin states resulting from antiferromagnetic coupling can explain the observation of some contact shift resonances arising from protons near the [4Fe-4S] center in 7Fe ferredoxin. This is because the thermally populated spin states of the 4Fe center is paramagnetic, even though the ground state of the [4Fe-4S] center is diamagnetic in its isolated oxidation state.

2.3 Nuclear Spin Relaxation in Paramagnetic Molecules

The presence of a paramagnetic center in ferredoxin also provides an efficient pathway for the nucleus to relax through dipolar and contact interaction between the fast relaxing unpaired electron and the resonating nucleus. The relationships most widely used to describe the relaxation of a

nucleus by an unpaired electron are the Solomon-Bloembergen equations (5, 6):

$$\frac{1}{T_{1M}} = \frac{2}{15}\frac{\gamma_I^2 g^2 \beta^2 S(S+1)}{r^6}\left(\frac{3\tau_{c1}}{1+\omega_I^2\tau_{c1}^2} + \frac{7\tau_{c2}}{1+\omega_S^2\tau_{c2}^2}\right) + \frac{2}{3}S(S+1)\left(\frac{2\pi A_c}{h}\right)^2\left(\frac{\tau_2}{1+\omega_S^2\tau_2^2}\right) \qquad (2.6)$$

and

$$\frac{1}{T_{2M}} = \frac{1}{15}\frac{\gamma_I^2 g^2 \beta^2 S(S+1)}{r^6}\left(4\tau_{c1} + \frac{3\tau_{c1}}{1+\omega_I^2\tau_{c1}^2} + \frac{13\tau_{c2}}{1+\omega_S^2\tau_{c2}^2}\right) + \frac{1}{3}S(S+1)\left(\frac{2\pi A_c}{h}\right)^2\left(\tau_1 + \frac{\tau_2}{1+\omega_S^2\tau_2^2}\right) \qquad (2.7)$$

where the first term describes dipolar relaxation, and the second term is contact relaxation. T_{1M} and T_{2M} are the longitudinal and transverse relaxation times of the nuclear spin I which arise from the interactions with the electron spin, τ_{c1} and τ_{c2} are the effective correlation times for the dipolar interactions, ω_I and ω_S are the Larmor frequencies for the nucleus and the electron, and τ_1 and τ_2 are the correlation times for contact coupling, which are in the absence of chemical exchange given by the longitudinal and transverse electron spin relaxation times, i.e. $\tau_1 = T_{1e}$ and $\tau_2 = T_{2e}$. The definitions of other terms remain the same as before. The total correlation times τ_{c1} and τ_{c2} are defined by equations (2.8):

$$\frac{1}{\tau_{c1}} = \frac{1}{\tau_c} + \frac{1}{T_{1e}} + \frac{1}{\tau_M}; \quad \frac{1}{\tau_{c2}} = \frac{1}{\tau_c} + \frac{1}{T_{2e}} + \frac{1}{\tau_M} \qquad (2.8)$$

where τ_c is the rotational correlation time of the molecule, and τ_M is the lifetime of the ion in the complex, which enters into the equations only in the case of a weak complex in fast exchange.

For ferredoxins the contact terms in the equations (2.6) and (2.7) can be neglected (7). This is because A_c/h is often of the order of 10^6 Hz, whereas the coefficient of the dipolar term is of the order of 10^{12} Hz. Therefore, the

rate of nuclear relaxation in a ferredoxin only depends on the dipolar interaction between nonpaired elections and nucleus.

One main objective of nuclear relaxation time measurements on paramagnetically perturbed macromolecules is to obtain the distances between a given nucleus and the paramagnetic center (8). This application is not valid in ferredoxin NMR studies. Iron atoms in Iron-sulfur clusters of ferredoxins are antiferromagnetic coupled. The effective paramagnetic center must be calculated from the molecular electronic wave functions. Such derivations are currently too complicated for iron-sulfur clusters.

2.4 One-Dimensional Nuclear Overhauser Effect

For two resonances arising from two dipole coupled nuclei, irradiation of one resonance results in an intensity change for the other resonance due to a change in population of the spin levels. This effect is called the nuclear Overhauser effect.

In 1D steady state NOE, the population distribution of one resonance is caused by applying a selective presaturation pulse for a period of several times longer than its T_1. The intensity change from a dipolar coupled nucleus is measured from the NOE difference spectrum accumulated either with or without selective irradiation pulse. The steady state nuclear Overhauser effect, NOE, for two protons, i and j, is defined as (9):

$$\eta_{i\rightarrow j} = (I_j - I_j^{\circ})/ I_i^{\circ} = \sigma_{ij} / \rho_j \qquad (2.9)$$

where $\eta_{i\rightarrow j}$ is the nuclear Overhauser effect for j upon saturating spin i; I_j and I_j° are intensities of the signal from the detected proton H_j with and without saturating the resonance of the spin H_i; and ρ_j is the selective relaxation rate. The cross-relaxation rate, σ_{ij}, for rigid molecules tumbling slowly in solution is given by equation (2.10) (10):

$$\sigma_{ij} = -\left(\frac{h}{2\pi}\right)^2 \gamma_H^4 \tau_c / 10 r_{ij}^6 \qquad (2.10)$$

where r_{ij} is the internuclear distance, τ_c is the correlation time of the protein and γ_H is the proton gyromagnetic ratio.

In the case of strongly paramagnetic systems, the dominance of paramagnetic influences minimizes the difference between the selective and nonselective T_1s (which implies that the T_1 is measured by *selective* or *nonselective* inversion) (11). The selective relaxation rate, ρ_j, in equation (2.9) can be replaced by nonselective spin-lattice relaxation time T_{1j}. Equation (2.9) can be rewritten as:

$$\eta_{i \to j} = \sigma_{ij} T_{1j}. \qquad (2.11)$$

However, when considering of a very broad paramagnetically shifted resonance, a high irradiation power is needed for complete saturation. This may cause a large spin-diffusion in the experiment. Since a very short spin-lattice relaxation time, T_{1j}, is expected for paramagnetically shifted resonance, a small nuclear Overhauser effect will be arisen between nuclei near paramagnetic centers, according to equation 2.11. Recently, Dugad, et al. (12) showed that a steady-state nuclear Overhauser effect still can be seen between paramagnetically shifted resonances in ^1H NMR spectra of strongly paramagnetic iron-sulfur proteins, even if these resonances are extremely broad and have very short relaxation times (T_1 and T_2).

The molecular wights of *A. vinelandii* ferredoxin I and *P. putida* ferredoxin are around 12 kDa. After correction for temperature and molecular weight differences, a correlation time of 1.4×10^{-8} can be estimated from the molecular weight (13) and the value experimentally obtained for apomyoglobin (14). For a β-proton on a cysteine liganded with iron in these two ferredoxins, the spin-lattice relaxation time, T_1, is

typically around 1.6 to 9.4 ms (see Chapter 5). A -4 % nOe is estimated for a geminal pair protons by using the equations 2.9 and 2.10 when 1.6 ms is used for T_1. This is within a modern FT NMR instrument capacity.

In diamagnetic systems, both σ_{ij} and ρ_j are proportional to correlation time τ_c in the slow motion limit (9). Therefore, the nuclear Overhauser effect, $\eta_{i\rightarrow j}$ is independent of τ_c in the absence of spin diffusion (15). However, for paramagnetic systems, due to strongly paramagnetic influence, T_{1j} (and hence ρ_j) is independent of τ_c , thus:

$$\eta_{i\rightarrow j}(\text{para}) \propto \tau_c \qquad (2.12)$$

The steady state NOE will be increased if the viscosity of the solvent is also increased. This is because the magnitude of correlation time depends on the size of a molecule and the viscosity of the solvent η. For spherical particles of radius a in a solvent of viscosity η, a correlation time can be estimated by the Stokes-Einstein relationship (16):

$$\tau_c = \frac{4\pi\eta a^3}{3kT} \qquad (2.13)$$

A doubling of the NOE upon increasing the viscosity by adding 30% (w/w) ethylene glycol was reported in myoglobin studies (17).

The distance between two protons also can be estimated by the NOE buildup curve when the spin-lattice relaxation time is unable to be directly measured. For a short saturation time, t, while saturating spin i, the truncated NOE results for spin j with the equation 2.13 (18):

$$\eta(t)_{i\rightarrow j} = \sigma_{ij}t \qquad (2.13)$$

This is independent of intrinsic relaxation, and hence independent of spin-lattice relaxation. σ_{ij} can be calculated from the slope of a nOe build up curve of plotting nuclear Overhauser effect vs the saturation time.

2.5 SM-NOESY (Short Mixing time NOESY)

The application for the 1D steady state NOE is limited due to the resonances overlapping in 1D spectra of large molecules. It is difficult to selectivly irradiate a resonance and to detect nOe peaks in crowded region of the NMR spectrum. This problem can be overcome by two-dimensional NOESY spectroscopy. Cross peaks in NOESY arise from homonuclear cross relaxation in longitudinal dimension for dipolar coupled proton pairs.

Since a strongly paramagnetic center present in a protein provides a strong source of external relaxation ($\gamma_e/\gamma_{1H} \approx 600$), any protons close to paramagnetic centers have fast relaxation which overwhelms the intramolecular cross relaxation. The nuclear Overhauser effect is extremely difficult to observe in paramagnetic proteins.

The time dependence of the integrated intensity of the NOESY cross-peaks, $I_{AB}(t_m)$, in an isolated two-spin system is given by Macura and Ernst as the following equation (19):

$$I_{AB} = \frac{M_0}{4} \frac{W_2^{AB} - W_0^{AB}}{|W_2^{AB} - W_0^{AB}|} \exp(-R_L t_m)\,[1 - \exp(-R_c t_m)] \qquad (2.15)$$

where W_0^{AB} and W_2^{AB} represent the zero quantum and double quantum transition probabilities. The cross relaxation rate constant, R_c, and the leakage relaxation rate constant, R_L, are given by equations:

$$R_c = 2\,|W_2^{AB} - W_0^{AB}| \qquad (2.16)$$

and

$$R_L = R_s + 2W_1^{AB} + W_0^{AB} + W_2^{AB} - |W_2^{AB} - W_0^{AB}| \qquad (2.17)$$

R_s is the external relaxation. In a strongly paramagnetic system, the value of R_s can be thought as approximately equaling to its T_1^{-1} in the slow motion limit.

In the case of a long correlation time, $\tau_c \gg 1/\omega_A$, $1/\omega_B$, the spin diffusion limit holds:

$$W_1^{AB} = W_2^{AB} = 0; \qquad W_0^{AB} = q\tau_c \qquad (2.18)$$

and

$$Rc = 2q\tau_c; \qquad R_L = R_s \qquad (2.19)$$

where

$$q = \frac{1}{10}\left(\frac{\mu_0}{4\pi}\right)^2 \gamma_H^4 \left(\frac{h}{2\pi}\right)^2 r_{ab}^{-6} \qquad (2.20)$$

here r_{ab} is the interproton distance. The equation 2.14 can be reduced to:

$$I_{AB} = -\frac{M_0}{4}\exp(-R_s t_m)\,[1 - \exp(-2q\tau_c t_m)] \qquad (2.21)$$

Thus, for a geminal pair protons with spin-lattice relaxation times of 7 ms (hence the Rs is about 150 sec^{-1}), the intensity of the cross-peak will reach to the maxima if a 4 ms mixing time is used.

Figure 2.1 shows the plot of the NOE cross-peak evolution of a proton geminal pair at different values of R_s when τ_c is 1.4×10^{-8} s. The result indicates that for a paramagnetic system, the intensities of cross-peaks in a NOESY spectrum is a sharp function of the mixing time.

Figure 2.2 shows that the downfield SM-NOESY spectra of *A. vinelandii* FdI are recorded with four different mixing times, 1, 5, 10, and

Figure 2.1 Cross-peak Evolution of a Proton Pair

1: R_s is 0 sec^{-1}

2: R_s is 10 sec^{-1}

3: R_s is 25 sec^{-1}

4: R_s is 50 sec^{-1}

5: R_s is 100 sec^{-1}

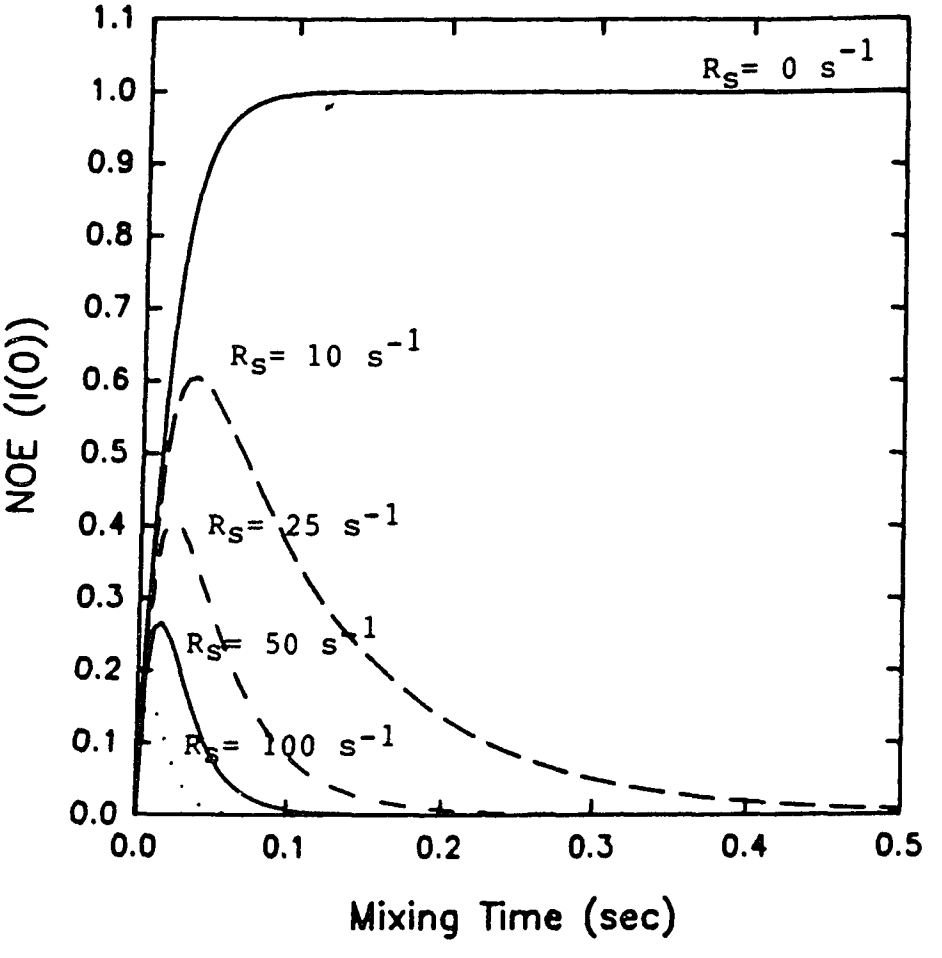
1.1
1.0
0.9
0.8
0.7
0.6
0.5
0.4
0.3
0.2
0.1
0.0
NOE (I(0))
R_S= 0 s^{-1}
R_S= 10 s^{-1}
R_S= 25 s^{-1}
R_S= 50 s^{-1}
R_S= 100 s^{-1}
0.0
0.1
0.2
0.3
0.4
0.5
Mixing Time (sec)

Figure 2.2 The Downfield of NOESY Spectra of *A. vinelandii* Ferredoxin I (5 mM) with Different Mixing Times at 7 °C

5 mM protein in a 50 mM Tris-HCl buffer containing 50 mM NaCl with a pH value of 7.4

1. 1 ms for the mixing time
2. 5 ms for the mixing time
3. 10 ms for the mixing time
4. 20 ms for the mixing time

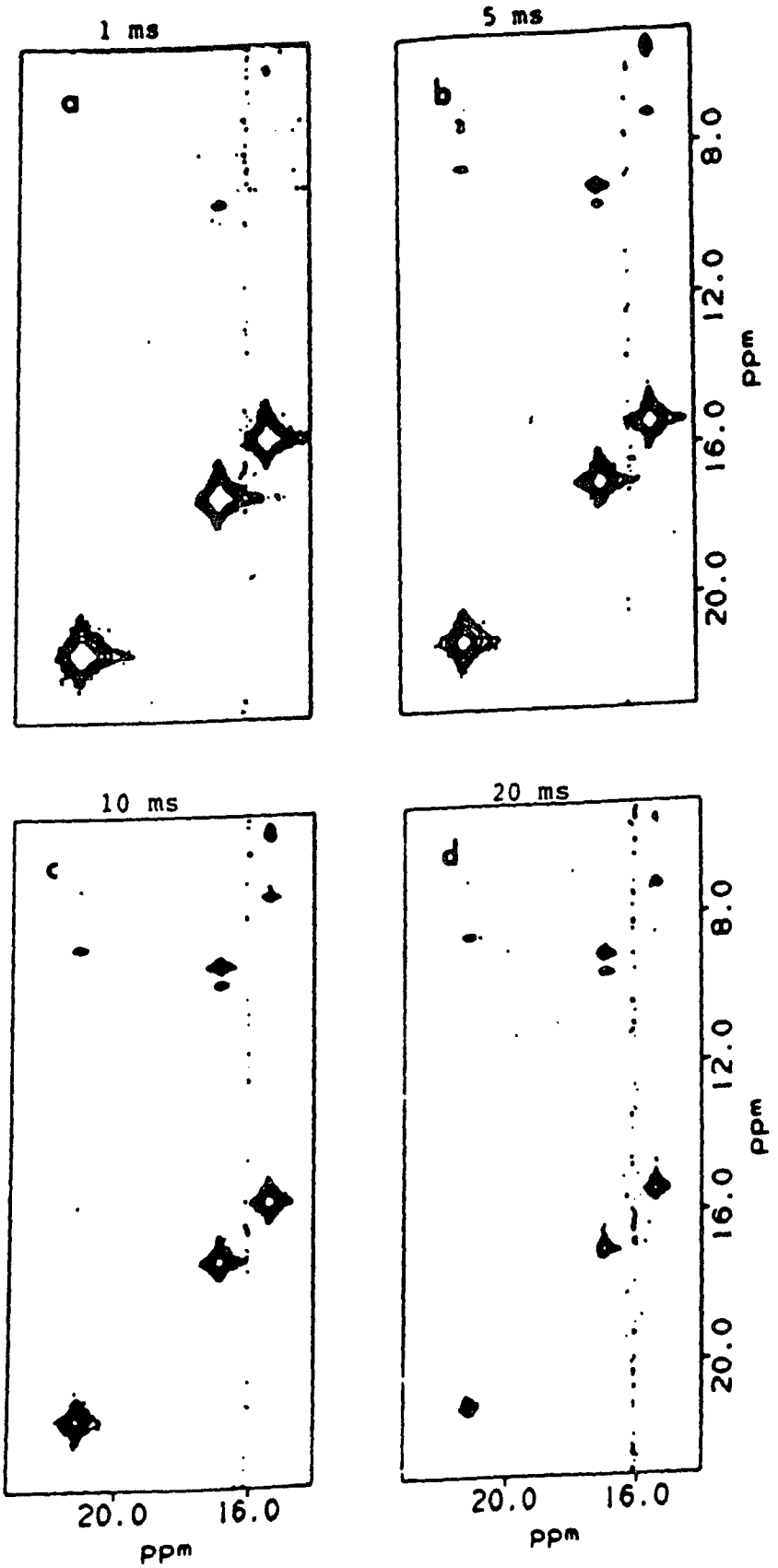
1 ms
a
5 ms
b
8.0
12.0
16.0
20.0
ppm
10 ms
c
d
20 ms
20.0
16.0
ppm

20 ms. Comparing these spectra, it is clearly seen that the intensity of the cross-peak at 15.5 ppm /5.6 ppm is first increased with mixing times of 1 ms to 5 ms, and then decreased in the spectra recorded with mixing times of 10 and 20 ms. The cross-peak at 21.1 ppm/7.2 ppm can only be seen in the spectrum recorded with a mixing time of 5 ms. Thus, a 5 ms mixing time was used in the NOESY experiment to observe a NOE cross-peak arising from the nuclei near a iron-sulfur center.

2.6 References

(1) Bloembergen, N. (1957) *J. Chem. Phys.* **27**, 595-596

(2) Poe, M., Philips, W. D., Mcdonald, C. C., and Lovenberg, W. (1970) Proc. Natl. Acad. Sci. **65**, 797-804

(3) Cowan, J. A. and Sola, M. (1990) *Biochemstry* **29**, 5633-5637

(4) McConnell, H. M. and Robertson, R. E. (1958) *J. Chem. Phys.* **29**, 1361-1365

(5) Soloman, I. and Bloembergen, N. (1956) *J. Chem. Phys.* **25**, 261-266

(6) Dwek, R. A. (1973) in "Nuclear Magnetic Resonance in Biochemistry: Applications to Enzyme System" Oxford Univ. Press (Clarendon), London and New York

(7) Jardetzky, O., & Roberts, G. C. K. (1981) in "NMR in Molecular Biology", Academic Press, New York

(8) Krishnamoorthi, R., Markley, J. L., Cusanovich, M. A., and Przysiecki, C. T. (1986) *Biochemistry*, **25**, 60-67

(9) Noggle, J. H., Sirmer, R. E. (1971) *The Nuclear Overhauser Effect*; Academic; New York

(10) Soloman, I. (1955) *Phys. Rev.* **99**, 559-565

(11) Lecomte, J. T. J., and La Mar, G. N. (1986) *Eur. Biophys. J.* **13**, 373-381

(12) Dugad, L. B., La Mar, G. N., Banci, L., and Bertini, I. (1990) *Biochemistry* **29**, 2263-2271

(13) Malthouse, J. P. G. (1986) *Prog. NMR Spec.* **18**, 1-59

(14) Marshall, A. G., Lee, K. M., and Martin, P. W. (1980) *J. Am. Chem. Soc.* **102**, 1460-1462

(15) Kalk, A; Berendsen, H. J. C. (1976) *J. Magn. Reson.* **24**, 343-366

(16) Nauhans, D. and williamson, M. (1989) in " The Nuclear Overhauser Effect in Structural and Conformational Analysis" VCH publisher, New York

(17) La Mar, G. N., and Dugad, L. B. (1988) *personal communication*

(18) Wagner, G. and Wüthrich, K. (1979) *J. Magn. Reson.* **33**, 675-680

(19) Macura, S., and Ernst, R. R. (1980) *Mol. Phys.* **41**, 95-117

CHAPTER 3

GENERAL METHODS

3.1 Bacterial Growth

Azotobacter vinelandii (ATCC 13705, OP strain) was cultured on Burk's nitrogen-free medium. The recipe is shown in Table 3.1. The cells of *Pseudomonas putida* (ATCC 15175) were aerobically grown on the medium (Table 3.2) described by Daijiro (1). The pH of the media for these two bacterial growth was adjusted to 7.4. The medium was autoclaved before using, and phosphate salts were separated out when autoclaved.

The pure cultures were initially bought from ATCC (American Type Culture Collection). The lyophilized cell was first aerobically inoculated in a 1-L Erlenmeyer flask which contained 300 mL medium with a cotton stopper. The Erlenmeyer flask was subsequently incubated in an orbit environ-shaker (Lab-Line) at 26 °C, with a shaking speed of 140 rpm. After the bacteria grew, the culture medium was diluted to 3 liters with sterile medium to grow continuously in nine 1-L Erlenmeyer flasks. The cells were then transferred into a Fermatron-150 fermenter which contained 90 liters of medium. It was noted that the bacterial metabolism caused the pH of the medium to drop steadily as growth progressed. If there was not contamination, a final pH of 6.5 would be reached. When the Klett turbidometric (Klett-Summerson Photoelectric Colorimeter, Model: 800-3, Klett mfg. Co., Inc. U. S. A.) reading reached approximately 450, bacteria were harvested by using a CEPA cell harvester. Generally, the yield was 6

Table 3.1 Recipe of Growth Medium for *A. vinelandii* (OP)

K_2HPO_4	0.64 gram
KH_2PO_4	0.16 gram
$MgSO_4 \cdot 7H_2O$	0.2 gram
$CaCl_2 \cdot 2H_2O$	0.05 gram
$FeSO_4$	0.0042 gram
Na_2MoO_4	0.001 gram
Sugar	20 gram
H_2O	1 liter

Table 3.2 Recipe of Growth Medium of *P. putida* (ATCC 15175)

Na_2HPO_4	7.4 gram
KH_2PO_4	1.5 gram
$MgSO_4 \cdot 7H_2O$	0.01 gram
$CaCl_2 \cdot 2H_2O$	0.002 gram
$FeSO_4 \cdot 7H_2O$	0.01 gram
$(NH_4)_2SO_4$	4 gram
Glucose	10 gram
H_2O	1 liter

g/L from one growth cycle for *A. vinelandii* and 4 g/L for *P. putida*. The cells were stored at -20 °C in a Ziploc storage bag.

For radioactive labeling, bacterial growth was the same as previously mentioned, except 10 μCi of radioactive (1-^{14}C)-d,l-cystine (Research Products International (RPI), specific activity: 97 mCi/mol) were added together with 0.25 mM of nonradioactive d,l-cystine into a 100 L of fermenter medium.

For isotopic labeling, if the culture was native *P. putida*, cells were first incubated in a normal medium containing of 0.25 mM isotopic d,l-cystine. After the bacteria grew, the culture medium was transferred into a Fermatron-150 fermenter which contained 50 liter batches of medium with 6 g of isotopic d,l-cystine. The yield was generally around 400 g for each growth cycle. Whereas, in the case of *P.putida* cystine auxotroph, the mutant cell was first inoculated in a 1-L Erlenmayer flask. A normal medium containing 0.25 mM d,l-cystine was used. The culture medium was then transferred into a fermenter which contained 50 liter batches of medium and 2 g of isotopic d,l-cystine. About 270 g of bacteria cells were obtained for each growth cycle.

Since *Azotobacter vinelandii* is a nitrogen fixing bacteria, a nitrogen-free medium is used. The incubation can be started by directly adding 30 g of frozen cells into the fermenter with 100 L medium.

3.2 Ferredoxin Isolation

Several methods for the purification of these two 7Fe ferredoxins have

been published (*P.putida*: D. Ohmori (1) and (2), T. Matoumoto et al (3). *A. vinelandii*: D. C. Yoch et al. (4) and Y. I. Shethua (5)) since they were first isolated. A procedure with a high and repeatable yield of ferredoxin from any of these published methods is desired. However, the yields of ferredoxin from them were not high (0.014 mg per gm of wet bacteria by Daijiro Ohmori(1976) method) and variation in yield was noted (varied from 0.35 mg to 16.0 mg per kg of wet bacteria (6)). Therefore, a modified process of protein isolation was designed based on previously published methods. The general procedure is the same for isolation *A. vinelandii* FdI and *P. putida* 7Fe Fd. The main difference between these two ferredoxin isolations is the method of applying cell lysate to the first DEAE-cellulose column.

The detailed procedure is described below:

3.2.1. Cell Destruction

Extracting the protein from a biological source such as a cell culture requires a process of cell destruction. Several methods can be used for this cellular disintegration, e.g., sonication, homogenizing cells by grinding with quartz sand, cleaving the cell walls by using lysozyme, or suspending cells in a 25% butanol and buffer mixture to weaken the cell wall for subsequent lysis. In this research, a detergent-wash/osmotic-shock procedure was used for cell destruction. The detergent-washing can sensitize the cell wall to the attack of the enzyme, and osmotic-shock forces lysozyme molecules through the outer membrane (Gram-negative bacteria) (7). Although *A.vinelandii* and *P.putida* both are lysozyme sensitive Gram-negative bacteria, the cell concentration can be remarkably increased if this method is used (7), i.e., the ratio of culture/lysate could be large than 2.

The wet cells from the harvest were suspended in a 0.05 M Tris-HCl buffer with a pH value of 7.4 (0.5 g/mL of buffer). In this solution, 0.5 mg lysozyme per gram cells, 10 μg DNase per mL of solution, 0.1% Triton X-100 and 1% butanol were added. After stirring for 1 hour at room temperature, the suspension was sonicated three times. A Sonifier Cell Disruptor (Model W185, Heat System-Ultrasonics, Inc.) was used. Each time, about 350 mL cell solution was filled into a sonicate beaker for sonication 3 minutes in an ice bath with full power. During this step, color of the suspension darkened steadily and the pH of the extract dropped to about 6.4, indicating that the cellular membrane was disrupted and ferredoxin was released into the buffer solution. The pH was adjusted back to 7 by adding solid Trizma base before centrifugation.

The cell lysate was then centrifuged at 10,000 xg for 1 hour, while the temperature was 0 to 4°C. After centrifugation, the supernatant was cloudy.

3.2.2.Ion Exchange Chromatography

After centrifugation, an anion exchange column was used. Two different methods of applying cell lysate to the column, batch and open column, were used for the first DEAE anion exchange chromatography depending on the culture source and amount of cells. The open column method gave a higher yield than the batch method (8). However, due to the speed of centrifugation, there were some cell segments remaining in the supernatent after centrifugation. These small cell segments stacked on the top of the column and caused a sluggish flow rate. To avoid this problem, a batch method was used when purifying *A. vinelandii* ferredoxin I. Although *A. vinelandii* and *P. putida* both are Gram negative bacteria, the

supernatant obtained directly from decantation in *P. putida* 7Fe ferredoxin purification was much clearer, a open column method was used during the purification.

A batch method was also used when a large amount of protein was purified for *P. putida* ferredoxin (for ferredoxin isolation from more than 1 kg cells in one purification cycle) and thus the purification could be faster.

For *A.vinelandii* ferredoxin I isolation, a batch method was generally used in this step. The settled DEAE-cellulose (Whatman DE-52), which was equilibrated with a 0.1 M Tris-HCl buffer and pH of 7.4, was added into the supernatant (0.3 mL DEAE-cellulose per g cell) from the centrifugation. The mixture was centrifuged at 2500 xg for 3 minutes. The cloudy supernatant was discarded. At the same time, the sedimentary DEAE-protein "slush" was suspended in a 0.05 M Tris-HCl, pH 7.4 buffer, and was recentrifuged as before. This procedure was repeated until the color of the supernatant became faintly yellow. Finally, this washed DEAE-protein slush was resuspended by a 0.05 M Tris-HCl, pH 7.4 buffer and poured into a 5 x 30 cm column. This column was then washed by a 0.05 M Tris-HCl, pH 7.4 buffer, until the column elution became clear. The DEAE-bound proteins, which include cyctochrome C, flavin and ferredoxins, were eluded with a 0.1 M Tris-HCl and 0.4 M NaCl buffer, pH 7.4. Once the brown ferredoxin containing band had reached the bottom of the column, the eluant was collected.

The brown fraction was dialysed overnight at 4 °C against 4.5 gal distilled water with about 200 mL of 0.1 M Tris-HCl, pH 7.17 (room temperature) buffer. A 6,000 - 8,000 molecular weight cutoff dialysis bag

(Spectrapor membrane tubing 1) was used. The dialysed protein was rechromatographed on the second DEAE-cellulose column.

For small amount of *P.putida* ferredoxin purification (isolated from below than 1 kg cells), an open column method was typically used. The supernatant from the first stage centrifugation was directly passed through a 5 x 15 cm DEAE-cellulose (Whatman DE-52) column, which was previously equilibrated with a 0.1 M Tris-HCl pH 7.4 buffer. The column was then washed by a 0.1 M Tris-HCl and 0.1 M NaCl pH 7.4 buffer until a clear eluate was reached. Ferredoxin remained bound to the top part of the cellulose column and was eluted by 0.4 M NaCl.

Ferredoxin-containing fractions, having a dark brown color, had a shoulder at 400 nm in a UV-VIS spectrum. They were combined and incubated with 50 mg each of DNase (Sigma Deoxyribonuclease I from Bovine Pancreas Type IV) and RNase (Sigma Ribonuclease A from Bovine Pancreas Type III-A), and 0.5 g of $CaCl_2$ (which was required for the activity of RNase). After overnight room temperature incubation, a centrifugation was used to remove all the precipitates. A high absorption peak around 260 nm was observed for the solution of the redissolved precipitate. The clear supernatant was diluted four-fold by using distilled water for the next DEAE-cellulose chromatography.

For both *A. veinlandii* ferredoxin I and *P.putida* ferredoxin isolations, ion exchange chromatography was repeated on a second DEAE-cellulose (Whatman DE-52) column (3x 25 cm). The proteins were eluted by using a linear concentration of NaCl gradient from 0.005 M to 0.4 M NaCl (500 mL each) in 0.1 M Tris-HCl buffer (pH 7.4). 7Fe ferredoxins were

eluted at 0.20 ~ 0.25 M NaCl. After this step, the 7Fe ferredoxin-containing fractions still contained nucleic acid and showed a high absorption peak around 260 nm in a UV-VIS spectrum.

3.2.3.Gel Filtration

In the ferredoxin eluted from the second DEAE-cellulose column, 50 mg each of DNase I (Sigma Deoxyribonuclease I from Bovine Pancreas Type IV) and RNase A (Sigma Ribonuclease A from Bovine Pancreas Type III-A), and 0.5 g $CaCl_2$ were added. The solution was incubated overnight at room temperature. A centrifugation might be required to remove any precipitates from the solution after the incubation. The ferredoxin was then concentrated by ultrafiltration (PM 5 membrane, Amicon) to 3 mL. The concentrated ferredoxin was further purified by passing it through a Sephadex G-75 (Pharmacia, Superfine) column (2.5 x 90 cm) with 0.1 M Tris-HCl pH 7.4 buffer containing 0.1 M NaCl.

The viscosity of solution could broaden the protein band on the gel filtration column, and decrease the resolution. In order to avoid this problem, as in the case of purification a large amount protein weighting more than 20 mg, the ferredoxin was prepurified by a DEAE-sephacel (Pharmacia) column (3 x 10 cm) before applying to a gel filtration column. The DEAE-sephacel column was step washed by 0.1 M NaCl, 0.15 M NaCl, 0.2 M NaCl and 0.25 M in 0.1 M Tris-HCl, pH of 7.4, buffers, until ferredoxin was eluted. Then the ferredoxin was concentrated by a Amicon ultrafiltration system to 3 mL and chromatographed on a G-75 gel filtration column.

After gel filtration, a DEAE-sephacel (Pharmacia) column (1.5 x 10 cm) was used to remove the last trace of impurity. The column was washed by 250 mL each of 0.1 M NaCl, 0.15 M NaCl and 0.2 M NaCl in 0.1 M Tris-HCl pH 7.4 buffer. The brown ferredoxin was eluted by 0.25 M NaCl in 0.1 M Tris-HCl buffer (pH 7.4) and then concentrated by using Amico ultrafiltration system to approximately 3ml and again applied to a G-75 column. The protein was eluted by 0.1 M NaCl in 0.1 M Tris-HCl buffer (pH 7.4).

The fractions with a ratio of A_{400}/A_{283} above 0.55 were combined. The ferredoxin was concentrated by using a Amicon ultrafiltration system with YM5 membrane to 1 mL and stored in liquid nitrogen for future works. Comparing the previously reported method, the yield of the ferredoxin was improved to about 20 ~ 25 mg per kg cell for both bacteria, the maximum yield was only 16 mg per kg of wet bacteria for the previously reported method (6), and reproducible during the research.

3.3 *Pseudomonas putida* Cystine Auxotroph Isolation

Two reasons, increasing isotopic labeling on cysteine of ferredoxin and decreasing the concentration of isotopic cystine in the medium, make it desirable to isolate a cystine auxotroph.

Radioactive labeling studies showed that *P.putida* would directly take cystine from media and integrate it into protein without degradation (see Chapter 4). Whereas no such activity was seen in *A.vinelandii* (10). So, *P.putida* was chosen as the precursor of the auxotroph. A chemically induced mutation was employed since it gave a high frequency of mutation and less revertant compared with radiation mutation. The mutagent was

methyl methanesulfonate (MMS, Aldrich). The overall procedure followed the method described by Calhoun and Feary (11) and Rudner (12).

An 18-hr stationary culture in a 30 mL cystine-free medium (see Table 3.2) was centrifuged. The pellet was washed, suspended, and then spun down by 30 mL of salt solution (normal medium without glucose) twice. The washed pellet was subsequently resuspended in 18 mL of salt solution, and 2 mL methyl methanesulfonate was added (0.05 M MMS). This mixture was incubated for 30 minutes at 30 °C. The treatment was terminated by centrifugation and washed twice with 30 mL salt solution. The pellet was resuspended in 30 mL medium supplemented with cystine (1 mM). After 18 hr incubation, the suspension was diluted by a factor of 2 x 10^{-5} (it gave about 100 colonies per plate) and plated on the surface of cystine-enriched media of Petri dishes. After 2 days growth at room temperature, colonies (presuming there were some auxotrophs) were replicated on a cystine-free medium by means of a multiple inoculation device. If a colony only grew on the cystine-enriched medium but not on the regular medium whose position corresponded to the location on the original plate (cystine-enriched), the colony was presumed to be auxotrophic. The mutant was isolated and further verified by comparing the bacteria growing on a cystine enriched medium with its growth on a normal cystine-free medium. Only one mutant was found from 40 dishes containing approximately 4,000 colonies.

3.4 Synthesis of Isotopic Labeled Cystine

3.4.1 D,L-[2,2'-^{2}H]-Cystine

D, L-[2,2'-^{2}H]-cystine was made using a modified procedure from

Wood and Du Vigneaud (13). A schematized diagram for the synthesis is illustrated in Figure 3.1.

3.4.1.1 Preparation of 2-^{2}H-S-Benzyl-D,L-Cysteine

A scrupulously dry, 2-L, one-necked, round-bottomed flask was equipped with a 100 cm reflux condenser, and a drying tube containing KOH pellets. In the flask, 50 g of S-benzyl-L-cysteine, 120 mL of D_2O (99.9 % deuterium), and 750 mL of acetic anhydride were placed. The mixture was gently heated under reflux in a heating mantle and shaken occasionally. When all the amino acid dissolved, the reaction vessel was continuously heated for an additional 3 minutes. During this period, gentle heating and great caution were essential to prevent violent boiling during the reflux. The yellow solution containing the dissolved amino acid was allowed to cool to ambient temperature. Any unreacted acetic anhydride was hydrolyzed by adding an additional 50 mL of D_2O. The solvent was removed with a rotary evaporator at 60 °C and the resulting cake-like white product was dissolved in 400 mL of 6N HCl. This mixture was further refluxed with gently boiling for 16 hours and then cooled to ambient temperature. Upon cooling, a coffee brown precipitate formed. The pH of the solution phase was raised to 6 with concentrated NH_4OH. After the solution stood overnight at 4 °C, the precipitate was collected by filtration with suction, and the product was washed with water and then cold ethanol. The ethanol wash continued until the precipitate became a creamish light brown color. The precipitate was finally dried with anhydrous ethyl ether and stored *in vacuo* over anhydrous $CaCl_2$ overnight at room temperature. A typical yield for this step was 85%.

The dried crude product from the prior step was purified by recrystal-

Figure 3.1 Schematized Diagram for the Synthesis of D,L-α,α'-^{2}H- Cystine

(Adapted from Martin R. Gluck Ph.D Dissertation (14)

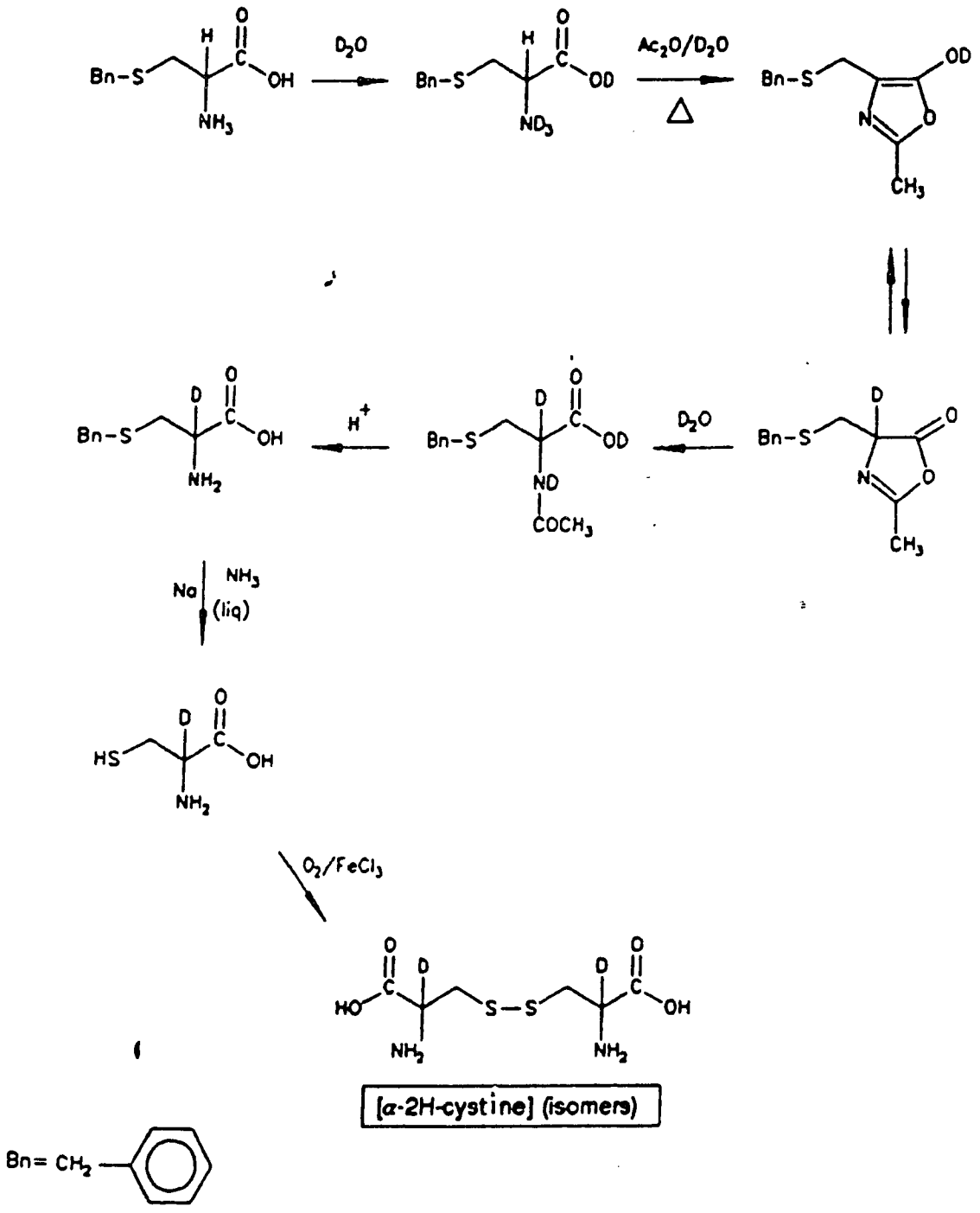
Bn-S
H
O
C
OH
NH3
D2O
OD
ND3
Ac2O/D2O
△
CH3
H+
D
NH2
ND
COCH3
Na
NH3
(liq)
HS
O2/FeCl3
HO
S—S
[α-2H-cystine] (isomers)
Bn= CH2

lization. With gentle heating, 49 g of the precipitate were added to 450 mL of 3N HCl. The solution was boiled with 1 g of Norite for about 5 minutes and then filtered through Whatman #2 filter paper by vacuum filtration. This step was repeated until the filtrate became nearly colorless. The clear solution was cooled to ambient temperature, and to the solution concentrated NH_4OH was added dropwise with a Pasteur pipet until significant precipitation was observed. The solution stood overnight at 4 °C for complete precipitation. The white crystals were collected by filtration with suction. The product was washed with ice water, 10% cold ethanol and finally diethyl ether. The crystals were dried *in vacuo* overnight over $CaCl_2$. Upon drying, colorless fluffy white crystals of 2-^{2}H-S-benzyl-D,L-cysteine appeared and 80% yield was afforded.

3.4.1.2 Debenzylation of 2-^{2}H-S-Benzyl-D,L-Cysteine

A dry, 1-L, three-necked, round-bottomed flask was equipped with a liquid air trap, a stirrer shaft, and a cork septum. In the large reservoir of the trap, acetone and dry ice were contained. Gaseous ammonia gas was introduced into the trap through the top jacket of the trap with an inlet. Condensed liquid ammonia was collected dropwise in the flask and cooled with an acetone ice bath. After about 700 mL of liquid ammonia was condensed, the flask was charged with 5 g of the 2-^{2}H-S-benzyl-D,L-cysteine. Strips of fresh sodium, cleaned by immersion in ethyl alcohol, were added to the ammonia until a dark blue color persisted. The reaction mixture was stirred to facilitate the dissolving of the amino acid. This sodium treatment was repeated when each 5 gram portion of amino acid was added. Before all of the reactant had been dissolved, enough sodium was added to maintain a constant blue color for about 5 minutes. Finally,

enough amino acid was added to remove the remaining blue color. The solvent was removed by evaporation at room temperature. The white residue was dissolved in 250 mL of ice/water mixture and transferred to a 500 mL separatory funnel, then extracted with three 200 mL portions of diethyl ether. The yellow aqueous layer containing 2-^{2}H-cysteine was heated in a water bath at 60 °C in order to remove any dissolved ether. The solution was then cooled to ambient temperature and the pH of the solution was adjusted to 10.5 by adding HCl or NaOH. Two drops of 10% (w/w) ferric chloride in water was added and the purple solution was gently bubbled with air for 48 hours after the color of the solution turned yellow. The pH was readjusted to 7.0 and the solution was allowed to precipitate overnight at 4 °C. The precipitate was filtered, washed with water and dissolved in a minimum amount of 1N HCl. The solution was decolorized with Norite as described before. A small amount of concentrated NH_4OH was added to the clear filtrate until an intense white precipitate was formed. The precipitate was left overnight at 4 °C, filtered, and then was washed first with distilled water followed by 10% (v/v) of ethanol in water. The crystals of D,L-[2,2'-^{2}H]-cystine were stored *in vacuo* over $CaCl_2$. The yield from this step varied from 50 to 70%. The ^{1}H NMR spectrum of this material showed about an 85% decrease in the intensity of the resonance corresponding to C_{α}H-cystine (Figure 3.2).

Higher labeling was observed (93%) if the S-benzyl-L-cysteine was pretreated with D_2O. This treatment was furnished by adding a small amount of clean sodium metal to a D_2O solution of S-benzyl-l-cysteine until the amino acid dissolved. Although this method led to a higher isotopic label, nearly 50% of the starting material was lost.

Figure 3.2 300 MHz ^{1}H NMR Spectrum of D,L-α,α'-^{2}H-Cystine in 6 N DCl/D_2O

Top: normal D,L-cystine

Bottom: α,α'-^{2}H-D,L-cystine

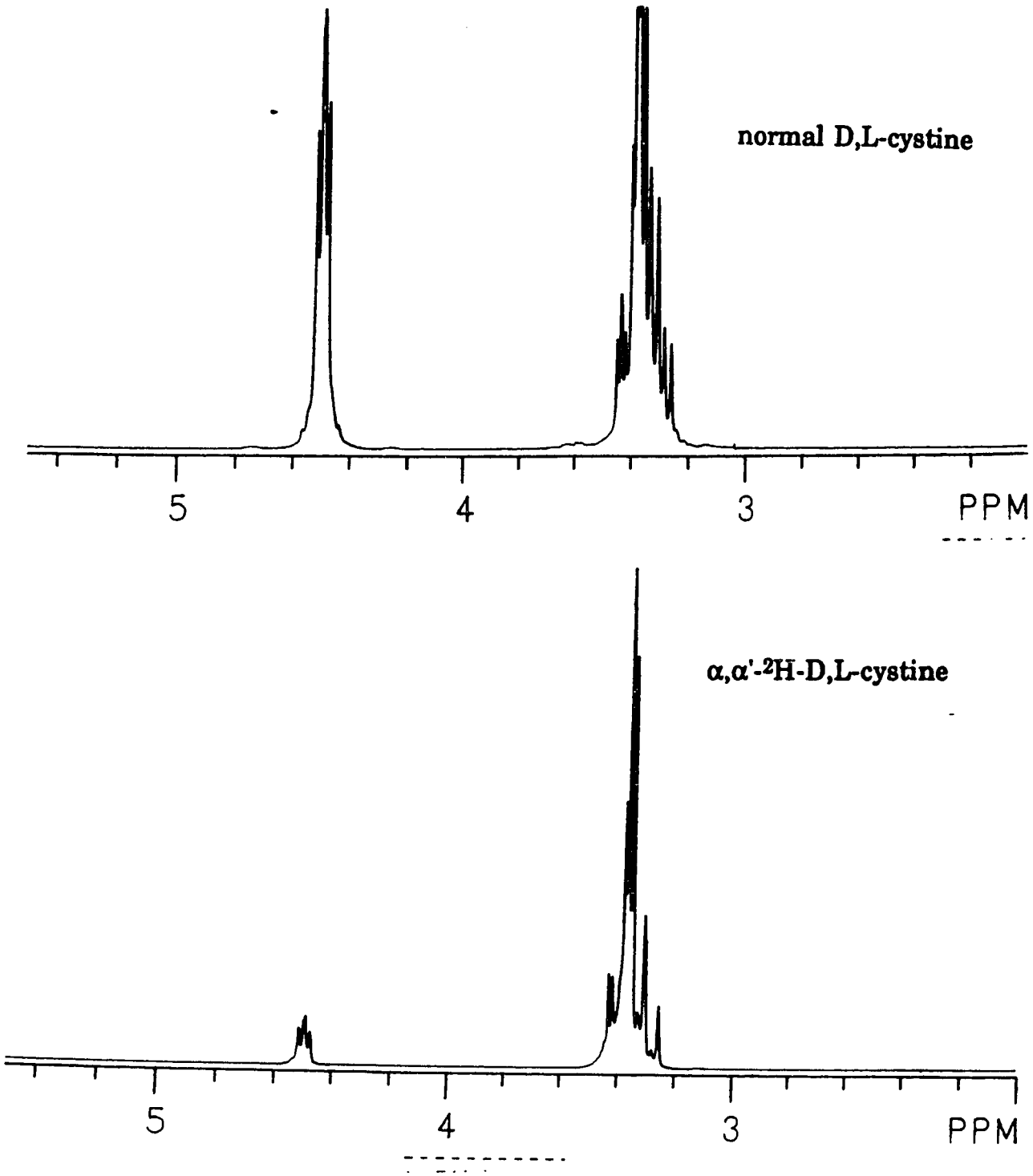
normal D,L-cystine
5
4
3
PPM
α,α'-²H-D,L-cystine
5
4
3
PPM

3.4.2 β-labeled Cystine Synthesis

D,L-[3,3'-^{2}H]-cystine and D,L-[3,3'-^{13}C]-cystine were prepared by Prof. Klaus Grohmann (Hunter College, Department of Chemistry) by the procedure of Wood and Du Vigneaud (13). The ^{1}H NMR spectrum of the synthesized D,L-[3,3'-^{2}H]-cystine is shown in Figure 3.3, and a 90% enrichment is indicated. Figure 3.4 is the ^{1}H NMR spectrum of the synthesized D,L-[3,3'-^{13}C]-cystine. The spectrum shows that two geminal β-cysteinyl proton resonances are splited about 150 Hz by β-cysteinyl carbon.

3.5 HPLC Amino Acid Analysis

3.5.1 Preparing of Cell Protein for HPLC

Two methods of cell protein preparation are commonly used in protein study (15). One is TCA (trichloroacetic acid) precipitation which entails directly adding 5% (w/v) trichloroacetic acid into the cell lysate to precipitate the cell protein. The another method is $(NH_4)_2SO_4$ precipitation. It involves first applying cell lysate to a DEAE-cellulose column. The DEAE-bound protein is then precipitated out from the eluate by 90% $(NH_4)_2SO_4$. In my experiment, a combined method was used to prepare cell protein because the presence of nucleic acids in the solution. This made the solvent exchange difficult in HPLC pre-column amino acid modification.

After growing two days, cells were harvested from 3 L of medium. Cell paste was dissolved in a 100 mL of 0.1 M Tris-HCl buffer, pH 7.4. To the solution 20 mg of lysozyme, 1 mg DNase, 0.1 mL Triton X-100 and 1 mL butanol were added. After incubating at room temperature for one hour with stirring, the solution was sonicated by a Sonifier cell disrupter (model W185 Heat System-Ultrasonics, Inc.) with full power for 3 minutes. The sonicated solution was centrifuged at 10,000xg for 15 minutes at a tempera-

Figure 3.3 300 MHz ^{1}H NMR Spectrum of D,L-β,β'-^{2}H-Cystine in 6 N DCl solution

Top: normal D,L-cystine

Bottom: β,β'-^{2}H-D,L-cystine

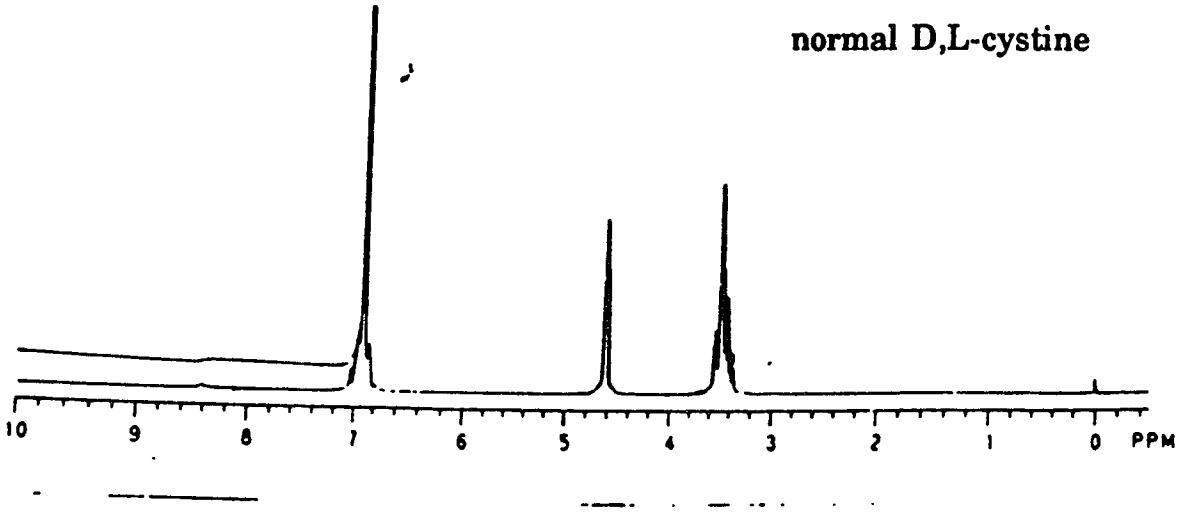
normal D,L-cystine
10
9
8
7
6
5
4
3
2
1
0
PPM

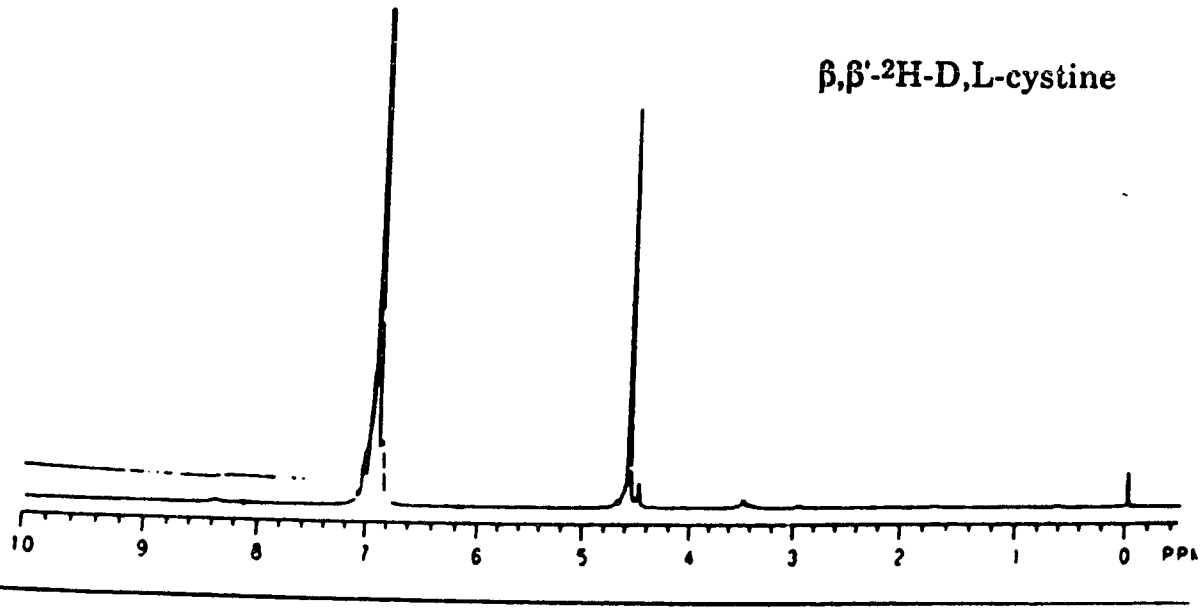
β,β'-²H-D,L-cystine
10
9
8
7
6
5
4
3
2
1
0

Figure 3.4 300 MHz ^{1}H NMR Spectrum of D,L-β,β'-^{13}C-Cystine in the Aliphatic Region

in DCl/D_2O (1:1 by volume)

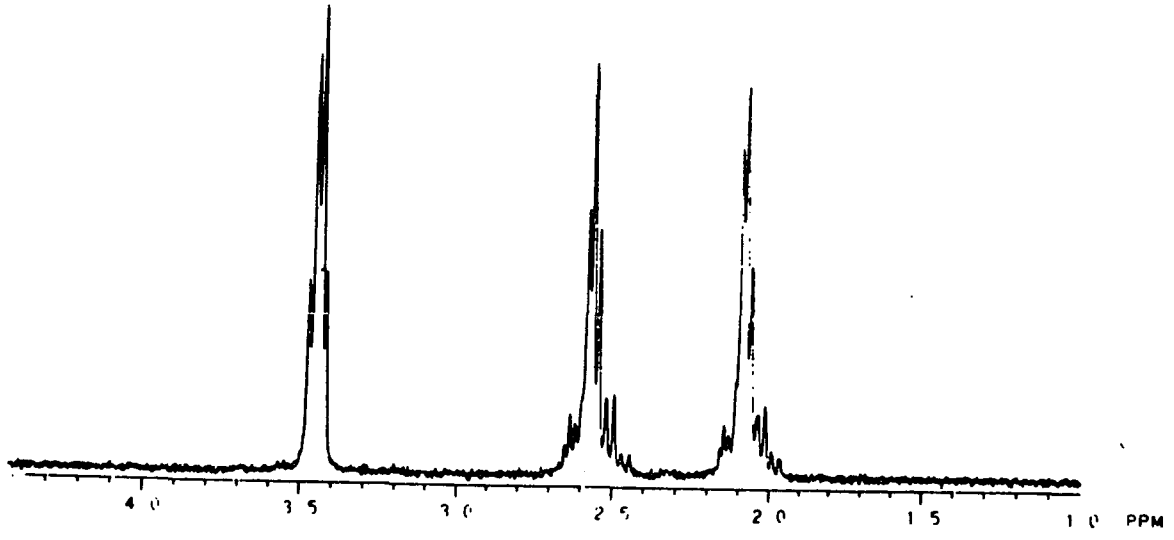
4 0
3 5
3 0
2 5
2 0
1 5
1 0
PPM

ture range of 0 ~ 4°C. The supernatant was applied to a DEAE-cellulose (Whatman DE-52) (2.5 x 10 cm) which was pre-equilibrated with the buffer. The protein band with a brown color was eluted with 0.4 M NaCl in 0.1 M Tris-HCl, pH 7.4, buffer and collected. To the protein solution 5 mg for each of DNase and RNase, and 0.5 g of $MgCl_2$ were added.

After overnight incubation at room temperature, the solution was centrifuged at 10,000xg for 15 minutes. Ammonium sulfate was added to the supernatant to 100% saturation. The precipitate was dissolved in 50 mL of water and dialysed against 20 L of water overnight using #3 Spectra/Por molecularporous membrane tubing (molecular weight cutoff 3,500).

After overnight dialysis, 2.5 g trichloroacetic acid (TCA) was added to the 50 mL dialysed solution to reach a final concentration of TCA of 5 % (w/v). The suspension stood in an icebath for one hour. The white precipitate formed was collected by centrifugation at 20,000xg for 1 hour. The precipitate was suspended in 50 mL of hot 5 % (w/v) trichloroacetic acid. Sonication was used to suspend all the precipitates. The solution was placed in a 90 °C hot water bath and incubated for 20 minutes to dissolve the nucleic acids. After 50 minutes of centrifugation at 20,000xg, the pellet was resuspended in 25 mL of 1.0 M Trizma base. All undissolved materials were removed from the solution by centrifugation at 4,000xg for about 15 minutes. The solution was dialysed twice against 20 L of distilled deionized water for 24 hours to remove all salt contained using a #3 Spectra/Por molecular porous membrane tubing (molecular weight cutoff about 3500). The solvent was then removed by lyophilization. The dry cell protein was stored in a vacuum desiccator ready for use. No significant nucleic acid contamination was found in the UV-visible spectrum of the cell protein (Figure 3.5). The ratio of A_{260}/A_{280} is 0.77 (this ratio is expected to be $\geq$ 1.7

Figure 3.5 UV-VIS Spectrum of *P.putida* Cell Protein

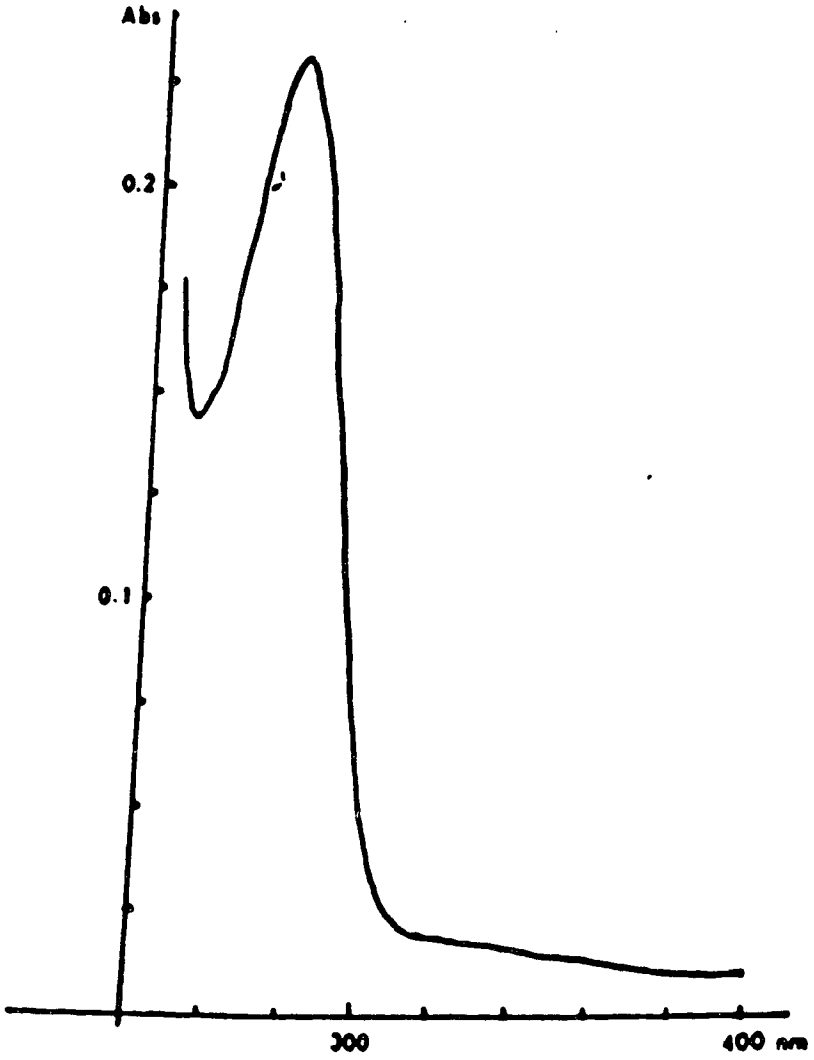
Abs
0.2
0.1
300
400 nm

for pure DNA and RNA).

3.5.2 Protein Hydrolysis

For protein hydrolysis, all the cysteines in a cell protein were first oxidized by performic acid as described by Hirs (16) and Moore (17).

The cell protein, isolated from cells grown in 3 L medium as described before, was dissolved in 2.5 mL of 88% formic acid (J & B Berge) and 2.5 mL performic acid. The performic acid was prepared by adding 1 mL of 30% H_2O_2 to 9 mL of 88% formic acid, letting the mixture stand for 1 hour at room temperature. After incubation at room temperature for 1 hour, the solution was diluted with 45 mL distilled water and subjected immediately to lyophilization.

A tube containing the dryed sample was then placed in a glass hydrolysis vessel containing 200 μL of constant boiling HCl (Pierce) and 1% phenol (Pierce). The entire vessel was incubated at 110°C for 24 hours. Any condensed HCl was further removed by a Savant "Speed-vac".

3.5.3 Free Amino Acids Pre-column Derivatization

Free amino acids were pre-column derivatized by reacting with phenylisothiocyanate (PITC) according to the procedure of Heinrikson and Meredith (18). The PTC amino acid derivatives formed from the reaction can remain stable for weeks, if keep them frozen in a neutral pH environment (18). The derivatives can be easily detected by UV absorption at 254 nm.

The procedure of derivatization followed the method developed by Stephen A. Bobin (Department of Biology, Hunter College). The hydrolyzed samples and amino acid controls (1 μmol amino acid) were first dissolved

in 1 mL of coupling buffer (ethanol (Pierce) : triethylamine (Pierce) : water; 15:2:3 by volume) and then dried down in a Savant "Speed-vac" speed evaporator. 0.5 mL of coupling buffer was then added to the cell protein, which isolated from cells grown in 3 L medium as described before, (0.1 mL for controls) followed by adding 20 μL of phenylthioisocyanate to cell protein (5 μL for each control). The reaction mixtures were allowed to stand for 3 hours at room temperature. After reaction, reagents were removed with a Savant "Speed-vac" speed evaporator. When the residues were dry, 0.5 mL of 20% acetonitrile (Fisher) was added to each of them. Samples were dried down again in a speed evaporator to remove any volatile side products and were then ready for HPLC amino acid analysis. The dry sample can be stored in a refrigerator for a short period. Before injecting into the HPLC column, the PTC derivatived dry samples were redissolved in a 0.5 mL mixture of 90% HPLC solvent A and 10 % HPLC solvent B (initial mobile phase composition).

3.5.4 HPLC Instrumentation and Method

Free amino acid separation was furnished with a HPLC system, composed of a Beckman Model 332 Gradient Liquent Chromatography system, a Beckman Model 420 Controller system, two Beckman Model 110A single-piston reciprocating pumps, a dynamically stirred gradient mixing chamber, a Model 210 sample injection valve, and a Beckman Model 163 variable wavelength detector with a 14 μL analytical flow cell. A 25 cm Phenomenex column packed with Ultres 5 micron C-18 material was used.

The two solvents were used for the mobile phases. Solvent A contained 0.415 M (34.02 g/L) sodium acetate (J.T. Baker) and 0.05 %

triethylamine (TEA), the pH was titrated to 6.08 with acetic acid, and solvent B
was a mixture of 60% acetonitrile and 40% water (HPLC grade).

A linear gradient (Table 3.3) was used to achieve separation. A 1 mL/min flow rate was used throughout and the temperature was controled at 38 °C.

3.6 NMR Instrumentation and Methods

3.6.1 NMR Spectra of Isotopic Labeled Cystine

All ^{1}H NMR or ^{13}C NMR spectra of isotopic labeled cystine were recorded on a GE QE-300 Fourier transform NMR spectrometer. 6 N DCl was used as solvent. For ^{1}H NMR, a 30° pulse was used, whereas a 45° pulse was used for ^{13}C NMR.

3.6.2 Preparation of Ferredoxin for NMR

Ferredoxin concentration and solvent exchange were performed using an Amicon ultrafiltration device with a YM5 or YM3 membrane under a nitrogen pressure of 40 psi. Generally, a 50 mM potassium phosphate D_2O buffer containing 50 mM sodium chloride, pD 7.4, was used. In the reduction with sodium borohydride, a 1 M potassium phosphate D_2O buffer, pD 7.4, was used. An internal standard of 5 μL of 1% DSS (sodium-2,2'-dimethyl-2-silapentane-5-sulphonate)(MSD) in $^{2}H_2O$ was added in pH and temperature dependent studies. For most experiments, the concentration of ferredoxin was about 1 mM. For 1D Overhauser experiments, six to seven millmolar ferredoxin was used, and samples were deoxygenated.

In the progressive reduction, 0.5 mL of 1 mM *P. putida* ferredoxin

Table 3.3 Program for HPLC Linear Gradient

time (min)	**%B**	**Duration** (min)
0.0	10	
0.1	25	2
2.1	100	30
32.1	100	5
37.1	9	10
47.1	9	13
60.1	alarm	0.1

was first reduced by 5 mg of solid sodium dithionite under fluxing of a nitrogen gas. The sample was then further reduced with 50 μL of 40 mM methyl viologen which was prereduced by acid-washed zinc under nitrogen. Finally, the partially reduced protein sample was reduced by adding 1 mg of solid sodium borohydride under fluxing nitrogen gas. The ^{1}H NMR spectra were recorded after every new reduction reagent was added. A 1 M phosphate buffer containing 50 mM with pH of 7.4 was used. The pD values were measured after each spectrum was recorded.

For the sodium dithionite and methyl viologen reduction experiment, 0.5 mL of 0.4 mM *P. putida* ferredoxin was partially reduced by a 50 μL mixture of 0.2 M sodium dithionite and 40 mM methyl viologen under fluxing of a nitrogen gas. The methyl viologen solution was prereduced by acid washed zinc. A 50 mM phosphate buffer containing 50 mM NaCl with pH of 7.4 was used.

In the reduction where methyl viologen was the only reductant, the sample was made by adding *A. vinelandii* ferredoxin I or *P. putida* ferredoxin into a nitrogen flushed vial which contained solid methyl viologen and acid washed zinc. When the color of the solution changed to deep blue, the reduced ferredoxin was transferred into a 0.5 mm o.d. NMR tube.

3.6.3 1D ^{1}H NMR Spectroscopy

The 1D ^{1}H NMR spectra of ferredoxins were recorded on a JEOL GX-400 Fourier transform NMR spectrometer. A 5 mm (o.d.) NMR tube containing 0.5 mL of solution was used. For most times, a 8 to 14 μsec pulse was used and 0.1 to 0.5 second delay time was employed. 16K to 64K data points per spectrum were used for 1D NMR. Adjustment of solution pH

was made by using solutions of DCl or NaOD in 99.9% D_2O. All pH values were measured on a pH meter (Radiometer Copenhagen pH Meter 26) which was calibrated by Fisher certified H_2O buffer solutions. Reported pH values for D_2O/NMR solutions were uncorrected for deuterium isotope effect and were reported as pD. For the pH titration and temperature dependence data, chemical shifts were referenced to 2,2-dimethyl-2-silapentane-5-sulfonate (DSS) at 0 parts per million (ppm). For all other spectra the HDO resonance was used for reference (4.78 ppm at 20°C). For titrations, pD values of samples were recorded both before and after acquiring NMR spectra with a Ingold combined glass electrode. The pK_a values for the titrations were obtained by fitting the appropriate data sets to an equation for a modified Henderson-Hasselbalch equilibrium:

$$\delta_{obs} = \frac{\delta_{HA} + \delta_{A^-} \times 10^{(pH - pK_a)}}{1 + 10^{(pH - pK_a)}} \qquad (3.1)$$

and Hill plot:

$$\log \frac{\delta_{A^-} - \delta_{obs}}{\delta_{obs} - \delta_{HA}} = - npK_a + npH \qquad (3.2)$$

where δ_{obs} is the observed chemical shift, δ_{HA} and δ_{A^-} are the chemical shifts for the protonated and unprotonated species respectively, and n is the Hill coefficient. One-dimentional spectra were recorded at a minimum of eleven pDs between pD 4 to pD 8. For temperature dependent studies, the temperature dependencies of the chemical shifts of contact shifted resonances were recorded by using one-dimensional spectra recorded at nine temperatures from 280K to 320K. The temperature values were corrected using a temperature calibration curve, a plot of thermometer readings in the probe vs. with the instrument setting values. The spin-

lattice (T_1) relaxation times were measured by using the inversion-recovery method at minimum 17 τ values from 0.1 to 100 ms. The pulse sequence is [PD - 180° - τ - 90° – AC]. PD is a pulse delay time, 90° and 180° represents magnetization rotation with rf pulses, τ is the evolution time, and AC is acquisition time. T_1s are calculated from fitting the intensity values to the equation:

$$M_z = M_0[1-2\exp(-\tau/T_1)] \qquad (3.3)$$

with two variables M_o and T_1. Here, M_o represents the macroscopic magnetic moment for a system at thermal equilibrium. It was taken to be proportional to the signal intensity at $\tau = 0$. Mz is the components of the macroscopic magnetic moment along the z axes. It was taken to be proportional to the signal intensity at time τ.

1D steady state saturation transfer NOE was performed with the pulse sequence [PD-T_i(selective saturation)-90°-AC], T_i representing the saturation time. For each irradiation frequency, 38,400 transients were acquired, cycling alternatively through several on-resonance frequencies and their controls in blocks of 128 scans. Difference spectra were obtained by subtracting the free induction decays of the on-resonance spectrum and the spectrum observed when the saturation pulse was symmetrically displaced from the chosen peak before Fourier transformation.

Spin diffusion was noted in the saturation pulses used for irradiation of peaks B, C, and E (see Figure 1.5). In order to minimize this, a minimum duration for the saturation pulse was estimated from the nuclear Overhauser effects between peaks A-B and C-E with three different irradiation times, 10, 30, and 50 ms (Table 3.4). The nuclear Overhauser effects between these peaks were saturated when a 30 msec saturation pulse was used. Therefore, a 30 msec saturation pulse was employed for all

Table 3.4 Nuclear Overhauser Effects with the Different Length of Irradiation Time

Duration Time (ms)	B* - A	C* - E	E* - C
10	- 8.3%	- 1.7%	- 1.4%
30	- 9.6%	- 2.1%	-2.0%
50	- 9.7%	- 2.2%	- 2.0%

a. With * is irradiated resonance, without * is nOe resonance.

b. The protein was *A. vinelandii* ferredoxin I. The data were recorded at temperature of 7 °C.

spectra. The interproton distances were calculated from the nuclear Overhauser effects using the formulas 2.10 and 2.11. A correlation time of 1.4×10^{-8} sec was used.

3.6.4 1D ^2H NMR Spectroscopy

^2H NMR spectra of the labeled ferredoxin and labeled cystine were recorded on a JEOL GX-400 Fourier transform NMR spectrometer. A 5 mm (o.d.) NMR tube containing 0.5 mL of solution was used.

3.6.5 2D ^1H NMR Spectroscopy

All 2D ^1H NMR spectra were recorded on the JEOL GX-400 spectrometer operating at 399.65 MHz, with a sample temperature of 20°C. All spectra were acquired in the phase-sensitive absorption mode with quadrature detection in both dimensions (19, 20). Generally, the carrier frequency was centered on the water signal, and a recycle delay of 0.5 sec was used in all spectra. The DQF-COSY spectra (21, 22), NOESY spectra (23) and TOCSY spectrum (also known as homonuclear Hartman-Hahn spectroscopy (HOHAHA)) (24, 25, 26) were recorded by the standard methods. A 150 ms mixing time was used for the NOESY spectrum. The spectral width was 6000 Hz in the acquisition period, t_2. All 2D spectra were collected in the following form: 1024 complex points in t_2, 384 complex FIDs in t_1, and 64 transients for each FID.

The SM-NOESY spectra were recorded by using a standard phase sensitive NOESY pulse sequence (23). A very short mixing time, 1 ms to 20 ms, was used. 1024 complex points were collected in t_2 for the each spectrum, 256 to 350 complex FIDs were recorded in t_1 with 384 transients for each FID. The spectral widths were from 15,000 to 16,000 Hz in the

acquisition period. A 12 μs deadtime (the time between the last 90° pulse and the beginning of FID accumulation) was used in order to achieve a flat baseline for the big spectral width used in the SM-NOESY experiment.

Processing 2D NMR data was done on a microVAX II computer using the program FTNMR (version 5.1) provided by Hare Research, INC.. Both time-domain data sets of each spectrum were multiplied by a 70° phase-shifted sine bell window function for D_2O-NOESY and TOCSY. A 70° phase-shifted skewed sine bell window function with a skew parameter of 0.6 for DQF-COSY. For SM-NOESY spectra, a cosine window function was applied in the t_2 time-domain, and a 70° phase-shifted sine bell window function was applied in t_1 time-domain. Zero filled to 1024 complex points along t_1 before transformation for all two dimensional spectra. The quadrature pairs of FIDs for the first t_1 value in all two dimensional spectra were multiplied by 0.5 after Fourier transformation along t_2 in order to reduce t_1 ridge artifacts (27). A polynomial baseline correction was applied to the NOESY, TOCSY and SM-NOESY spectra in both dimension. The baseline points were automatically selected by computer or manually selected.

3.6.6 1D ^{13}C NMR Spectroscopy

All 1D ^{13}C NMR spectra were recorded on the JEOL GX-400 spectrometer. It is operated at 100.4 MHz. A 90° pulse was used (around 20 μs). A 10 mm (o.d.) NMR tube containing about 2 mL of solution was used.

3.6.7 Proton Detected Heteronuclear Correlation NMR Spectroscopy

The proton detected HMQC was recorded on the JEOL GX-400 spectrometer with the standard pulse sequence (28, 29, 30, and 31). The

spectral widths were 14,300 Hz for the carbon dimension and 12,000 for the proton dimension. 2048 complex points were collected in t_2 for each spectrum, 96 complex FIDs were recorded in t_1 with 4,000 transients for each FID.

3.7 CD Instrumentation

All CD studies were performed with a ISA Auto-Dichrograph Mark V spectrometer and an Apple IIe computer was used for data processing. Spectra were recorded with a 0.5-nm step, and a time constant of 1 second. A pair of fluorescence cuvettes with 1 cm path-length was used. A total of eight scans was averaged for both sample and control. Solvent contributions were corrected by subtracting sample spectra with solvent spectra. The concentration of *P. putida* ferredoxin was measured by the visible absorption at 400 nm. The pHs were recorded before and after data recording.

3.8 Examination of the X-ray Structure

An Evans and Sutherland PS 390 system was used, employing the revised coordinates for *A. vinelandii* ferredoxin I deposited with the Brookhaven Protein Data Bank on 6/88. The reported interproton distances were obtained from these coordinates using the Dock software (version 5D) provided by the Fox Chase Cancer Center.

3.9 References

1. Ohmori, Daijiro (1976) *Biochem. and Biophys. Res. Commun.* **72** (No. 2), 566-574

2. Ohmori, Daijiro (1984) *Biochim. Biophys. Acta* **790**, 15-21

4. Yoch, D. C., Benneman, J. R., Valentine R. C., and Arnon, D. I. (1969) *Proc. Natl. Acad. Sci. USA* **64**, 1404-1410

5. Shethna, Y. I. (1970) *Biochim. Biophys. Acta* **205**, 58-62

6. Capetanaki, Semi (1979) Master Thesis, Hunter College, CUNY

7. Schwinghamer, E. A. (1980) *FEMS Microbio. Lett.* **7**, 157-162

8. Rossomand, Edward F. (1990) *Meth. Enzy.* **182**, 309-343

9. Buchanan, R. E. and Gibbons, N. E. (1974) "Bergey's Manual of Determinative Bacteriology", 8th Edison. The Williams & Wilkins Company, Baltimore

10. Malikayil, J. A. (1986) Ph.D dissertation, The City University of New York. New York

11. Calhoun, D. H. and Feary, T. W. (1969) *J. Bacteriol.* **97**, 210-216

12. Rudner, R. (1981) *Mutation Res.* **83**, 339-347

13. Wood, J. L., and Du Vigneaud, V. (1939) *J. Biol. Chem.* **131**, 267-274

14. Gluck, M. R. (1989) Ph.D dissertation, The City University of New York, New York

15. Packer, E. L. (1974) Ph.D dissertation, University of california, Berkeley. Berkeley, California

16. Hirs, C. H. W., *Meth. Enz.* **11**, 197-199

17 Moore, S. (1962) *J. Biol. Chem.* **238**, 235-237

18. Heinrikso, R. L. and Meredith, C. S. (1984) *Anal. Biochem.* **136**, 65-74

19. Müeller, L., and Ernst, R. R. (1979) *Mol. Phys.* **38**, 963-992

20. States, D. J., Harberkorn, R. A., and Reuben, D. J. (1982) *J. Magn. Reson.* **48**, 286-292

21. Piantini, U., Sorensen, O. W., and Ernst, R. R. (1982) *J. Am. Chem. Soc.* **104**, 6800-6801

22. Shaka, A. J., and Freeman, R. (1983) *J. Magn. Reson.* **51**, 169-173

23. Macura, S., and Ernst, R. R. (1980) *Mol. Phys.* **41**, 95-117

24. Braunschweiler, L. and Ernst, R. R. (1983) *J. Magn. Reson.* **53**, 521-528

25. Bax, A., and Davis, D. G. (1985) *J. Magn. Reson.* **63**, 207-213

26. Bax, A., and Davis, D. G. (1985) *J. Magn. Reson.* **65**, 355-360

27. Otting, G., Widmer, H., Wagner, G., and Wüthrich, K. (1986) *J. Magn. Reson.* **66**, 187-193

28. Müller, L. (1979) *J. Am. Chem. Soc.* **101**, 4481-4484

29. Bax, A., Griffey, R. H., and Hawkins, B. L. (1983) *J. Am. Chem. Soc.* **105**, 7188-7190

30. Bax, A., Griffey, R. H., and Hawkins, B. L. (1983) *J. Magn. Reson.* **55**. 301-315

31. Bendall, M. R., Pegg, D. T., and Doddrell, D. M. (1983) *J. Magn. Reson.* **52**, 81-117

CHAPTER 4

BACTERIA CYSTINE INCORPORATION STUDY

4.1 Radioactive ^{14}C-Cystine Labeling Studies

P. putida cystine uptake from its growth medium was first studied by radioactive labeling. *P. putida* ferredoxins isolated from cells grown in the presence of 10 μCi radioactive (1-^{14}C)-d,l-cystine (Research Products International (rpi), specific activity: 97 mCi/mol) and varied concentrations of non-radioactive cystine (1 mM, 0.5 mM, and 0.2 mM cystine) were isolated. The radioactivity of 1 mL bacteria's media (at the beginning time of each incubation) and 1 mL pure ferredoxins after isolation was counted by a scintillation counter (Beckman LS 6800) on a 10 minute counting scale. The concentration of protein was determined by visible absorbances at 400 nm. Their radioactive labeling percentages were calculated. All ferredoxins isolated from the cells grown in the presence of radioactive cystine were radioactive. The results are shown in Table 4.1.

The results indicated that the *P. putida* ferredoxin isolated from cells grown in the presence of radioactive ^{14}C-d,l-cystine was radioactive labeled. The highest labeling of cystine, 93.3%, was obtained from the ferredoxin isolated from bacteria grown on the medium containing 1 mM radioactive D,L-cystine. If the concentration of D,L-cystine of medium decreased to 0.2 M, the percentage of radioactive labeling of ferredoxin dropped to 29.0%.

Table 4.1 ^{14}C-Cystine Incorporation In *P.putida* Fd

Conc. of Cys	Description	% Labeling
1.0 mM	6 g of d,l-cystine/50 L	93.3%
0.5 mM	6 g of d,l-cystine/100 L	88.7%
0.2 mM	2.4 g of d,l-cystine/100 L	29.0%

4.2 HPLC-Amino Acid Labeling Distribution Studies

It was seen that the ferredoxin isolated from *P. putida* bacteria grown in the presence of radioactive cystine was radioactive. The radioactive labeling site was further examined by using HPLC amino acid labeling distribution analysis.

A radioactive cell protein and a nonradioactive cell protein were separately isolated as previously described (Chapter 2.5.1) from *P.putida* grown in a 3 L of radioactive cystine medium (containing 10 μCi of ^{14}-D,L-cystine and 0.36 g D,L-cystine) and 3 L of normal nonradioactive cystine medium (containing 0.36 g D,L-cystine in normal medium). After isolation, 0.1 μCi D,L-[1-^{14}C]-cystine was added into the nonradioactive TCA perceptible cell protein as a control sample. Cell proteins were hydrolyzed and their free amino acids were precolumn PTC-derivatized as described in Chapter Three (3.5.2 and 3.5.3). Other control samples were also made. They included commercial cysteic acid (Sigma), cystine (Sigma), cysteine (Sigma), alanine (Sigma) and standard amino acid mixture (Pierce). The commercial cystine was first oxidized to cysteic acid by performic acid as described before. Amino acid separations were performed by HPLC, as described in Chapter 3. Free amino acid elution profiles were determined by absorbance at 254 nm. The radioactivities of amino acid elution profiles for the cell protein samples were detected by scintillation counting. The eluate of cell protein samples from HPLC amino acid separations were directly collected into liquid scintillation vials manually at 15 second intervals. 10 mL of scintillation cocktail (ScintiVerse I, Fisher) was added into each vial and 1 minute counts was taken by using a Beckman scintillation counter (LS 6800).

Figure 4.1 shows the HPLC chromatogram of standard free amino acids. Under conditions used, cysteic acid had a 4.4 minute retention time on the HPLC chromatogram (Figure 4.2). Figure 4.3 shows the HPLC chromatogram of *P. putida* cell protein. The radioactive distributions were compared between radioactive cell protein (Figure 4.4) and its control (nonradioactive cell protein and 0.1 μCi of ^{14}C-d,l-cystine) (Figure 4.4). Both chromatograms of the radioactive cell protein and the noradioactive cell protein with radioactive cystine showed a major radioactive peak with a time scale of about 5 minutes. For radioactive cell protein, about 70% radioactivity of the the injected sample was recovered in the fractions correspond to this peak. A minor peak contained approximately 18% radioactivity of the injected sample was also observed, but its retention time (about 9.65 minute after correction) did not coincide with any of the standard free amino acids. Therefore, the cysteine is the major labeled amino acid in the cell protein isolated from cells grown in the presence of ^{14}C-d,l-cystine.

4.3 Deuterium NMR of α,α'-^{2}H-Cysteine Labeled Ferredoxin

5 mg α-^{2}H-cysteine labeled ferredoxin was isolated from *P. putida* grown on the medium containing 6 g of α,α'-^{2}H-D,L-cystine. The labeled ferredoxin was concentrated to about 1 mL and then oxidized with 30 mL of performic acid. Performic acid was prepared by mixing 9 volumes of 88% formic acid with 1 volume of 30% hydrogen peroxide. The solution was allowed to stand at room temperature for 1 hour and then cooled to 4°C for use. The reaction mixture of cell protein with performic acid was stood at 4°C for 4 hours with cover. After incubation, 2 mL of 48% HBr was added into the mixture with swirling to destroy the excess performic acid. Most of

Figure 4.1 HPLC Chromatogram of Standard Free Amino Acids

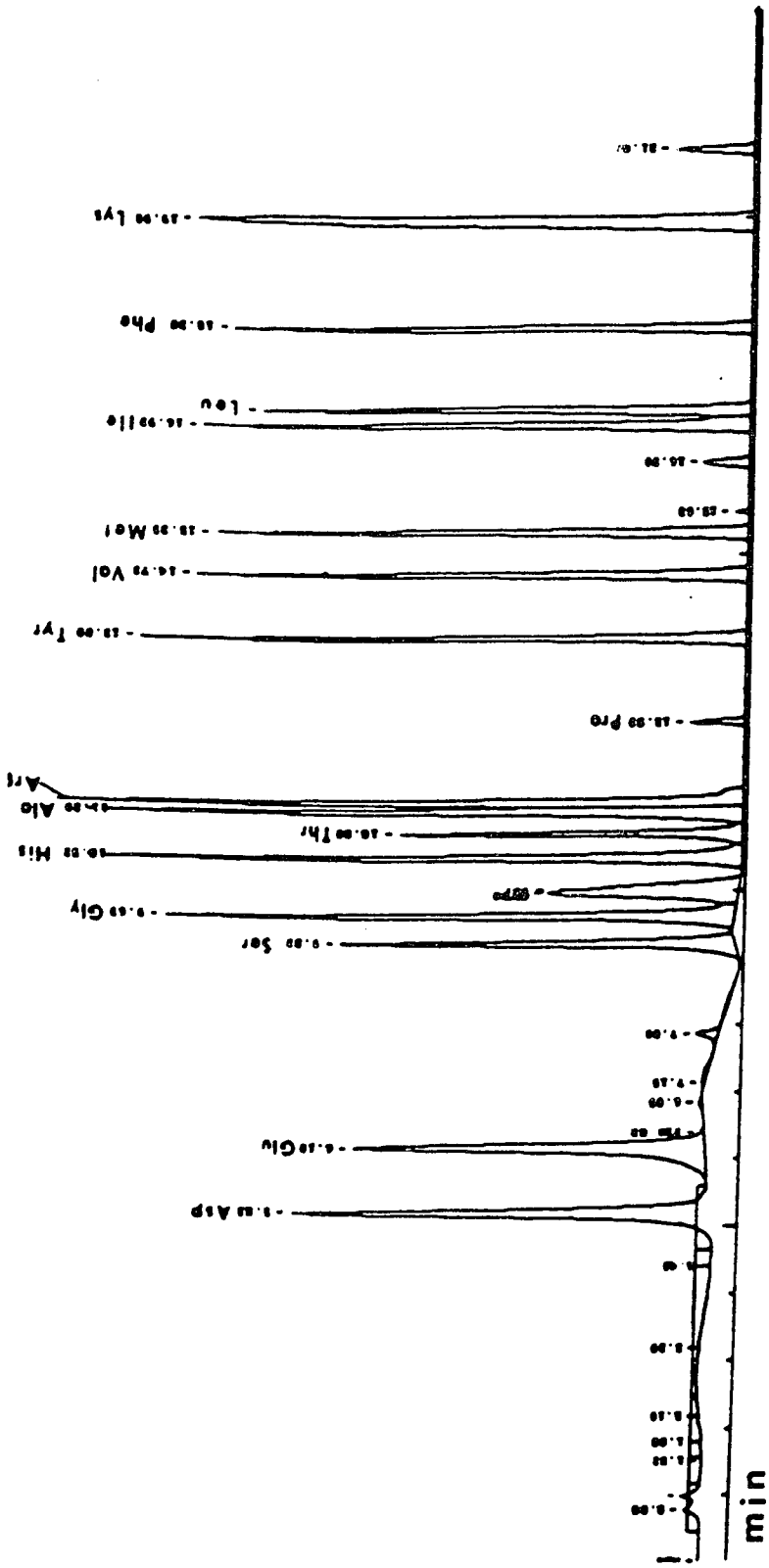
min

Figure 4.2 HPLC Chromatogram of Cysteic Acid

min
ASP
GLU
SER
GLY
ASN
ALA
TYR
VAL
ILE
PHE
LYS

Figure 4.3 HPLC Chromatogram of *P.putida* Cell Protein

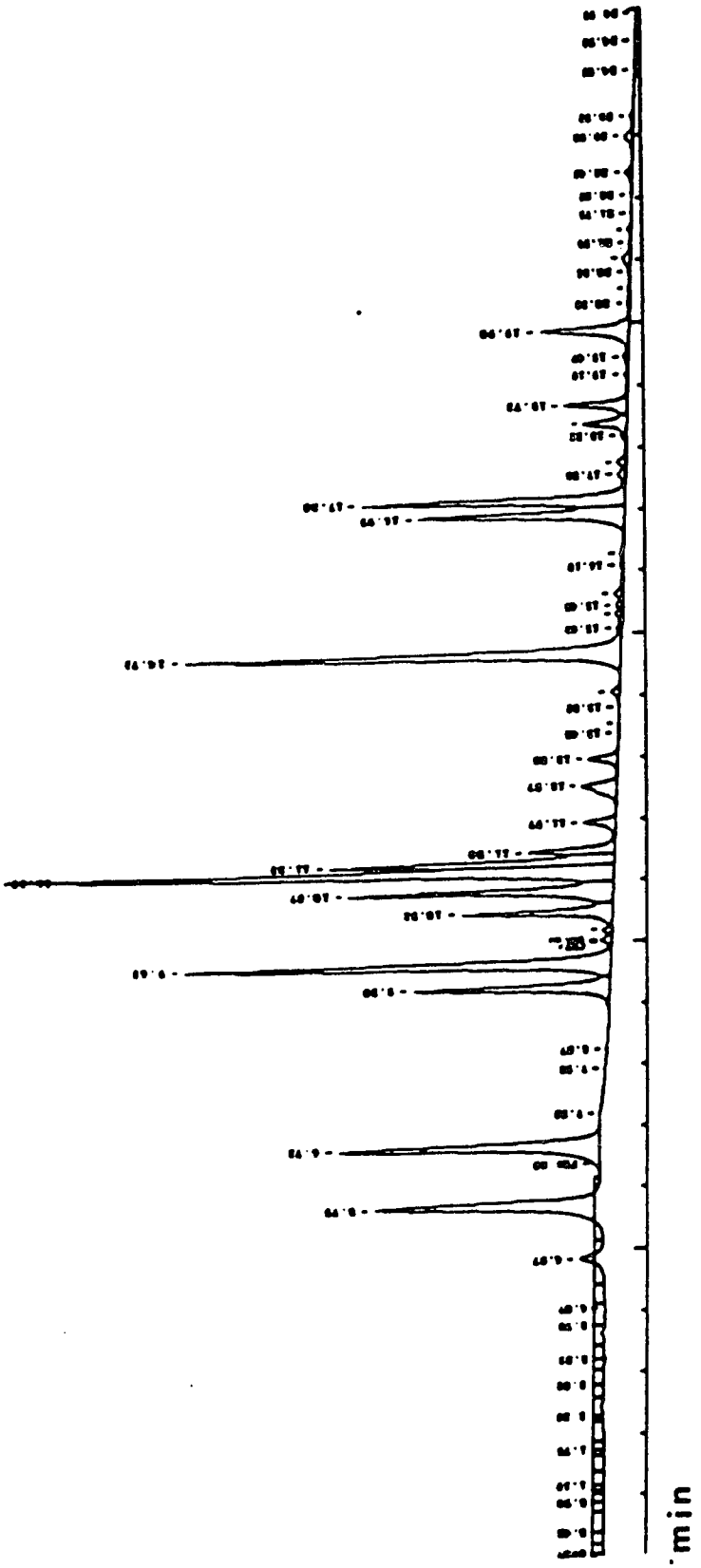
min

Figure 4.4 Radioactive Distribution of HPLC Elution Profiles

Top: 0.1 μCi radioactive of 1-^{14}C-cystine combined with nonradioactive normal cell protein

Bottom: radioactive cell protein isolated from the cells grown in the presence of radioactive cystine

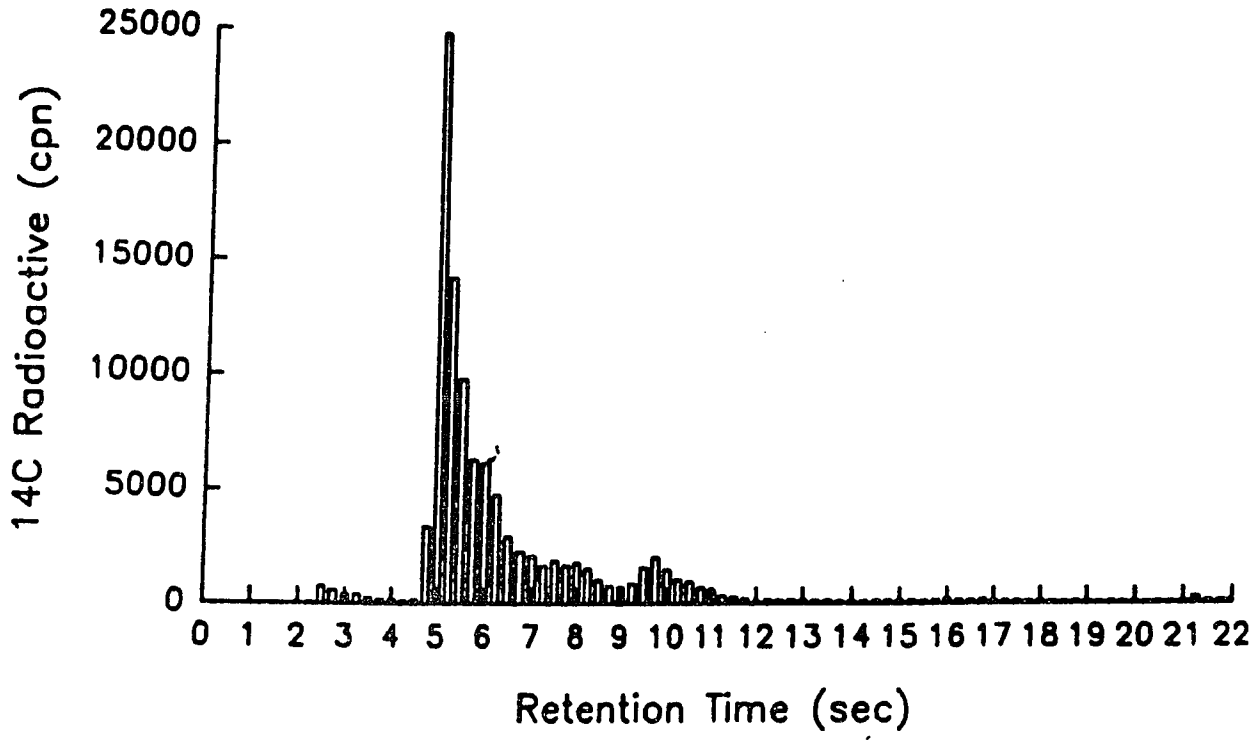
25000
20000
15000
10000
5000
0
14C Radioactive (cpn)
0 1 2 3 4 5 6 7 8 9 10 11 12 13 14 15 16 17 18 19 20 21 22
Retention Time (sec)

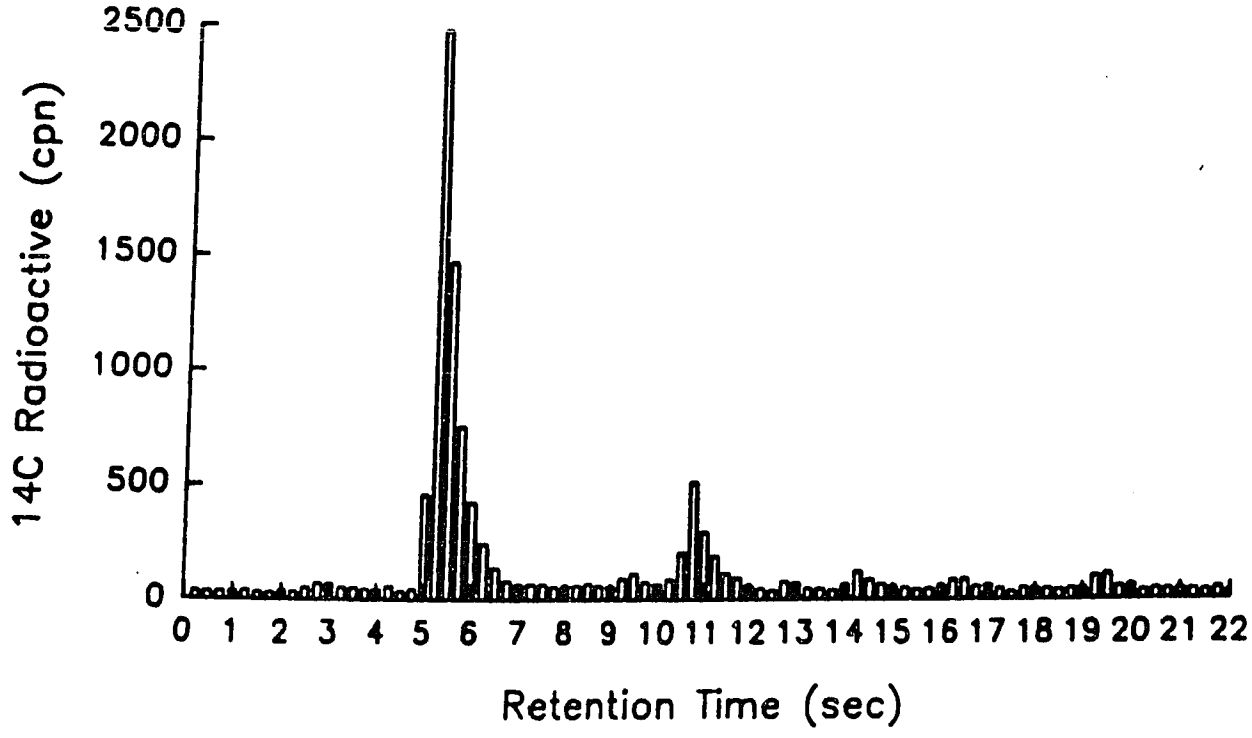
2500
2000
1500
1000
500
0
14C Radioactive (cpn)
0 1 2 3 4 5 6 7 8 9 10 11 12 13 14 15 16 17 18 19 20 21 22
Retention Time (sec)

the solvent was then removed by rotary evaporation at 45°C.

The residue of about 1 mL solution was transferred into a borosilicate test tube. The sample was dried completely by lyophilization. 0.6 mL of 6 N HCl was added to the residue. The tube was sealed under a gentle flow of nitrogen gas and incubated at 110 °C for 24 hours. After hydrolysis, the solution was directly transferred to a 5 mm (o.d.) NMR tube.

A 0.6 mg of α,α'-^{2}H-D,L-cystine was used as a control. It underwent both treatments of performic acid oxidized and hydrolysis as described for the labeled ferredoxin.

Only two peaks (6.5 ppm and 4.5 ppm) were observed in the ^{2}H NMR spectrum of α-^{2}H-cysteine labeled ferredoxin (Figure 4.5), and in the spectrum of oxidized and hydrolyzed α,α'-^{2}H-cystine (Figure 4.5). Comparison with ^{1}H NMR spectrum of commercial cysteic acid (Sigma) (Figure 4.6) shows that the peak at 4.5 ppm belongs to α-^{2}H of cysteic acid, and the peak around 6.5 ppm is contributed from the natural abundance of HDO. Inconjunction with the previous results from radioactive labeling and HPLC amino acid analysis, the result from this experiment showes that *P. putida* ferredoxin isolated from cells grown in the presence of α,α'-^{2}H-cystine is deuterium labeled on the appropriate position, α-cysteinyl position.

4.4 Cystine Auxotrophic Mutant

The cystine uptake of a *P. putida* cystine auxotroph was studied by growing cells in the presence of different cystine concentrations. First, a single colony of the mutant was inoculated in a 125 mL Erylenmeyer flask containing 30 mL of cystine enriched (0.5 mM L-cystine) medium as a cell

Figure 4.5 ^{2}H NMR Spectra of Performic Acid Oxidized and Hydrolyzed α-^{2}H-cysteine Labeled *P. Putida* Ferredoxin and Its Control in 6N HCl

Top: Performic Acid Oxidized and Hydrolyzed α-^{2}H-cysteine Labeled *P. Putida* Ferredoxin

Bottom: Performic Acid Oxidized and Hydrolyzed α,α'-^{2}H-Cystine

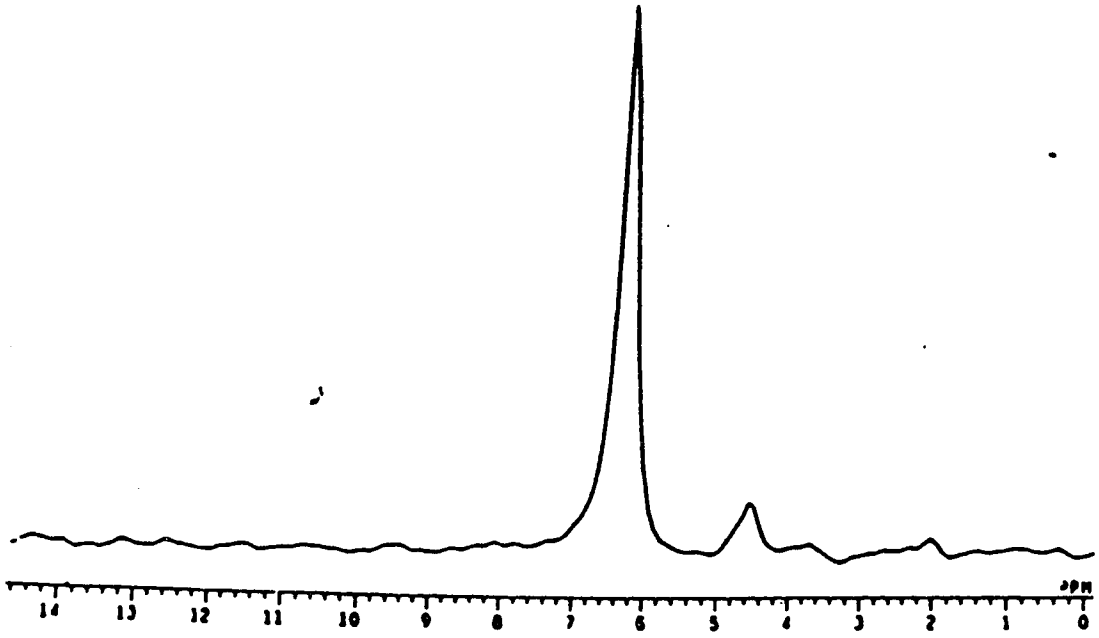
PPM
14 13 12 11 10 9 8 7 6 5 4 3 2 1 0

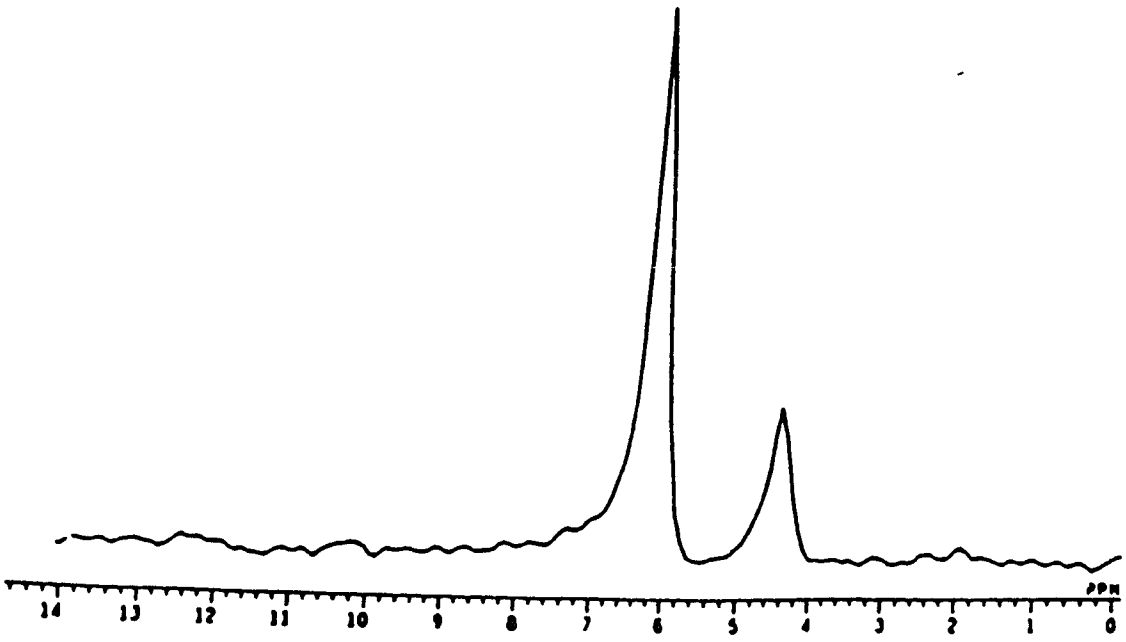
PPM
14 13 12 11 10 9 8 7 6 5 4 3 2 1 0

Figure 4.6 300 MHz ^{1}H NMR Spectrum of Commercial Cysteic Acid

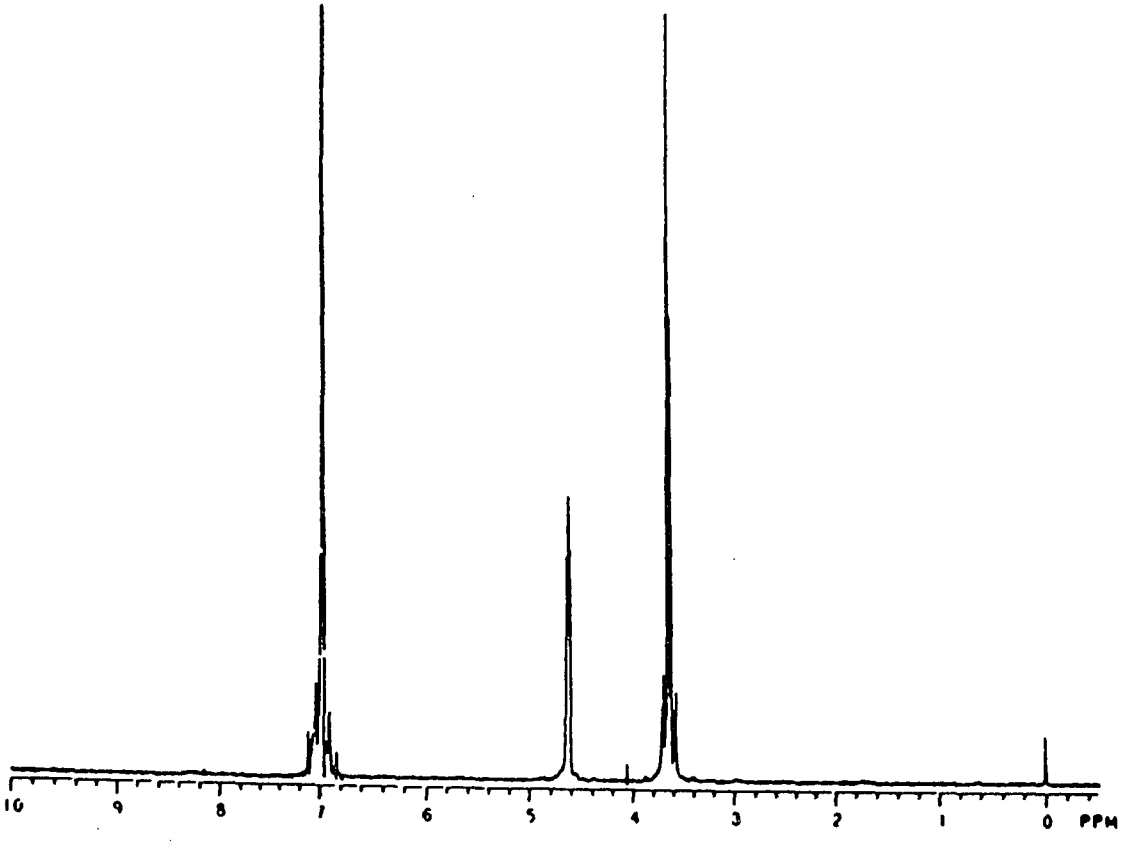
10
9
8
7
6
5
4
3
2
1
0
PPM

source. After overnight incubation with shaking, 100 μL of overnight grown bacteria were transferred into each of sixteen 125 mL Erylenmeyer flasks which contained 30 mL of medium and different concentrations of cystine. Varying concentrations of cystine were made by mixing cystine-free medium and cystine contained medium (0.5 mM cystine) in different volume ratios. Bacterial growth in each concentration of cystine was tested. After another overnight growth, the numbers of cells in each flask were determined by Klett turbidity and absorbances at 600 nm. The result is shown in Table 4.2. Figure 4.7 shows the curve of Klett turbidometric readings versus varying concentrations of cystine.

NMR spectrum of ferredoxin isolated from auxotroph cells grown in the presence of β,β'-^{2}H-cystine (0.17 mM) was also recorded (see Chapter 5). The intensities of the five most downfield resonances were diminished (about 50%), with respect to the overall aromatic ring-proton region.

In theory, the cysteines in ferredoxin isolated from the cystine auxotroph cells grown in the presence of deuterium labeled cystine should be 100% labeled. The reason for only 50% labeling is still not known.

4.5 Comparison of Cystine Uptake by *A. vinelandii* and *P. putida*

The results from radioactive cystine labeling study, HPLC amino acid analysis, and deuterium NMR spectroscopy study clearly demonstrate that *P. putida* bacterium can uptake cystine and integrate it into ferredoxin. This has been further proved by later ^{1}H and ^{13}C NMR data. The intensities of the resonances which arose from the isotopic labeled nuclei were diminished in the NMR spectra of ferredoxins isolated from the cells grown in the presence of isotopic cystine (see Chapter 5).

Table 4.2 Auxotrophic Mutant Growth at Varied Concentration of Cystine

0.5 mM Cystine	0 mM Cystine	Conc. of L-Cystine	Average Abs_{600}	Average Klett
0.0 mL	30.0 mL	0 mM	0.077	35
1.2 mL	28.8 mL	0.01 mM	0.390	128
2.4 mL	27.6 mL	0.02 mM	0.636	200
3.6 mL	26.4 mL	0.03 mM	0.994	312
4.8 mL	25.2 mL	0.04 mM	1.402	500
6.0 mL	24.0 mL	0.05 mM	1.498	650
18.0 mL	12.0 mL	0.15 mM	1.469	820
30.0 mL	0.0 mL	0.25 mM	1.440	570

Figure 4.7 Growth Curve of *P. putida* Cystine Auxotrophic Mutant with Different Concentrations of Cystine

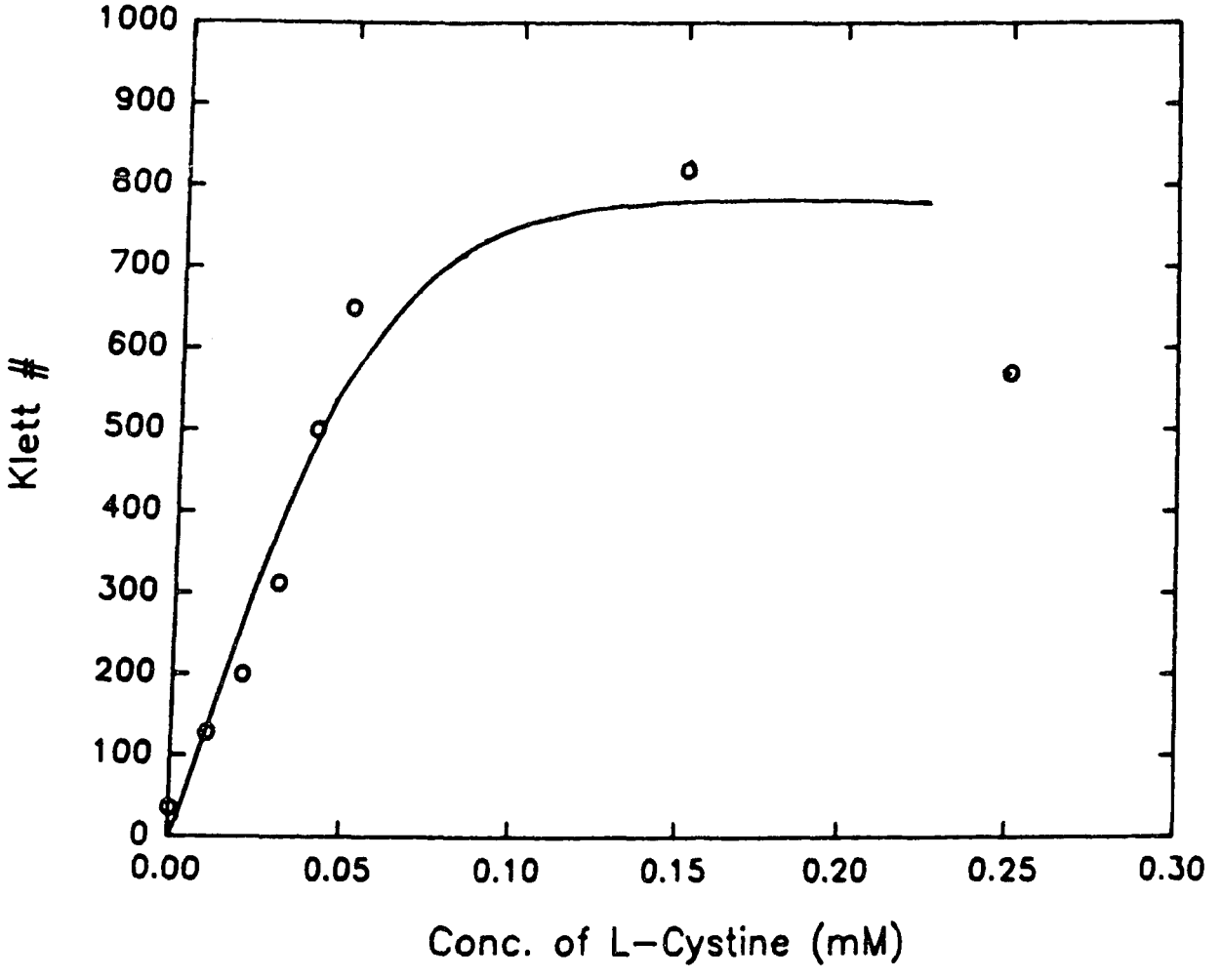
1000
900
800
700
600
500
400
300
200
100
0
Klett #
0.00
0.05
0.10
0.15
0.20
0.25
0.30
Conc. of L-Cystine (mM)

However, *A. vinelandii* only uptakes cystine from its growth medium but does not integrate it into ferredoxin. No radioactivity was found in the ferredoxin I isolated from the *A. vinelandii* cells grown in the presence of radioactive cystine. In the HPLC examination of radioactivity cell protein, only 3.9% radioactivity was recovered from the input radioactive cell protein (1). Furthermore, no differences were found between the NMR spectra of isotopic cystine "labeled" *A. vinelandii* ferredoxin I and the spectra of native unlabeled ferredoxin. Therefore, *P. putida* was used in labeling studies. However, *A. vinelandii* ferredoxin I is the only 7Fe ferredoxin that its structure has been reported by X-ray crystallography. Thus *A. vinelandii* ferredoxin I was used for the NOE experiments.

The pathway of cystine utilization is different for these two bacteria, *A. vinelandii* and *P. putida*. *P. putida* can uptake cystine from its growth medium, transfer it into the cell and then integrate it into protein. In contrast to this, *A. vinelandii* can not. No publications have discussed cystine uptake differences between these two bacteria.

4.6 References

(1). Malikayil, J. A. (1986) Ph.D Dissertation, City University of New York, New York

CHAPTER 5

NMR SPECTROSCOPY

5.1 Cysteinyl Proton Resonances Assignments

5.1.1 Deuteration, pH and Temperature Studies

Figure 5.1 is the ^1H NMR spectrum of native *P. putida* ferredoxin in the isolated form at 23 °C. Six isolated most downfield resonances (A-F) were visible, lying near 31.0, 25.8, 17.6, 15.7, and 10.5 ppm. The integrated intensities of the five most downfield peaks were approximately the same. Searching from +200 to -50 ppm, no new resonances were found. The temperature dependencies of these resonances are shown in Figure 5.2. Resonances A and B exhibited Curie dependencies, while C, D, and E displayed anti-Curie dependencies. Peak F was not a single resonance. It splits into two peaks with similar intensities, F' and F", when the temperature was either over 30 °C or below 15 °C (Figure 5.3). Resonance F' was Curie temperature dependent, while resonance F" exhibited anti-Curie dependence. The spin-lattice relaxation times, T_1s, of these resonances are very about 1.4 ~ 10.6 ms in these two 7Fe ferredoxins (Table 5.1). Specially, the spin-lattice relaxation time, T_1, of peak B was only 1.4 ms in *P. putida* ferredoxin and 1.6 ms in *A. vinelandii* ferredoxin I (Table 5.1).

The downfield region of the NMR spectrum of *P. putida* ferredoxin isolated from cells grown in the presence of 0.5 mM D,L-[3,3'-^2H]-cystine is shown in Figure 5.4. The five most downfield resonances, A-E, exhibited only about 30% of the intensity of the equivalent resonances in the spectrum of native ferredoxin. This is more easily seen in the difference spectrum

Figure 5.1 400 MHz ^{1}H NMR Spectrum of the Isolated Form of *P. putida* Ferredoxin

0.5 mM of protein is dissolved in a 50 mM Tris-DCl buffer containing 50 mM NaCl with a pH of 7.4

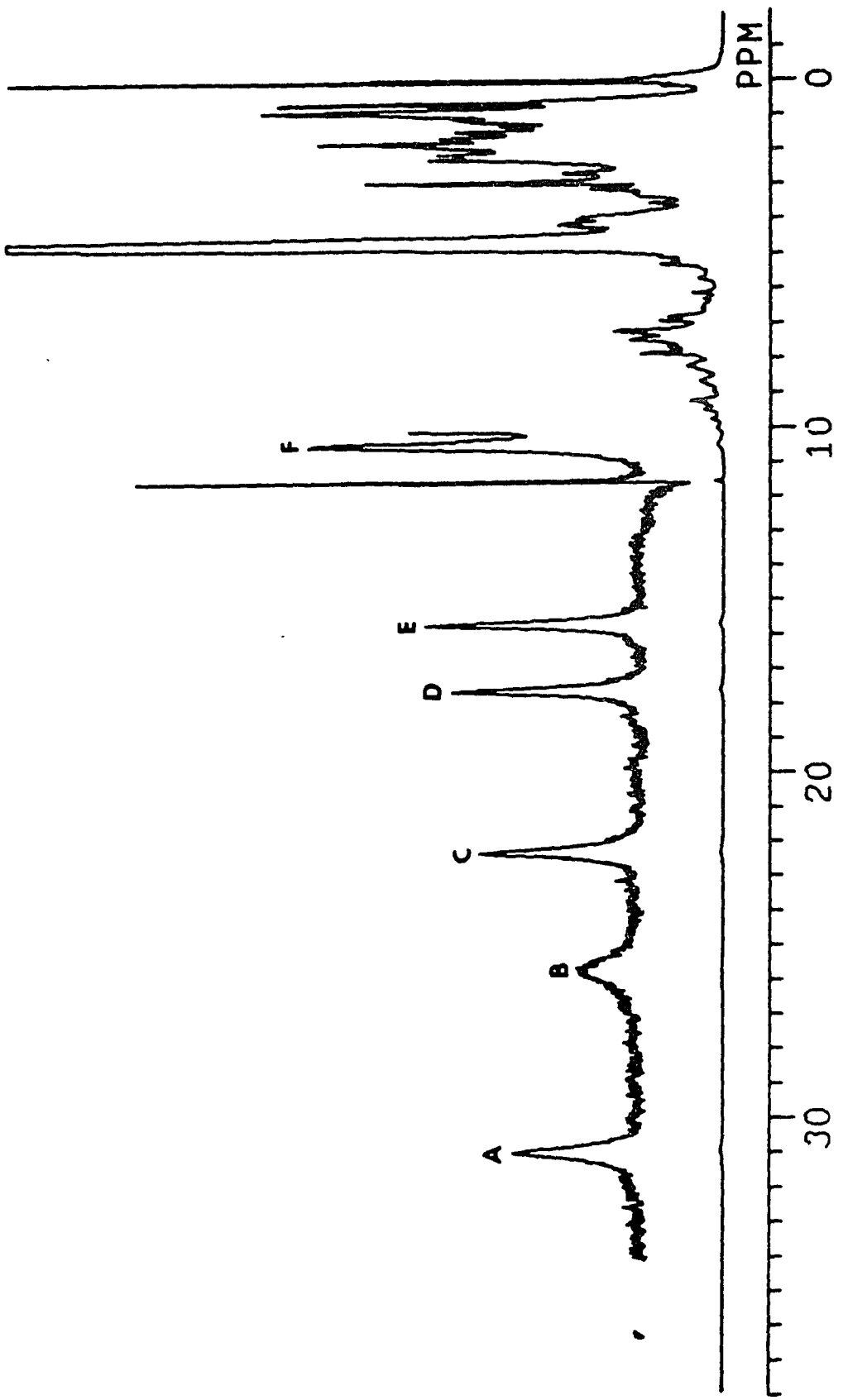
PPM
0
10
20
30
A
B
C
D
E
F

Figure 5.2 Temperature Dependences of the Most Downfield Resonances in ^{1}H NMR Spectrum of the Isolated Form of *P.putida* Ferredoxin

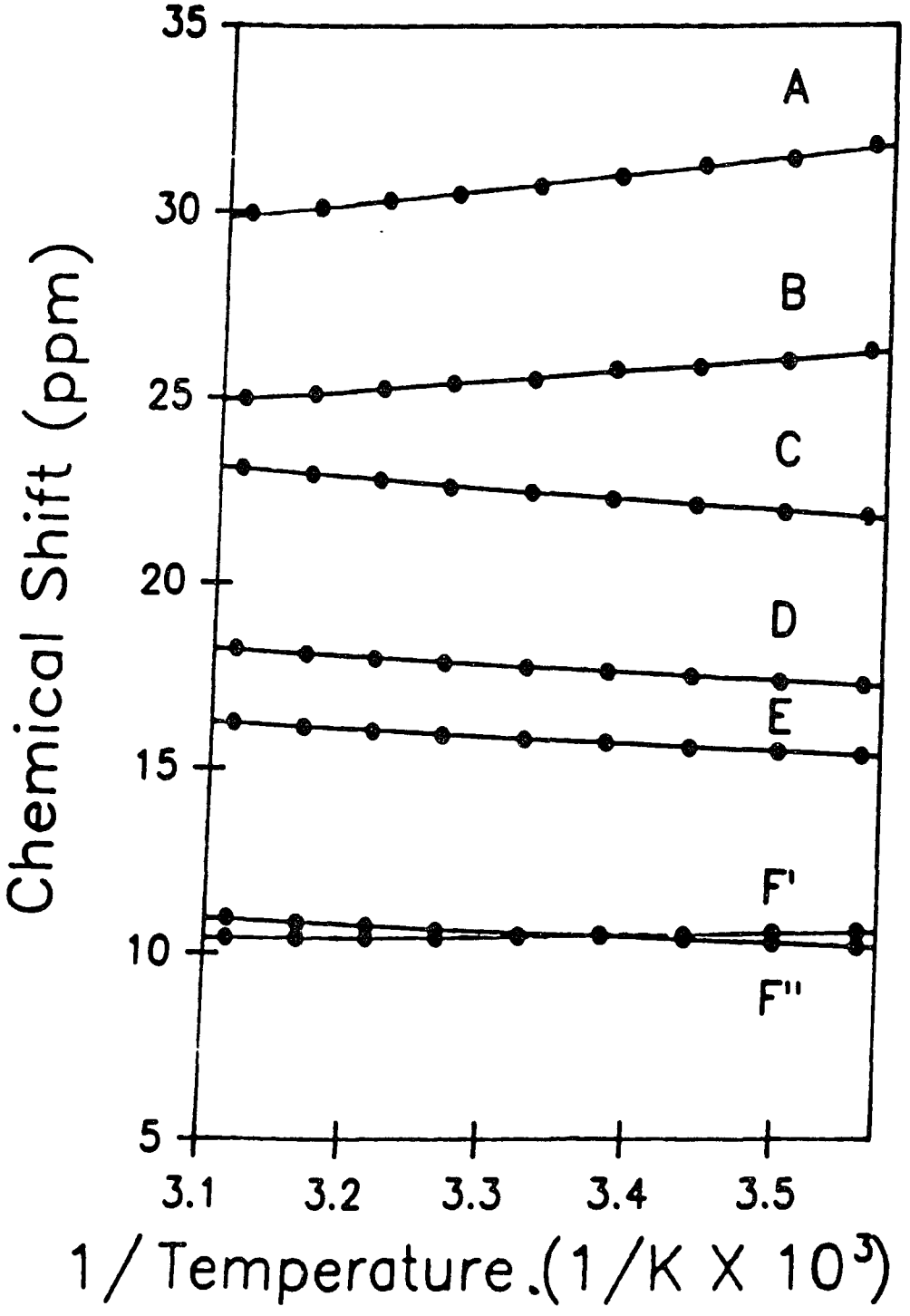
35
30
25
20
15
10
5
A
B
C
D
E
F'
F''
Chemical Shift (ppm)
3.1
3.2
3.3
3.4
3.5
1/ Temperature .(1/K X 10³)

Figure 5.3 Resolution of the Peaks F' and F'' in the Temperature Dependence Study

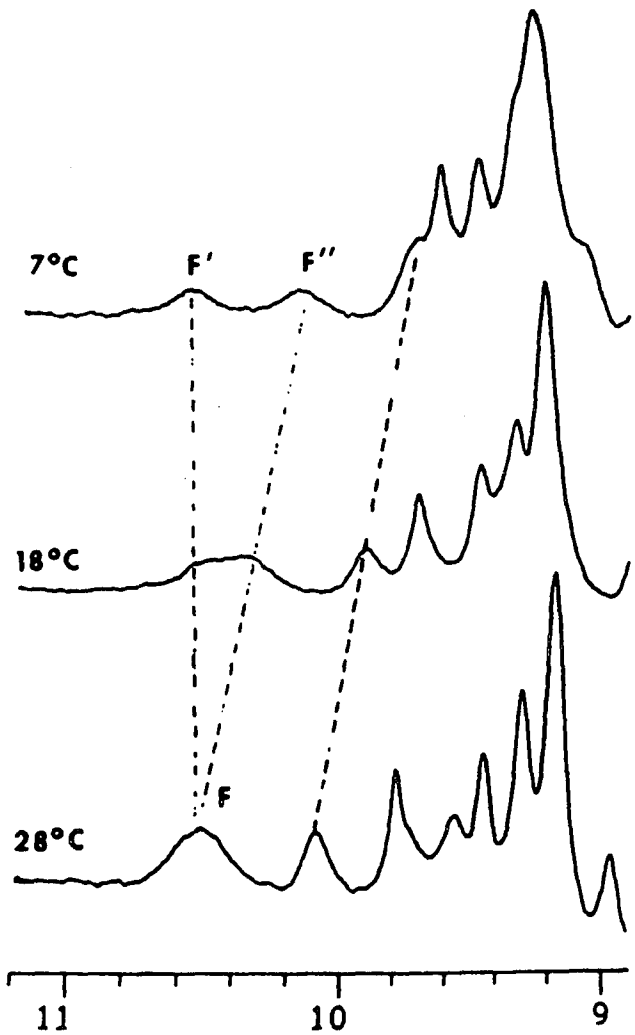
7°C
F'
F''
18°C
F
28°C
11
10
9

Table 5.1 T_1 Values and Assignments for the Most Downfield Resonances of Two 7Fe Ferredoxins (7 °C)

	P.putida		*A. vinelandii*		
Peak	ppm	T_1 (ms)	ppm	T_1 (ms)	Assignment
A	31.8	4.8	32.3	5.2	3Fe-4S β-cysteinyl proton
B	26.3	1.4	26.5	1.6	3Fe-4S β-cysteinyl proton
C	21.8	6.7	21.1	7.3	Cys16 β-proton
D	17.3	8.4	17.1	8.0	Cys39(42?)[d] β-proton
E	15.3	8.6	15.5	9.4	Cys45 β-proton
F'	10.2	5.8	10.2	*	not α- or β- cysteinyl proton
F"	10.6	6.2	10.4	*	not α- or β- cysteinyl proton
G	10.1[e]	10	10.1[e]	12	β-cysteinyl proton
H	9.6	25	9.8	21[c]	4Fe-4S α-cysteinyl proton
I	9.2		9.2	8.8[c]	4Fe-4S β-cysteinyl proton

a. T_1 values are the results of a fit to the equation 3.3.

b. The chemical shifts are referenced to the water peak at 4.78 ppm.

c. The T_1 value for resonance are estimated from an NOE build-up curve.

d. from one of the β-protons on either Cys39 or Cys42.

e. The chemical shifts are measured at 27 °C

Figure 5.4 400 MHz ^{1}H NMR Spectra of *P. putida* Ferredoxin Isolated from the Cells Grown in the Presence of β',β''-^{2}H Cystine

0.5 mM proteins dissolved in a 50 mM Tris-DCl buffer containing 50 mM NaCl with a pH of 7.4

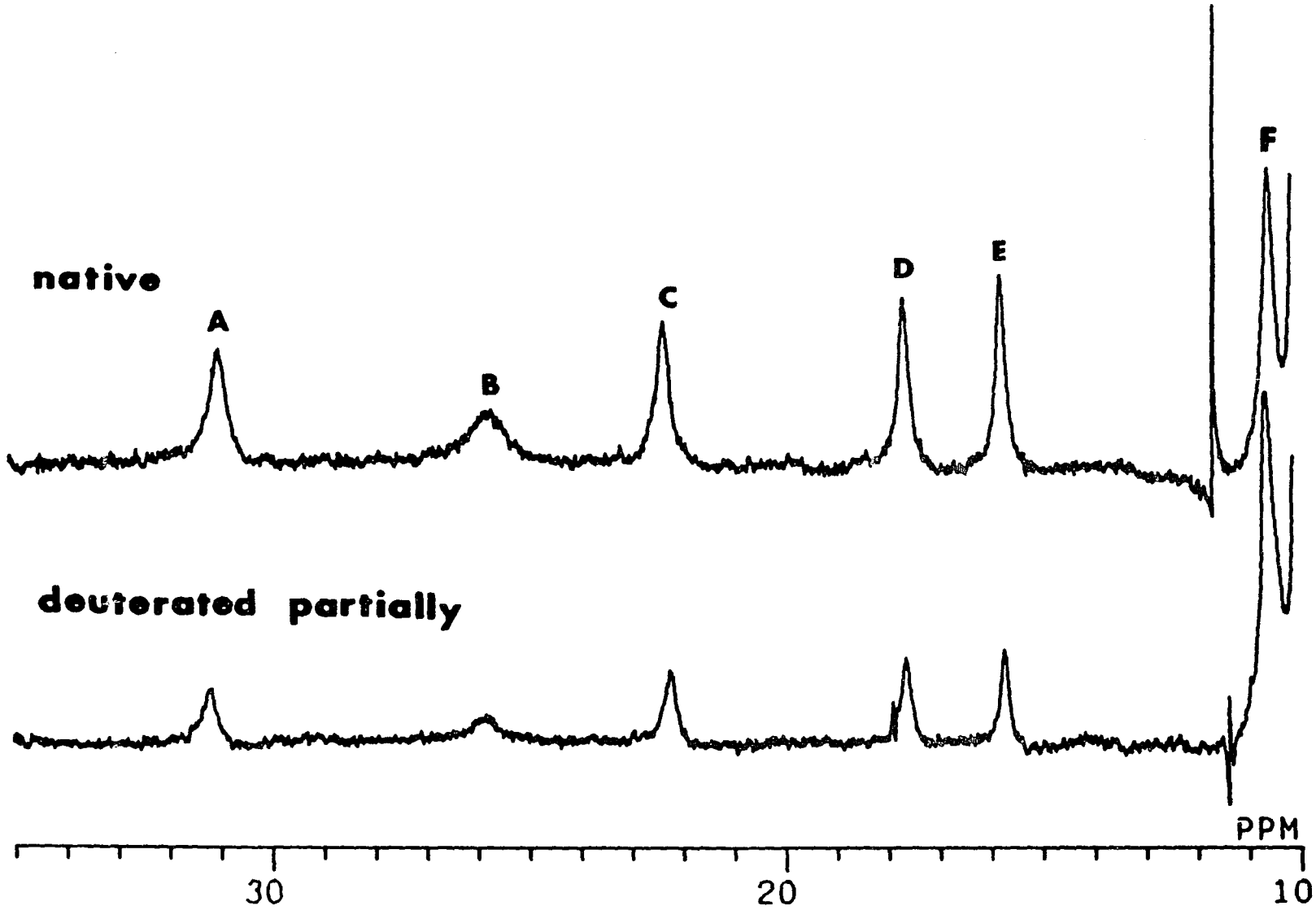
native
A
B
C
D
E
F
deuterated partially
PPM
30
20
10

Figure 5.5 The Downfield Region of the 400 MHz ^{1}H NMR Spectrum of *P. putida* Ferredoxin Isolated From Cells Grown in the Presence of β',β''-^{2}H-Cystine

A: Native Ferredoxin

B: β-^{2}H-Cysteine Labeled Ferredoxin

C: Difference Spectrum Obtained from subtracting the Spectrum of Native Ferredoxin (A) from that of the Labeled Ferredoxin (B)

all proteins are dissolved in a 50 mM Tris-DCl buffer containing 50 mM NaCl with a pH of 7.4

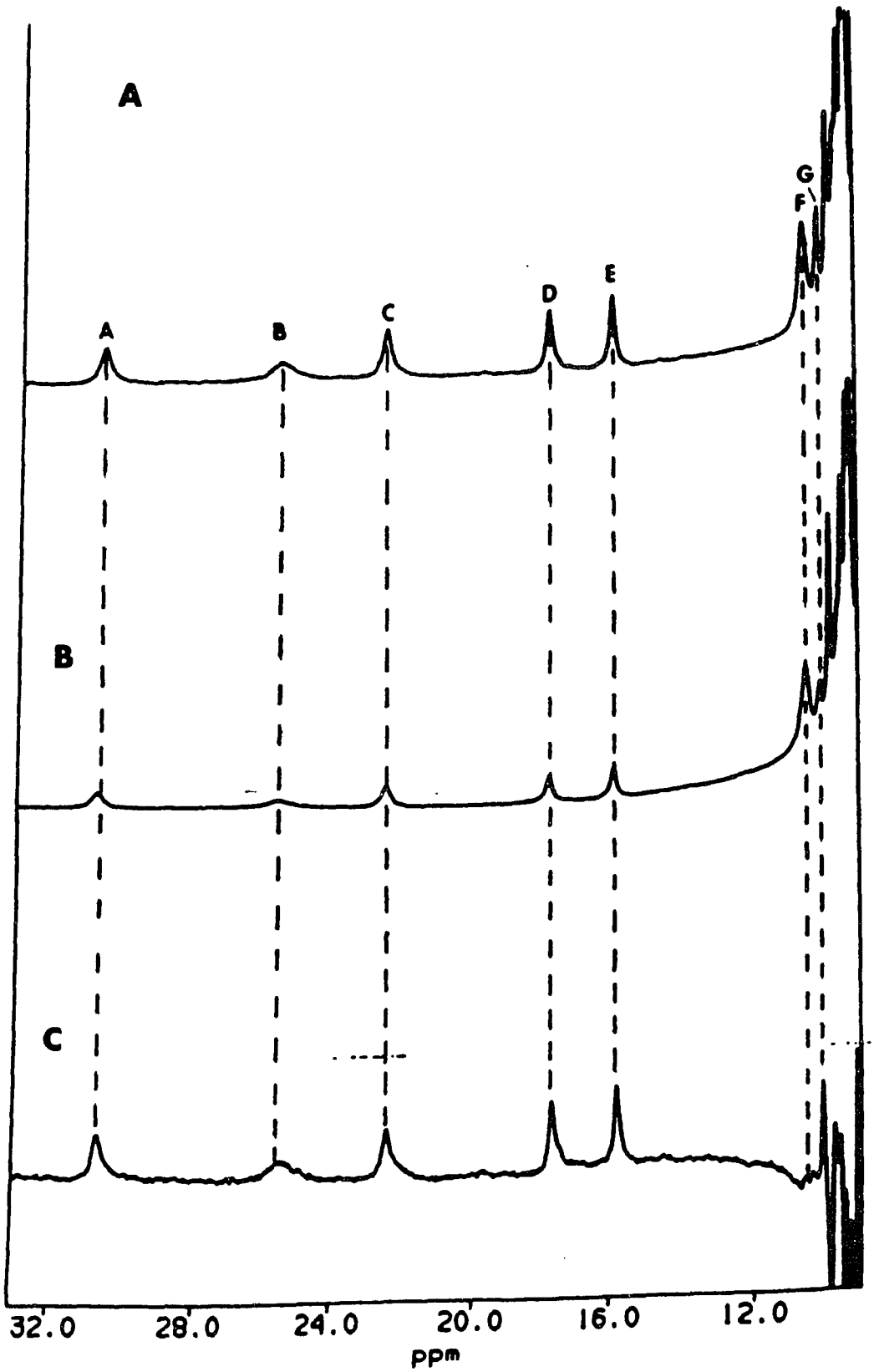
A
B
C
A
B
C
D
E
F
G
32.0
28.0
24.0
20.0
16.0
12.0
ppm

(Figure 5.5). Figure 5.5c shows the result from subtracting the spectrum of native ferredoxin (Figure 5.5a) from that of the labeled ferredoxin (Figure 5.5b). When peak F was completely subtracted along with other aromatic resonances, the five most downfield peaks, A-E, were still in the difference spectrum. Thus, peaks A-E were considered to be β-CH_2 cysteinyl protons. Their downfield chemical shift positions, broad line widths, short T_1 times, and temperature dependencies are consistent with these cysteines acting as ligands to iron atoms.

Although near 100% labeling was expected, the ^1H NMR spectrum of *P. putida* ferredoxin isolated from cystine auxotroph only showed about 50% intensity reduction for these five most downfield resonances, when compared with the NMR spectrum of native ferredoxin. The cystine auxotroph cells were grown in the presence of 2 g D,L-[3,3'-^2H]-cystine of 50 L medium. The reason for the lower labeling is not understood.

In contrast to the result obtained with β-^2H-labeled cystine, resonances A-F in the spectrum of *P. putida* ferredoxin isolated from cells grown in the presence of 0.5 mM D,L-[2,2'-^2H]-cystine were undiminished in intensity relative to the spectrum of unlabeled ferredoxin. Studies using ^{14}C-labeled cystine and the results of the deuterium β-labeling study indicated that the cysteinyl α-protons would be 70-80% labeled under the conditions used. Deuterium NMR of hydrolyzed "labeled" ferredoxin demonstrated that [2-^2H]-cysteine was present in the protein. The ferredoxin was previously treated by performic acid in order to convert cysteine into cysteic acid.

Figure 5.6c is the difference ^1H NMR spectrum obtained from subtracting the spectrum of native *P. putida* ferredoxin (Figure 5.6a) from that of the α-^2H-cysteine labeled *P. putida* ferredoxin (Figure 5.6b) between 6

Figure 5.6 The Aromatic Region of the 400 MHz ^{1}H NMR Spectrum of α-^{2}H-Cysteine Labeled *P. putida* Ferredoxin

A: Native Ferredoxin

B: α-^{2}H-Cysteine Labeled Ferredoxin

C: The Difference Spectrum Obtained from subtracting the Spectrum of Native Ferredoxin (A) from that of the Labeled Ferredoxin (B)

all proteins are dissolved in a 50 mM Tris-DCl buffer containing 50 mM NaCl with a pH of 7.4

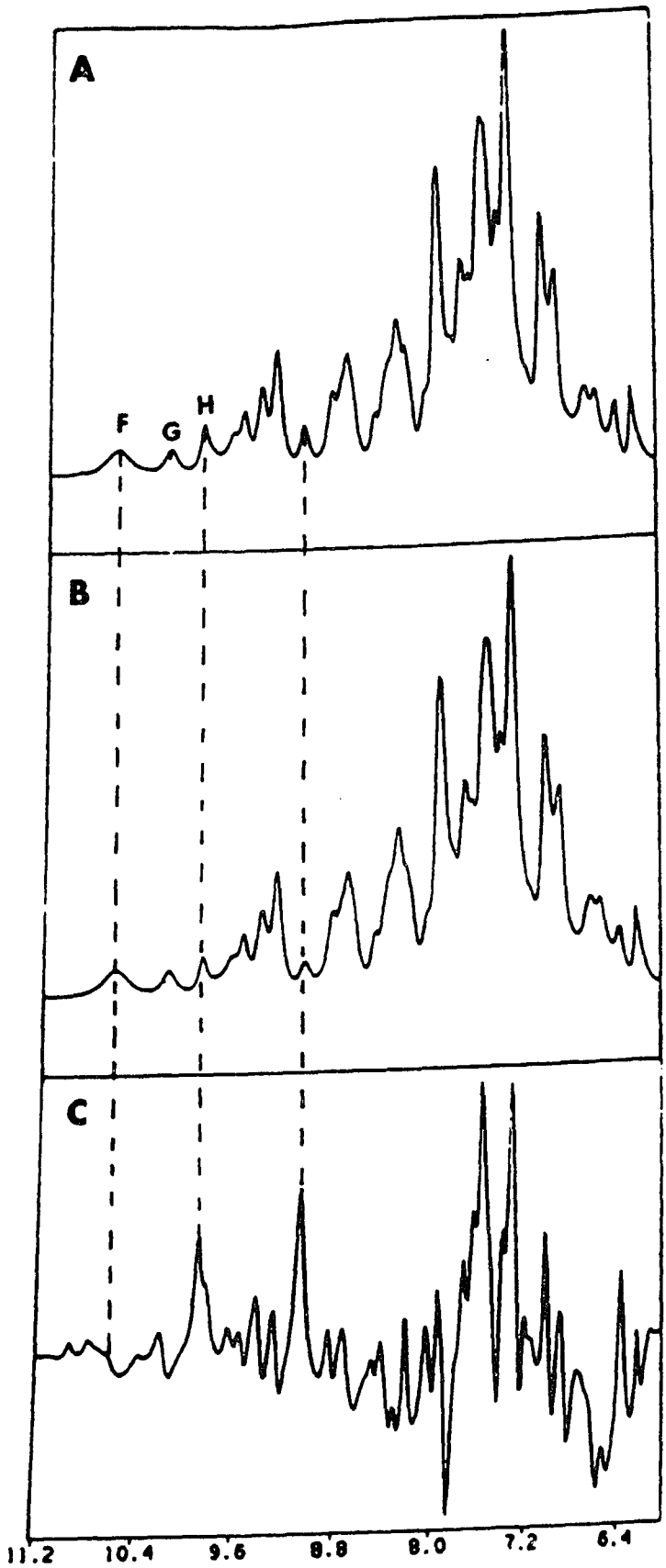
A
F
G
H
B
C
11.2
10.4
9.6
8.8
8.0
7.2
6.4

and 11.2 ppm. After the five most down field resonances, A-E, were completely subtracted out in the difference spectrum, four difference peaks were observed in the region between 5 and 10 ppm, lying near 9.84 (H), 9.0, 7.5, and 7.3 at 7 °C. These peaks were assumed to arise from the α-CH protons on cysteines liganded with iron-sulfur clusters due to their unusual large chemical shifts. The unobserved other five α-cysteinyl proton peaks may be not shifted out of the diamagnetic spectrum evenlope. Peak H around 9.8 ppm showed a anti-Curie temperature dependence. Others three α-cysteinyl proton peaks were not resolved from the diamagnetic envelope, and their temperature dependencies were not determinable.

Peaks F' and F'' were completely subtracted out in the α-^{2}H-cysteine labeled difference spectrum along with the five most downfield resonances, A-E. Considering the result from D,L-β,β'-^{2}H-labeled cystine study (Figure 5.5c), it appears that these peaks arise neither from α- nor β-cysteinyl protons.

The pH titration curves of six downfield cysteinyl proton resonances, A-E and H, of *A. vinelandii* ferredoxin I and *P. putida* ferredoxin at 27 °C are shown in Figure 5.7 and 5.8. Their pK_a values and Hill coefficients were calculated by nonlinear least square fit pH titration data to a modified Henderson-Hasselbalch equation (equation 3.1) and Hill plot (equation 3.2) for both ferredoxins at 7 °C and 27 °C. The results are shown in Table 5.2, 5.3, 5.4, and 5.5. For the pH titration of *A. vinelandii* ferredoxin I, the titration behavior of resonances A, B, and C were optimally fit with pK_a values of 5.5, 5.3 and 5.3 at 7 °C (Table 5.2), or 5.4, 5.3, and 5.3 at 27 °C (Table 5.3), although a reasonable fit for all three titration curves could be obtained with a single pK_a for each temperature. The titration curves of peaks D and

Figure 5.7 pH Titrations of Six Downfield Cysteinyl Proton Resonances in the ^{1}H NMR Spectrum of *A. vinelandii* Ferredoxin I (27 °C)

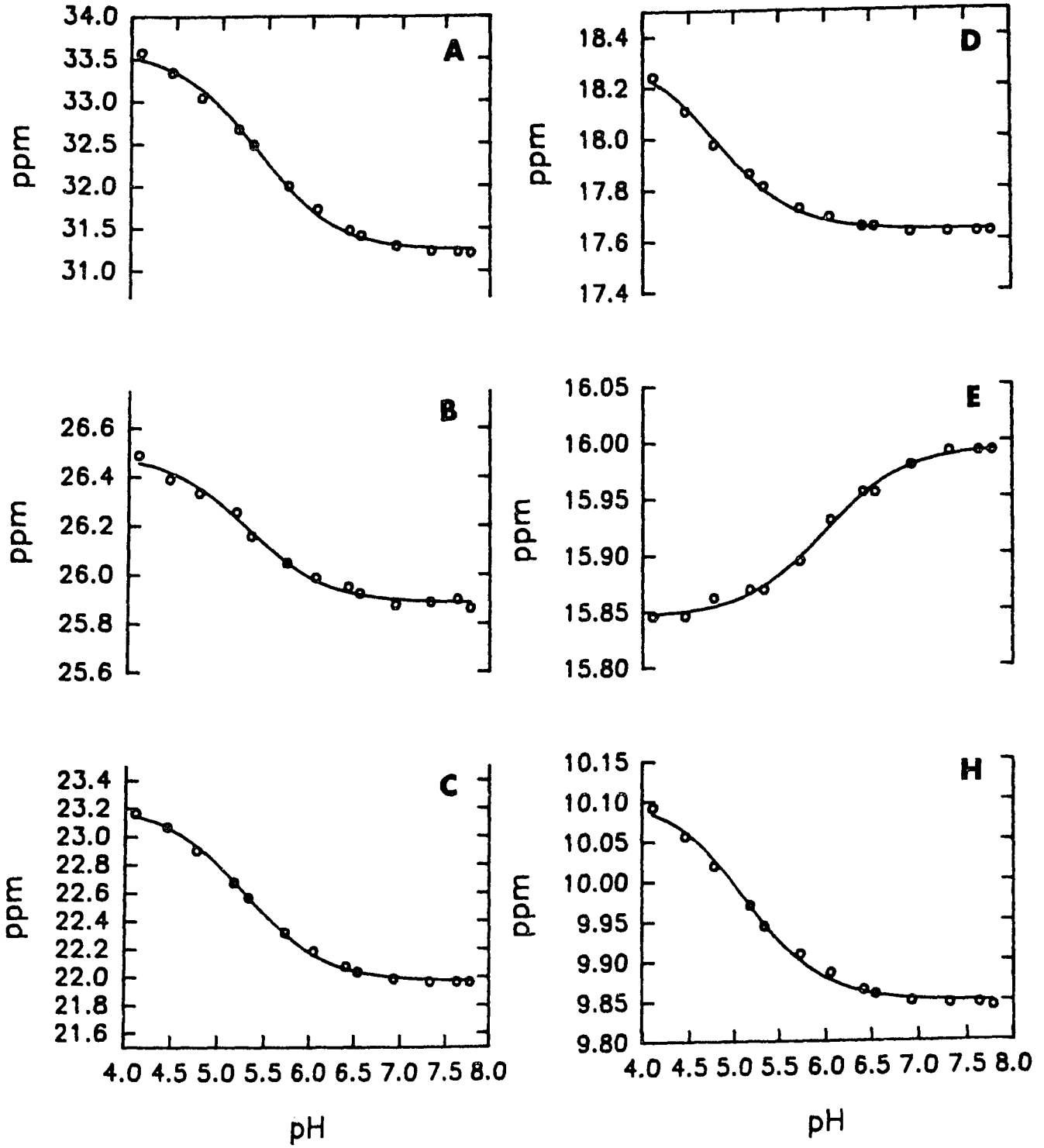
A
B
C
D
E
H
ppm
pH
34.0
33.5
33.0
32.5
32.0
31.5
31.0
26.6
26.4
26.2
26.0
25.8
25.6
23.4
23.2
23.0
22.8
22.6
22.4
22.2
22.0
21.8
21.6
18.4
18.2
18.0
17.8
17.6
17.4
16.05
16.00
15.95
15.90
15.85
15.80
10.15
10.10
10.05
10.00
9.95
9.90
9.85
9.80
4.0 4.5 5.0 5.5 6.0 6.5 7.0 7.5 8.0

Table 5.2 pH Titration Parameters of the Cysteinyl Residues of *A. vinelandii* Ferredoxin I at 7°C

Peak	Henderson-Hasselbalch Equation				Hill Plot	
	pKa	δ_{AH} (ppm)	δ_{A^-} (ppm)	$\Delta\delta_{AH,A^-}$ (ppm)	pK_a	Hill Coefficient
A	5.5	34.73	32.28	2.45	5.5	0.93
B	5.3	27.21	26.63	0.58	5.4	1.13
C	5.3	22.74	21.19	1.55	5.3	1.02
D	4.7	17.63	17.04	0.59	4.7	0.93
E	6.2	15.32	15.50	-0.18	6.2	1.12
H	5.0	9.92	9.68	0.24	5.1	1.00

a. δ_{AH}, δ_{A^-} are the results of a nonlinear least-square fit to a modified Henderson-Hasselbalch equation and the chemical shifts are referenced to DSS at 0 ppm.

b. pK_a are the results either of a nonlinear least-square fit to a a modified Henderson-Hasselbalch equation or a Hill plot

Table 5.3 pH Titration Parameters of the Cysteinyl Residues of *A. vinelandii* Ferredoxin I at 27°C

Peak	Henderson-Hasselbalch Equation				Hill Plot	
	pKa	δ_{AH} (ppm)	δ_{A^-} (ppm)	$\Delta\delta_{AH,A^-}$ (ppm)	pK_a	Hill Coefficient
A	5.4	33.61	31.25	2.36	5.4	0.93
B	5.3	26.50	25.88	0.62	5.3	0.85
C	5.3	23.22	21.97	1.25	5.3	1.00
D	4.8	18.34	17.64	0.70	4.8	1.00
E	6.0	15.85	15.99	-0.14	6.0	1.21
G	5.7	10.01	10.13	-0.12	5.7	0.96
H	5.1	10.11	9.85	0.26	5.2	0.99

a. δ_{AH}, δ_{A^-} are the results of a nonlinear least-square fit to a modified Henderson-Hasselbalch equation and the chemical shifts are referenced to DSS at 0 ppm.

b. pK_a are the results either of a nonlinear least-square fit to a a modified Henderson-Hasselbalch equation or a Hill plot

Figure 5.8 pH Titrations of Six Downfield Cysteinyl Proton Resonances in the ^{1}H NMR Spectrum of *P. putida* Ferredoxin I (27 °C)

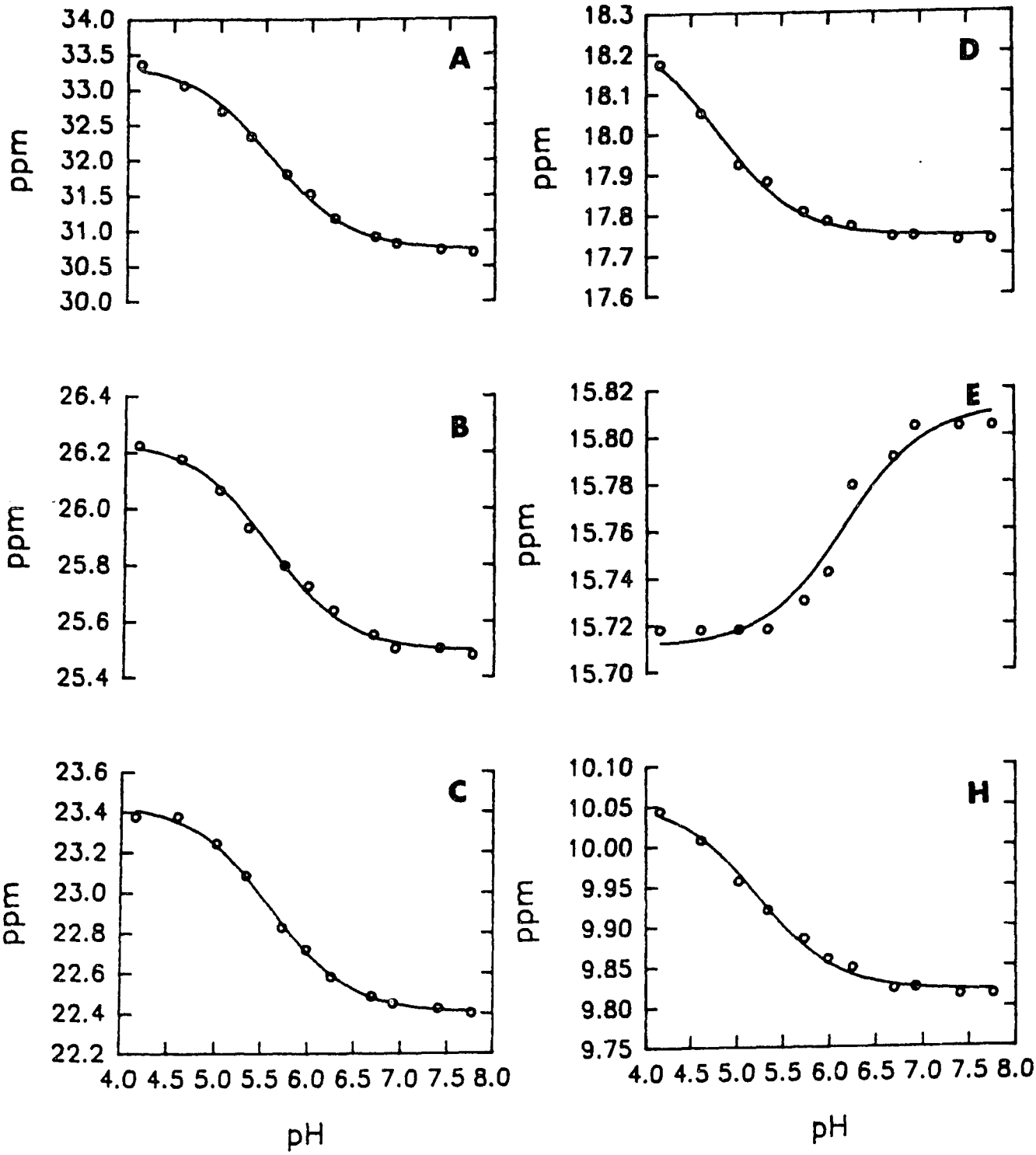
A
B
C
D
E
H
ppm
pH
34.0
33.5
33.0
32.5
32.0
31.5
31.0
30.5
30.0
26.4
26.2
26.0
25.8
25.6
25.4
23.6
23.4
23.2
23.0
22.8
22.6
22.4
22.2
18.3
18.2
18.1
18.0
17.9
17.8
17.7
17.6
15.82
15.80
15.78
15.76
15.74
15.72
15.70
10.10
10.05
10.00
9.95
9.90
9.85
9.80
9.75
4.0 4.5 5.0 5.5 6.0 6.5 7.0 7.5 8.0

E were fit with pK_a values of 4.7 and 6.2 at 7 °C (Table 5.2), or 4.8 and 6.0 at 27 °C (Figure 5.7 and Table 5.3). Similar results were obtained from the titration of *P. putida* ferredoxin. The best fits for peaks A, B, and C were obtained with pK_a values of 5.8, 5.7, and 5.6 at 7 °C (Table 5.4), or 5.5, 5.6, and 5.6 at 27 °C (Table 5.5 and Figure 5.8). However, all three titration curves could reasonably be fit with a single pK_a if a modified Henderson-Hasselbalch equilibrium equation (equation 3.1) was used. pK_a values of 4.7 and 6.3 produced the best fits for the titration curves of peaks D and E at 7 °C (Table 5.4). At 27 °C the pK_a values for D and E were 4.8 and 6.2 respectively (Table 5.5 and Figure 5.8). Peaks G and H had pK_a values of 5.7 and 5.1 at 27 °C for *A. vinelandii* ferredoxin I (Table 5.3 and Figures 5.7, 5.9), and 5.5 and 5.2 for *P.putida* ferredoxin (Table 5.5 and Figure 5.8, 5.9). At temperature of 7 °C, the pK_a values of peak Hs are 5.0 (Table 5.2) and 5.2 (Table 5.4) for *A. vinelandii* ferredoxin I and *P. putida* ferredoxin respectively. Peak G was pH dependent and shifted into the spectrum envelop during pH titration at 7 °C. Its pK_a could not be determined at this temperature.

5.1.2 1D Steady State NOE studies

Small negative Overhauser effects were observed between resonances A and B and between C and E (Table 5.6). Figure 5.10a shows the spectrum obtained when peak B (26.5 ppm) is irradiated. A proper control spectrum should be designed in order to distinguish off-resonance saturation effects from nuclear Overhauser effects. Figure 5.10b shows the control spectrum for quantitative evaluation of the NOE between peaks A and B. For this spectrum an irradiation pulse was applied at 38.1 ppm, whose position is the mirror image of peak B respective to peak A. Figure 5.10c shows the

Table 5.4 pH Titration Parameters of the Cysteinyl Residues of *P. putida* Ferredoxin I at 7°C

	Henderson-Hasselbalch Equation				Hill Plot	
Peak	pKa	δ_{AH} (ppm)	δ_{A^-} (ppm)	$\Delta\delta_{AH,A^-}$ (ppm)	pK_a	Hill Coefficient
A	5.8	34.40	31.66	2.74	5.7	0.97
B	5.7	26.87	26.16	0.71	5.7	1.05
C	5.6	23.07	21.70	1.37	5.6	1.18
D	4.7	17.62	17.19	0.43	4.7	1.05
E	6.3	15.19	15.34	-0.15	6.3	0.94
H	5.2	9.89	9.65	0.24	5.3	0.97

a. δ_{AH}, δ_{A^-} are the results of a nonlinear least-square fit to a modified Henderson-Hasselbalch equation and the chemical shifts are referenced to DSS at 0 ppm.

b.pK_a are the results either of a nonlinear least-square fit to a a modified Henderson-Hasselbalch equation or a Hill plot

Table 5.5 pH Titration Parameters of the Cysteinyl Residues of *P. putida* Ferredoxin I at 27°C

Peak	Henderson-Hasselbalch Equation				Hill Plot	
	pKa	δ_{AH} (ppm)	δ_{A^-} (ppm)	$\Delta\delta_{AH,A^-}$ (ppm)	pK_a	Hill Coefficient
A	5.5	33.38	30.72	2.66	5.8	0.95
B	5.6	26.24	25.49	0.75	5.6	0.95
C	5.6	23.44	22.40	1.04	5.6	1.00
D	4.8	18.26	17.74	0.52	4.8	0.92
E	6.2	15,70	15.81	-0.11	6.2	1.36
G	5.5	9.92	10.12	-0.20	5.5	0.95
H	5.2	10.06	9.82	0.24	5.3	0.98

a. δ_{AH}, δ_{A^-} are the results of a nonlinear least-square fit to a modified Henderson-Hasselbalch equation and the chemical shifts are referenced to DSS at 0 ppm.

b.pK_a are the results either of a nonlinear least-square fit to a a modified Henderson-Hasselbalch equation or a Hill plot

Figure 5.9 pH Dependencies of Peaks G's in the ^{1}H NMR Spectra of *A. vinelandii* Ferredoxin I and *P. putida* Ferredoxin (27 °C)

A: *A. vinelandii* Ferredoxin I

B: *P. putida* Ferredoxin

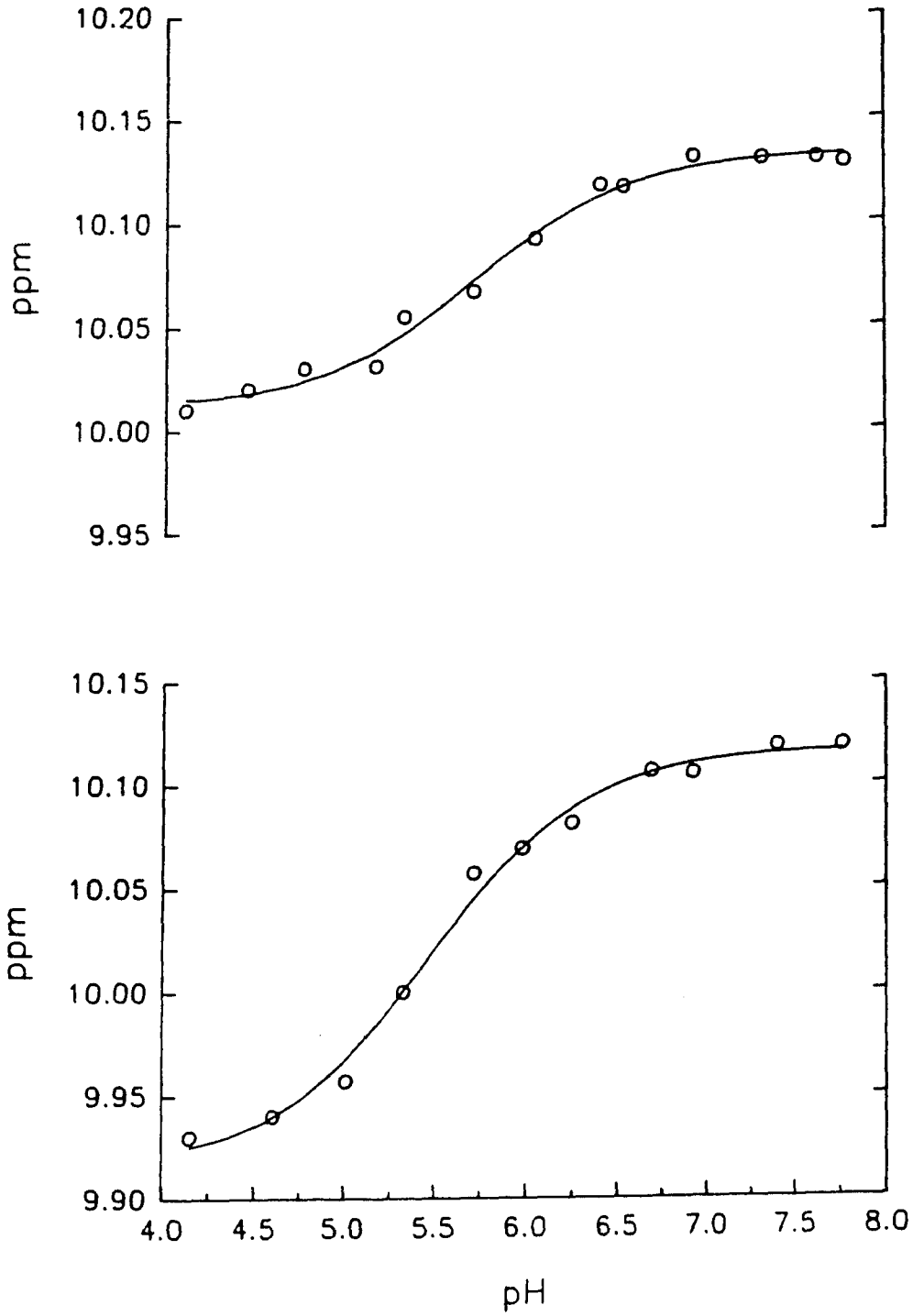
10.20
10.15
10.10
10.05
10.00
9.95
ppm
10.15
10.10
10.05
10.00
9.95
9.90
ppm
4.0
4.5
5.0
5.5
6.0
6.5
7.0
7.5
8.0
pH

Table 5.6 Observed Nuclear Overhauser Effects and Calculated Distances Between Downfield Resonances in the NMR spectrum

Obsd Peaks	Saturated Peaks				
	A	B	C	D	E
A	-	-8.9%/1.9 Å	-	-	-
B	-2.3%/1.9 Å	-	-	-	-
C	-	-	-	-	-1.3%/2.8Å
E	-	-	-1.3%/2.9Å	-	-
H	-	-	-	-6.3%/2.5Å[b]	-
I	-	-	-	-20.0%/1.8Å[b]	-

a. All distances are the results of calculations by using equations 2.10 and 2.11, and all nuclear Overhauser effects were measured at temperature of 7 °C.

b. The data were obtained from the NOE build up curves

Figure 5.10 Nuclear Overhauser Effect Between Peaks A and B (7 °C)

A: irradiation peak B

B: control spectrum

C: difference spectrum obtained from subtracting from the FID of spectrum A from the FID of spectrum B

6 mM protein is dissolved in 50 mM Tris-DCl buffer containing 50 mM NaCl with a pH of 7.4

Irradiation of Peak B (irradiation at 26.5 ppm)

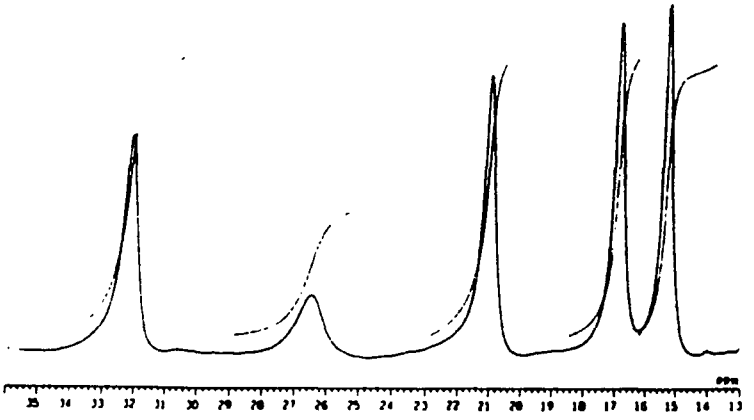

Control Spectrum (irradiation at 38.1 ppm)

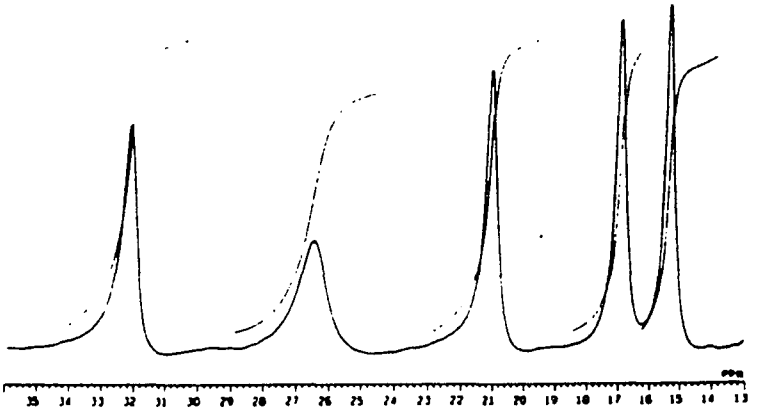

Difference Spectrum

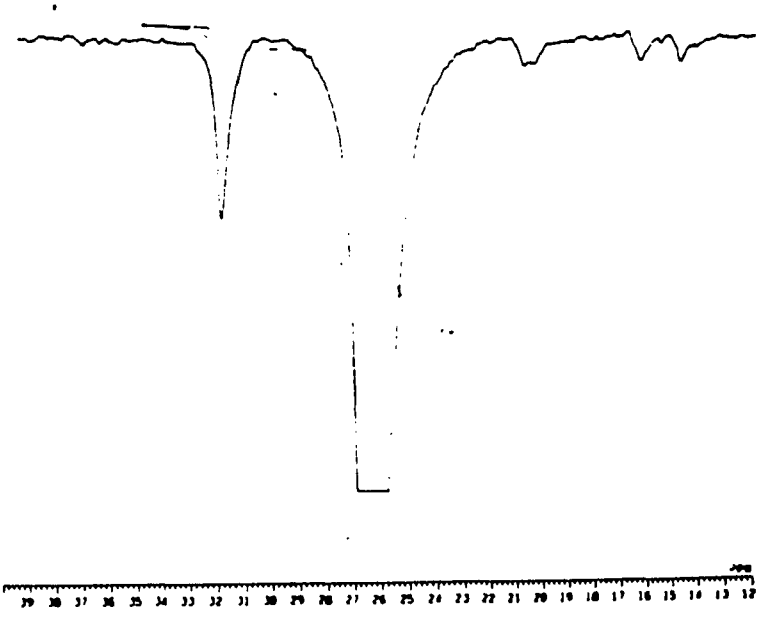

difference spectrum after subtracting the FID (free induction decay) of the spectrum with irradiation of peak B (Figure 5.10a) from that of the control spectrum (Figure 5.10b). A nuclear Overhauser effect of -8.9% was seen at resonance A (Table 5.6). Using the T_1 of peak A (5.4 ms) 1.9 Å was obtained from a interproton distance r_{AB} calculation based on equations 2.10 and 2.11. Although the complementary experiment of irradiation of peak A with a control yielded a considerably smaller Overhauser effect (-2.3%) at peak B (Table 5.6), using the shorter T_1 of 1.6 ms for peak B, the same interproton distance for r_{BA} (1.9 Å) was obtained (Table 5.6). Thus the calculated distance from the complementary experiments was essentially the same.

Figure 5.11a shows the difference spectrum obtained for the measurement of the Overhauser effect at peak C (21.1 ppm) due to irradiation of peak E (15.8 ppm). For the control in this case, the irradiation pulse was placed at 26.8 ppm. The apparent positive Overhauser effects seen at peaks A and B (Figure 5.11a) resulted from off-resonance saturation in the control spectrum. Similarly, the apparent negative Overhauser in peak D (Figure 5.11a) arose from off-resonance saturation during the irradiation of peak E. A 2.8 Å interproton distance was obtained from the calculation based the -1.3% of nuclear Overhauser effect at peak C with irradiation of peak E. The complementary experiment observing an -1.3 % of Overhauser effect at peak E from irradiation of C yielded almost the same interproton distance of 2.9 Å (Table 5.6 and Figure 5.11b). No evidence of an Overhauser effect between peak E and any peak other than C was observed.

When peak D was irradiated, two negative NOE peaks were obtained in the difference spectrum at 9.8 (H) and 9.2 ppm (I) (Figure 5.12). Since peak I is inside the spectrum envelop, its spin-lattice relaxation time, T_1, is

Figure 5.11 NOE Difference Spectra When Peak C or E Is Irradiated (7 °C)

A: peak E is irradiated

B: peak C is irradiated

6 mM protein is dissolved in a 50 mM Tris-DCl buffer containing 50 mM NaCl buffer

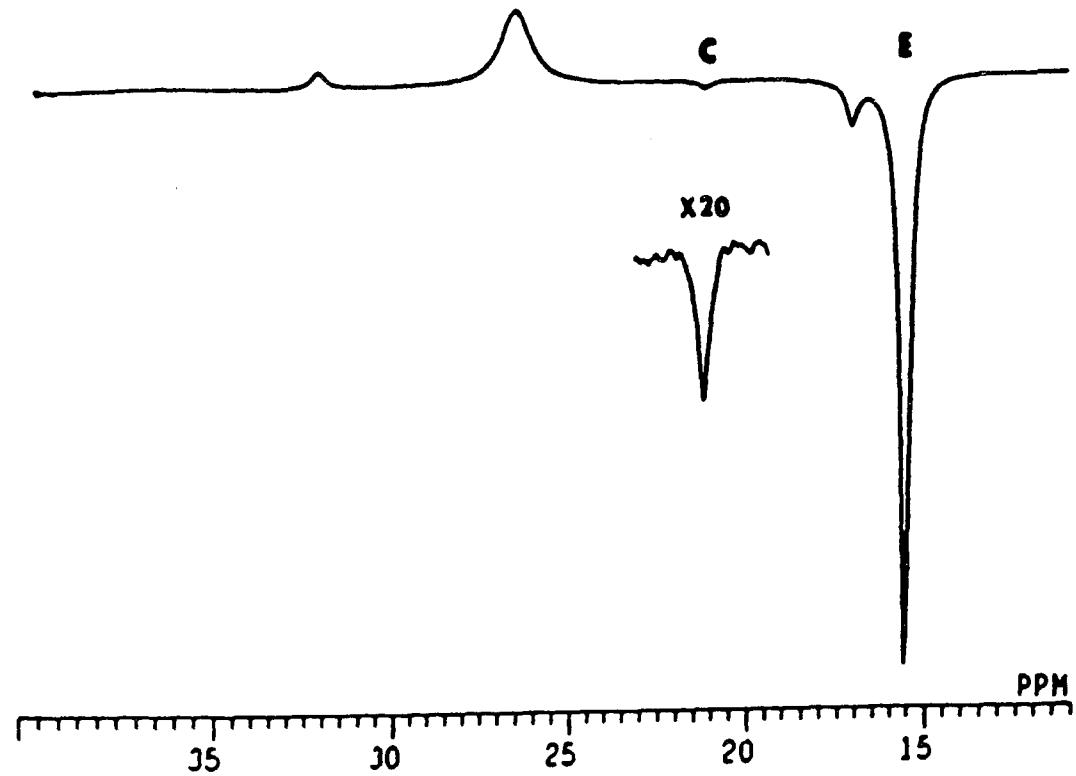
C
E
X20
PPM
35
30
25
20
15

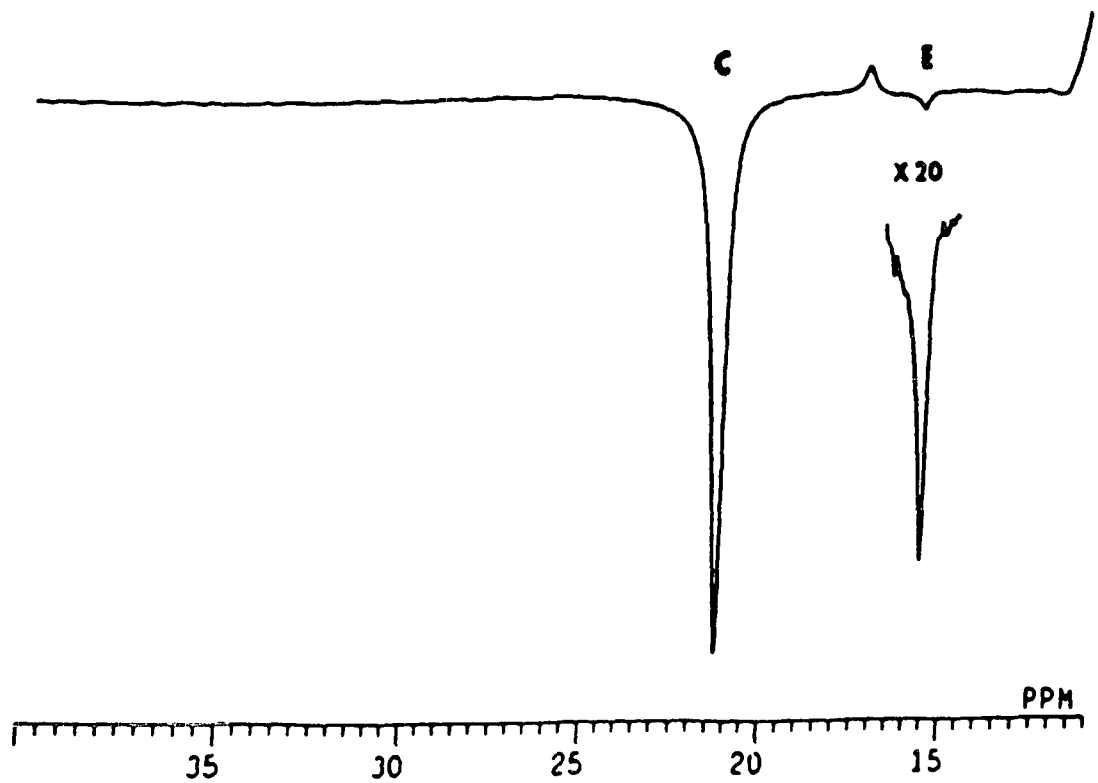
C
E
X 20
PPM
35
30
25
20
15

Figure 5.12 400 MHz ^{1}H NMR NOE Difference Spectrum when the Peak D is Irradiated (7°C)

6 mM protein is dissolved in 50 mM Tris-DCl buffer containing 50 mM NaCl with a pH of 7.4

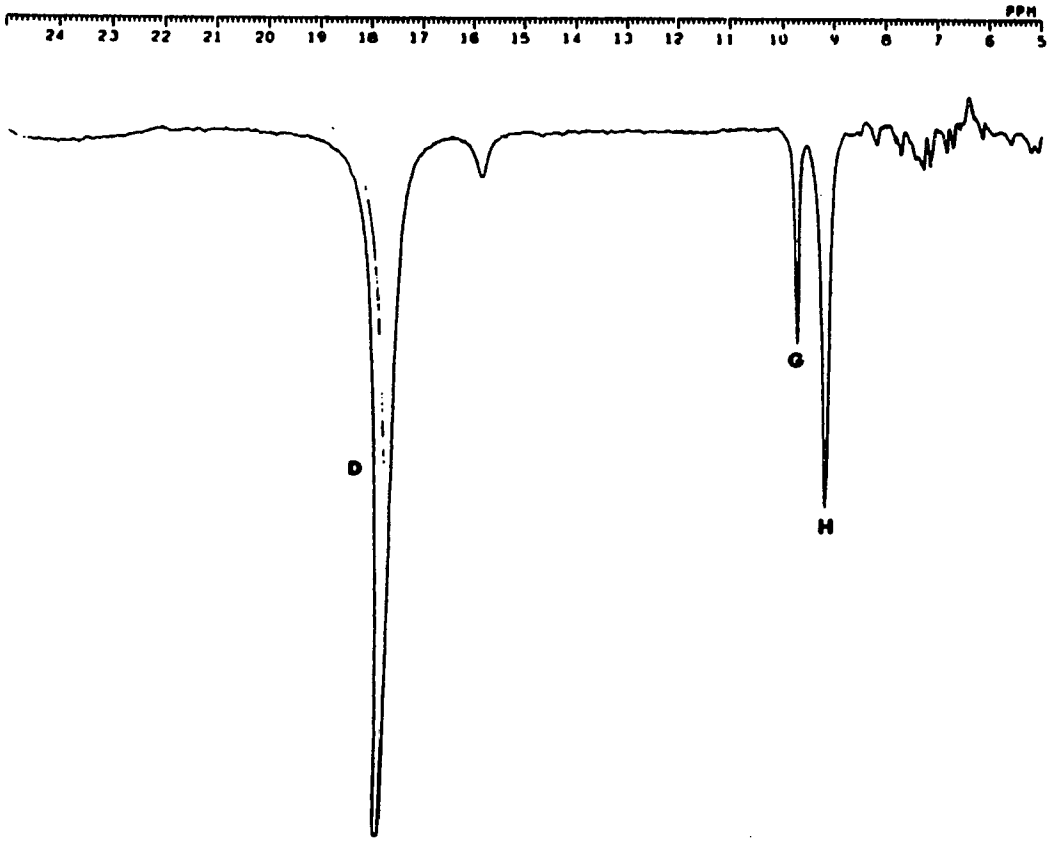
PPM
24 23 22 21 20 19 18 17 16 15 14 13 12 11 10 9 8 7 6 5
D
G
H

not directly measurable. The interproton distances between protons giving rise to peaks D and H or peaks D and I were obtained from the NOE buildup curves (Figure 5.13 and Table 5.6). The cross relaxation rates calculated from the slopes of the NOE buildup curves were 3.0 s^{-1} for peak H and 22.7 s^{-1} for peak I. This led to a 1.8 Å interproton distance for r_{DH} and a 2.5 Å for r_{DI} from equation 2.10. Using equation 2.11, the spin-lattice relaxation times estimated from the NOE buildup experiment were 8.8 ms and 21 ms for peaks I and H respectively.

5.1.3 SM-NOESY Spectroscopy

Figure 5.14 is the downfield region of the SM-NOESY (short mixing time NOESY) spectrum of *A. vinelandii* ferredoxin I. A 5 ms mixing time was used. Nine α-β or β-β cysteinyl proton NOE cross-peaks were seen in the spectrum. Their assignments are given in Table 5.7 based on their chemical shifts, line width, and in conjunction with results from 1D steady state NOE and deuteration experiments and will be disscused in the discussion section

One NOE cross-peak (#5) which arose from the dipole correlation between β-cysteinyl proton resonance D and a possible methyl proton resonance was also seen in the spectrum (Figure 5.15). Based on the X-ray structure and assuming that the solution structure is essential the same as the crystal structure, this cross-peak is tentatively assigned and will be disscused in the discussion section (Table 5.7).

5.1.4 Reduction Studies

The NMR spectra of reduced *A. vinelandii* and *P. putida* ferredoxins have been studied in three different experiments. In the progressive

Figure 5.13 NOE Buildup Curves of Peaks H and I when the Peak D is Irradiated (7 °C)

(*A. vinelandii* Ferredoxin I)

A: NOE buildup curve for peak H

B: NOE buildup curve for peak I

Appropriate data was lease-square non-linear fitted to a exponential decay function

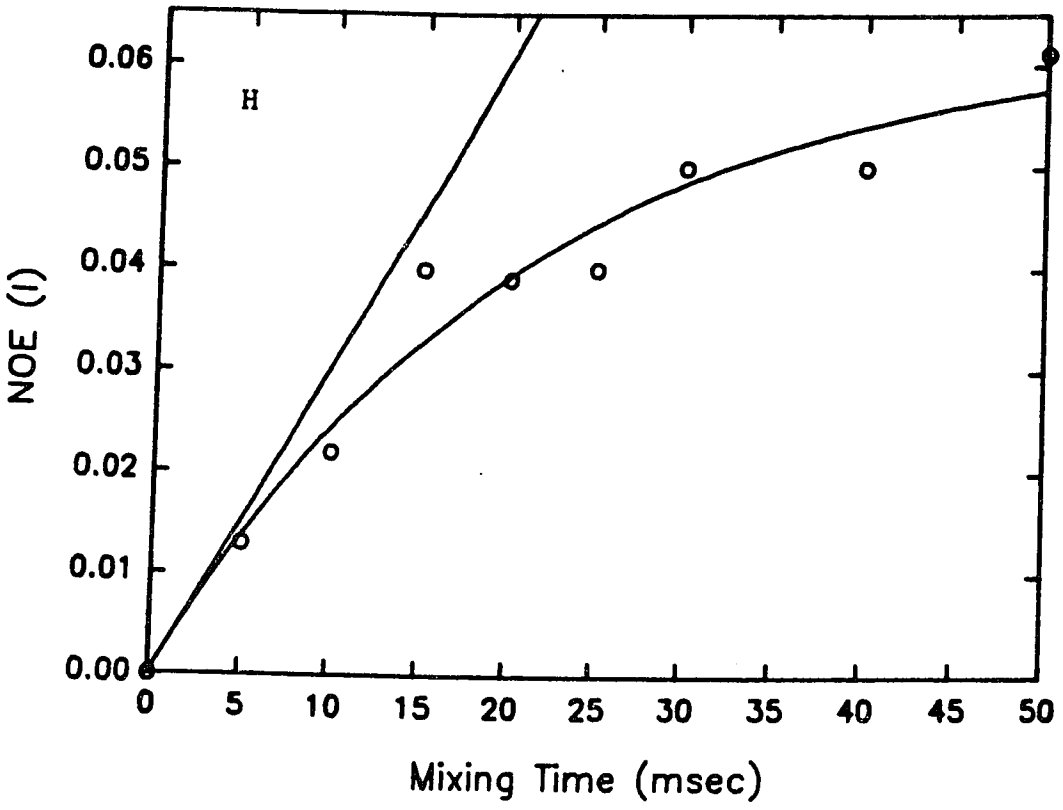
H
NOE (I)
0.06
0.05
0.04
0.03
0.02
0.01
0.00
0
5
10
15
20
25
30
35
40
45
50
Mixing Time (msec)

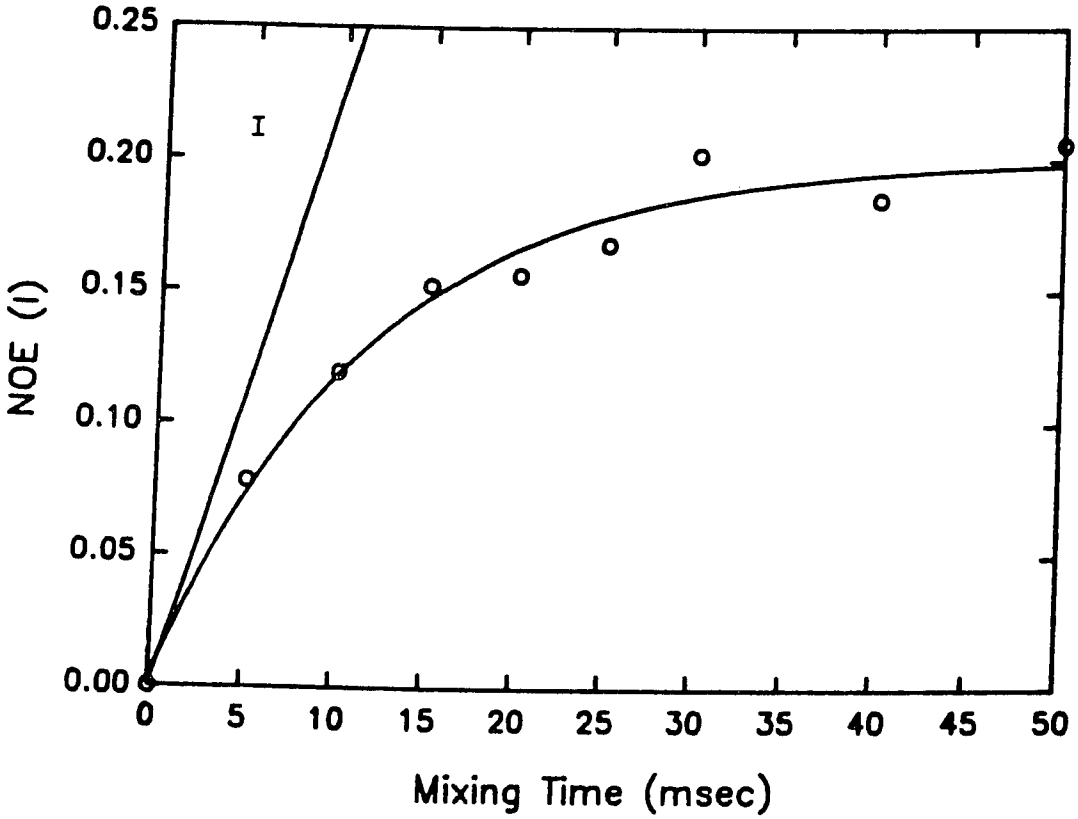
I
NOE (I)
0.25
0.20
0.15
0.10
0.05
0.00
0
5
10
15
20
25
30
35
40
45
50
Mixing Time (msec)

Figure 5.14 The Downfield Region of SM-NOESY (τ_m: 5 ms) of *A. vinelandii* Ferredoxin I in the Isolated Form (7 °C)

7 mM protein is dissolved in 50 mM Tris-DCl buffer containing 50 mM NaCl with a pH of 7.4

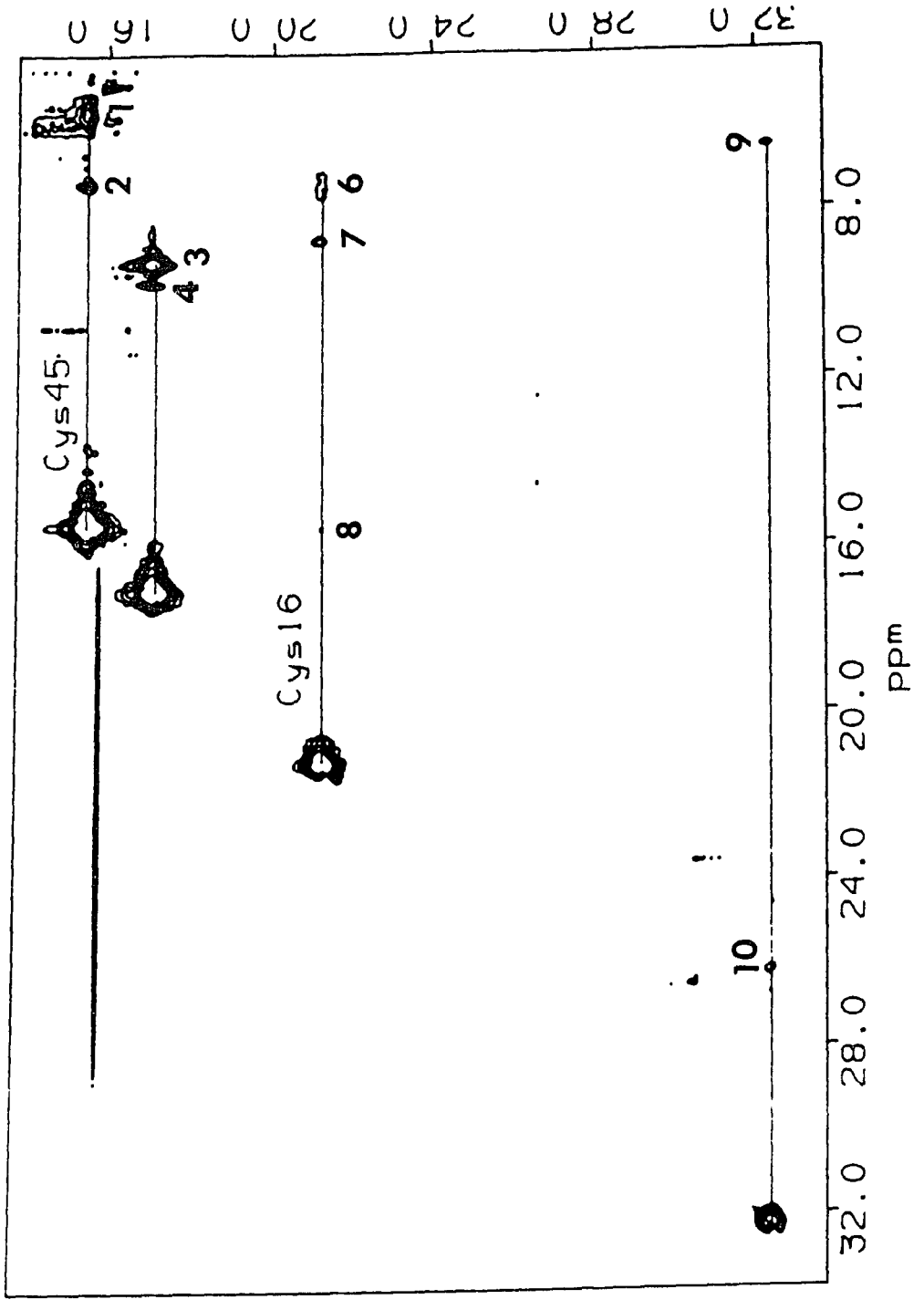
Cys45
Cys16
1
2
3
4
5
6
7
8
9
10
8.0
12.0
16.0
20.0
24.0
28.0
32.0
ppm

Figure 5.15 The NOE Cross Peaks Associated with Peaks D and E in the SM-NOESY (τ_m: 5 ms) of *A. vinelandii* Ferredoxin I in the Isolated Form (7 °C)

7 mM protein is dissolved in 50 mM Tris-DCl buffer containing 50 mM NaCl with a pH of 7.4

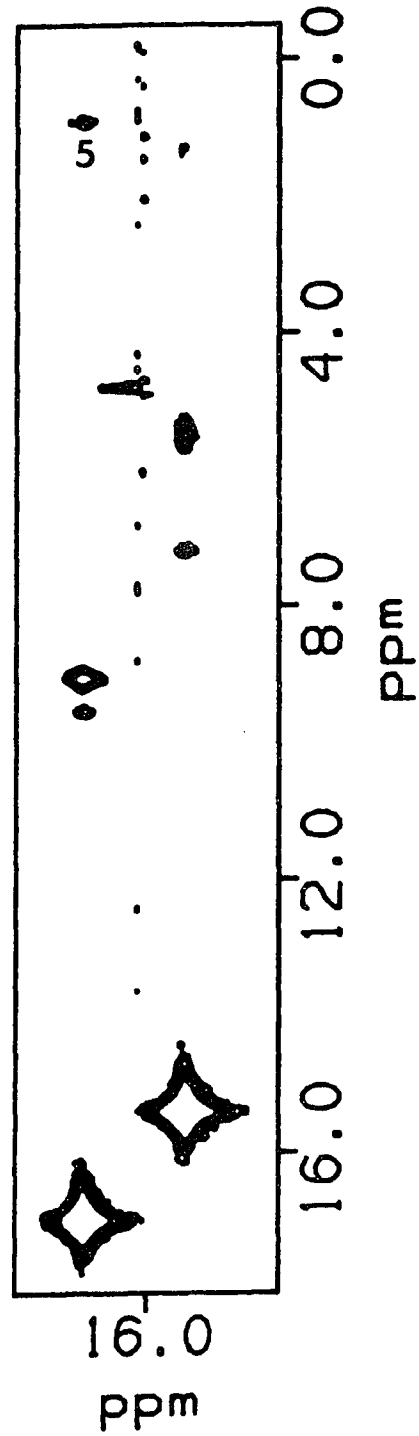
5
0.0
4.0
8.0
12.0
16.0
ppm
16.0
ppm

Table 5.7 The Cross Peaks in the Downfield Region of 400 MHz SM-NOESY of *A. vinelandii* Ferredoxin I (7 °C)

#	ω1 (ppm)	ω2 (ppm)	Assignment
1	15.2 ppm (E)	5.6 ppm	Cys45 α–β cross-peak
2	15.2 ppm (E)	7.3 ppm	Cys45 β–β cross-peak
3	16.9 ppm (D)	9.1 ppm (I)	Cys39 (42?) β–β cross-peak
4	16.9 ppm (D)	9.6 ppm (H)	Cys39 (42?) α–β cross-peak
5	16.9 ppm (D)	0.93 ppm	β-Cys39 (42?) and methyl protons
6	21.1 ppm (C)	7.2 ppm	Cys16 α–β cross-peak
7	21.1 ppm (C)	8.6 ppm	Cys16 β–β cross-peak
8	21.1 ppm (C)	15.2 ppm (E)	Cys16 and Cys45 β–β cross-peak
9	32.2 ppm (A)	6.5 ppm	[3Fe-4S] Cysteine α–β cross-peak
10	32.2 ppm (A)	26.1 ppm (B)	[3Fe-4S] Cysteine β–β cross-peak

reduction experiment, *P. putida* ferredoxin was first partially reduced by sodium dithionite, the partially reduced ferredoxin was then further reduced by addition of zinc reduced methyl viologen, and finally almost completely reduced by addition of sodium borohydride. In another reduction experiment, *P. putida* ferredoxin was reduced by a mixture of sodium dithionite and zinc reduced methyl viologen. In the third reduction experiment, *A. vinelandii* ferredoxin I and *P. putida* ferredoxin were separately reduced by only zinc reduced methyl viologen.

The results from Mössbauer, EPR and resonance Raman experiments indicate that sodium dithionite partially reduces the 3Fe center while the 4Fe center is unaffected. The 3Fe center is further reduced by addition of zinc reduced methyl viologen, still leaving the 4Fe center unaffected. Addition of sodium borohydride leads to almost complete reduction of the 3Fe center, while the 4Fe center is only slightly reduced (see Chapter 1).

Figure 5.16 shows the downfield regions in the progressive reduction of *P. putida* ferredoxin. Figure 5.17 are the NMR spectra of *P. putida* ferredoxin in the aromatic and aliphatic regions in the progressive reduction. Comparing the ^{1}H NMR spectrum of native ferredoxin (Figure 5.16a and 5.17a, e), the aromatic and aliphatic proton resonances (Figure 5.17b and 5.17f) were broadened after adding sodium dithionite. However, the five most downfield resonances, A-E, were almost not changed (Figure 5.16b). With the continual adding of zinc-reduced methyl viologen, the resonances A, B and C became broad and the intensity of resonance E decreased (Figure 5.16c). Finally, after addition of sodium borohydride, resonances A, B, C, and E disappeared from the ^{1}H NMR spectrum (Figure 5.16d) and the resonances in the aromatic and aliphatic regions were fur-

Figure 5.16 The Downfield Region of the 400 MHz ^{1}H NMR Spectra of *P. putida* Ferredoxin in the Progressive Reduction

a: the native *P. putida* ferredoxin

b: the protein was reduced by 5 mg of solid sodium dithionite

c: the protein was further reduced by 50μL of 40 mM zinc reduced methyl viologen

d: the protein was final reduced by 1 mg of solid sodium borohydride

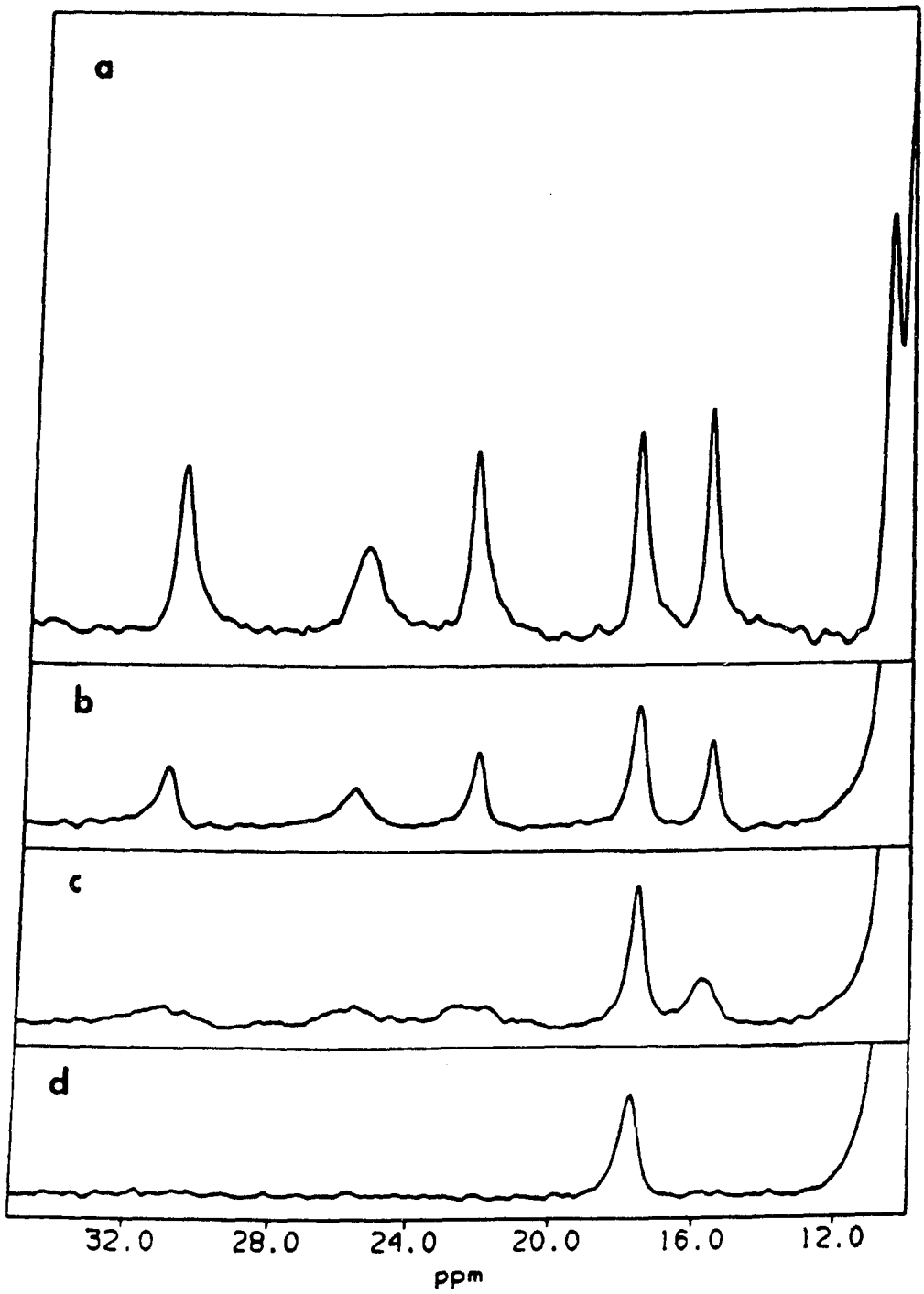
a
b
c
d
32.0
28.0
24.0
20.0
16.0
12.0
ppm

Figure 5.17 The Aromatic and Aliphatic Region of the 400 MHz ^{1}H NMR Spectra of *P. putida* Ferredoxin in the Progressive Reduction

a and e: the native *P. putida* ferredoxin

b and f: the protein was reduced by 5 mg of solid sodium dithionite

c and g: the protein was further reduced by 50μL of 40 mM zinc reduced methyl viologen

d and h: the protein was final reduced by 1 mg of solid sodium borohydride

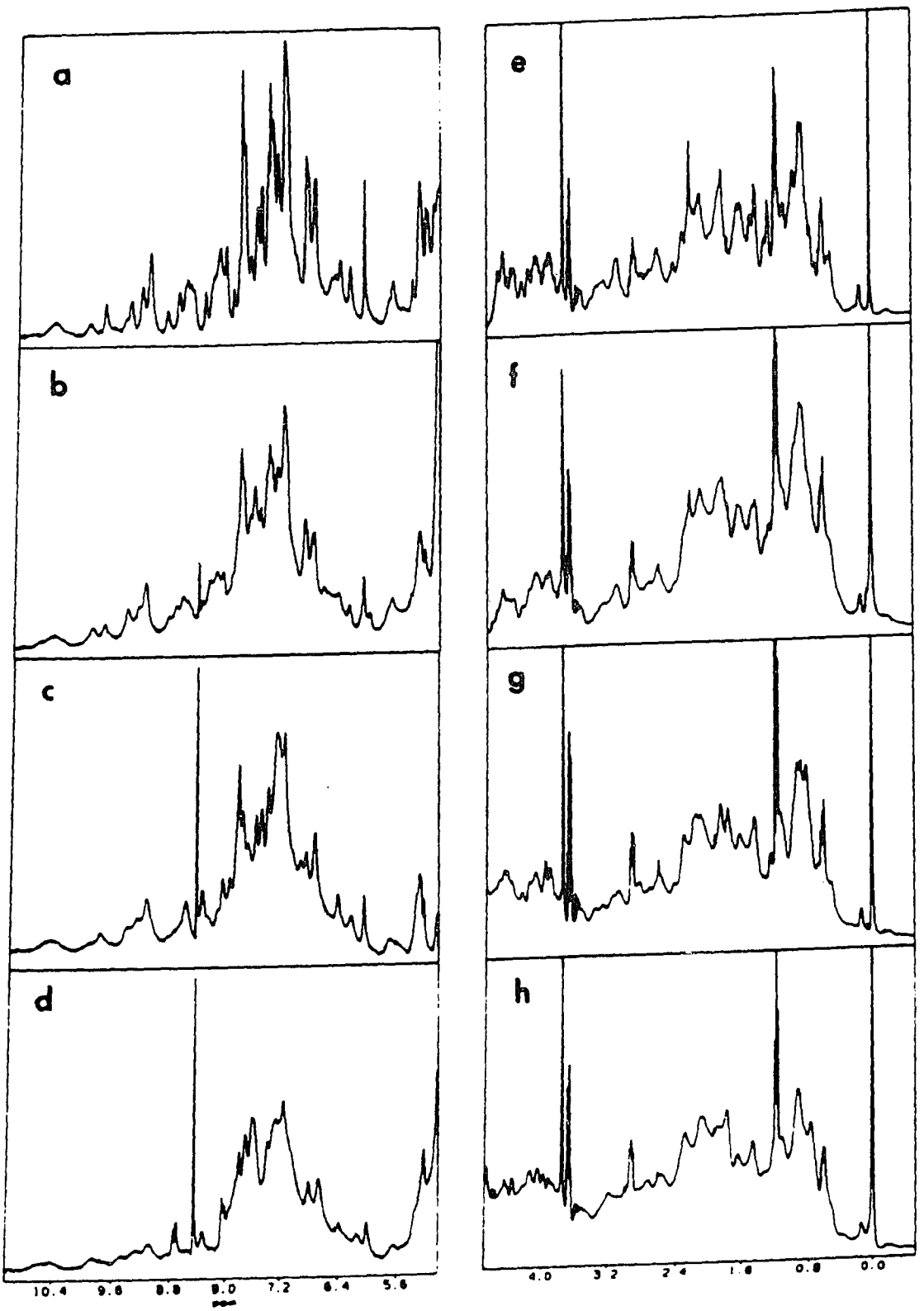
a
b
c
d
e
f
g
h
10.4
9.6
8.8
8.0
7.2
6.4
5.6
4.0
3.2
2.4
1.6
0.8
0.0

ther broadened (Figure 5.17d and h).

The ^{1}H NMR spectrum of *P.putida* ferredoxin was recorded after the ferredoxin was partially reduced by a mixture of sodium dithionite and zinc-reduced methyl viologen (Figure 5.18). The spectrum shows that the resonances A, B, and C are much more broad (Figure 5.18 bottom) than they were in the isolated from (Figure 5.16). Resonances D and E are almost unchanged (Figure 5.18 bottom). A broadening was also seen for other resonances in the aromatic and aliphatic proton regions (Figure 5.18 top and middle).

Figure 5.19 shows the ^{1}H NMR spectra of *A. vinelandii* and *P. putida* ferredoxins reduced by only zinc-reduced methyl viologen. The downfield regions (Figure 5.19c and f) of the spectra look similar to the spectrum of ferredoxin in the progressive reduction experiment after the sodium dithionite and methyl viologen reduction. Resonances A, B, and C were broader than they were in the isolated form and the intensity of resonance E was diminished. A broadening effect for the resonances in the aromatic and aliphatic proton regions was also seen in these two spectra (Figure 5.19a, b, d, and e).

The behavior of the five most downfield resonances in the reduction indicated that resonances A, B, and C were from protons near the 3Fe center and the resonances D was from a proton near the 4Fe center. The origin of resonance E was not clear since the results obtained from the reduction studies and those previously reported (refs. 1-4) were not in accord with each other.

Comparing all the results from the reduction studies, the degree of the intensity decrease for resonance E was not proportional to that of line-width changes for resonances A, B, and C. The intensity change for

Figure 5.18 The 400 MHz ^{1}H NMR Spectrum of Partially Reduced *P. putida* Ferredoxin by the Mixture of Sodium Dithionite and Zinc Reduced Methyl Viologen

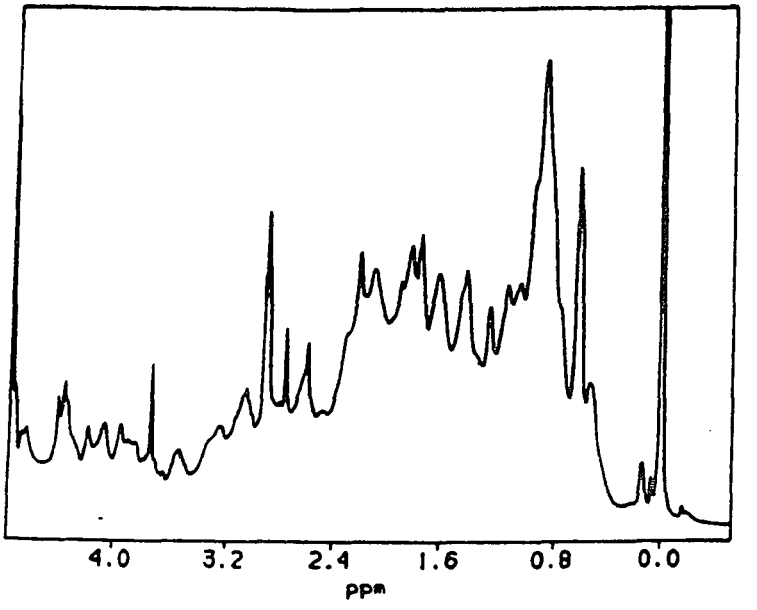
4.0
3.2
2.4
1.6
0.8
0.0
ppm

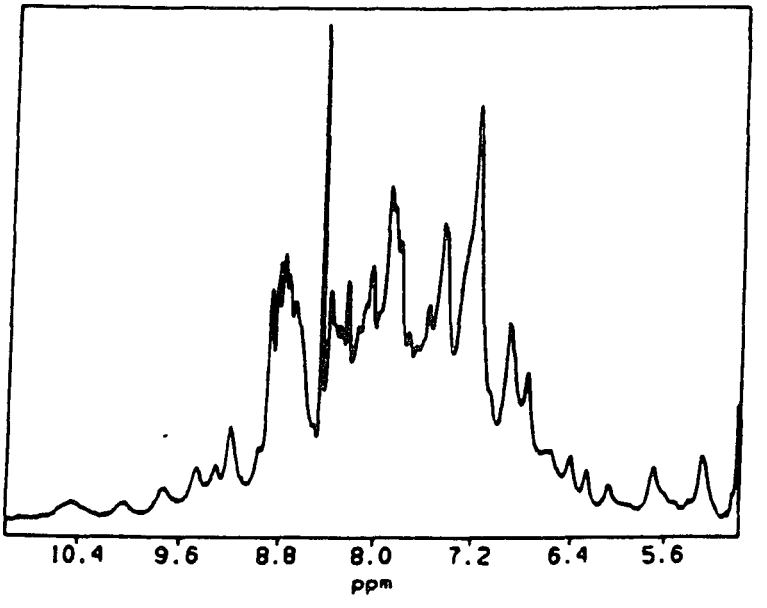
10.4
9.6
8.8
8.0
7.2
6.4
5.6
ppm

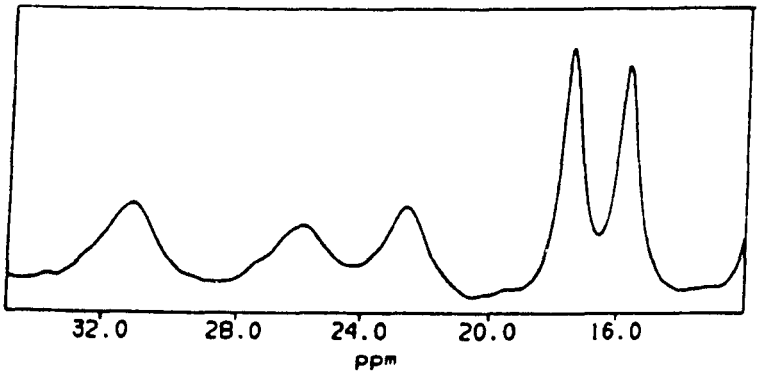
32.0
28.0
24.0
20.0
16.0
ppm

Figure 5.19 The 400 MHz ^{1}H NMR Spectra of the Partially Reduced *P. putida* Ferredoxin and *A. vinelandii* Ferredoxin I by Zinc Reduced Methyl Viologen

a, b, and c: *P. putida* ferredoxin

d, e, and f: *A. vinelandii* ferredoxin I

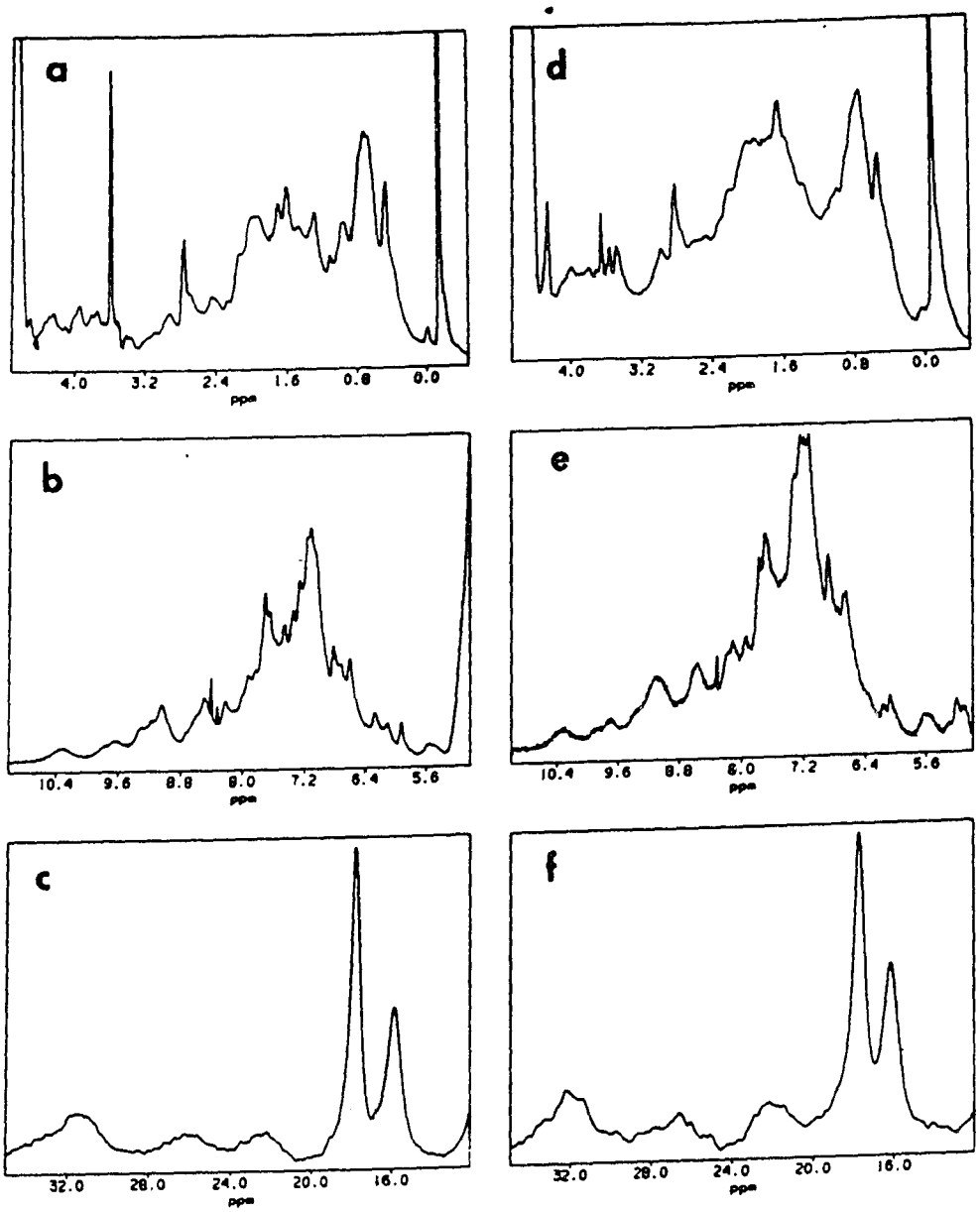
a
4.0
3.2
2.4
1.6
0.8
0.0
ppm
d
4.0
3.2
2.4
1.6
0.8
0.0
ppm
b
10.4
9.6
8.8
8.0
7.2
6.4
5.6
ppm
e
10.4
9.6
8.8
8.0
7.2
6.4
5.6
ppm
c
32.0
28.0
24.0
20.0
16.0
ppm
f
32.0
28.0
24.0
20.0
16.0
ppm

resonance E in the reduction was not the same while similar broadening effects at resonances A, B, and C were seen (Figure 5.16, 5.18, and 5.19) in different reduction experiments.

5.1.5 H_2O Exchangeable Protons

In order to identify exchangeable proton resonances, the ^1H NMR spectrum of *P. putida* ferredoxin in 90% ^1H_2O was recorded at 7 °C. The spectrum exhibited no new resonances in the 15-35 ppm region, and no intensity change was seen for peaks A-E and F". Four new resonances were visible at 10.4, 10.6, 10.8 and 10.9 ppm (Figure 5.20). Their chemical shifts are similar to those of four proton exchangeable peaks (10.0, 10.5, 10.6 and 11.1 ppm at 22 °C) in the ^1H NMR spectrum of *A. vinelandii* ferredoxin I reported by W. Sweeney (1). It was noticed that one of these four proton exchangeable peaks was right on peak F'.

5.1.6 Discussion

Deuteration: The results obtained from HPLC amino acid analysis with radioactive scintillation counting demonstrated that no amino acid other than cysteine was significantly labeled under experimental conditions (Chapter 4). Therefore, the decrease in intensity of resonances A-E seen in the proton NMR spectrum of ferredoxin isolated from cells grown in the presence of β-deuterium cystine (Figure 5.4 and 5.5) unambiguously demonstrates that these resonances arise from β-protons on cysteinyl residues. The T_1 values observed for these resonances, being 1.4 to 8.6 ms in *P. putida* (Table 5.1) and 1.6 to 9.4 ms in *A. vinelandii*, are in reasonable agreement with the 2.5 to 4.3 ms T_1 values obtained for β-cysteinyl protons on residues coordinating the [4Fe-4S] center in oxidized high potential iron

Figure 5.20 400 MHz ^1H NMR (7 °C) of the Isolated form of *P. putida* Ferredoxin in 90% ^1H_2O

top: recorded in 90% ^1H_2O

bottom: recorded in D_2O

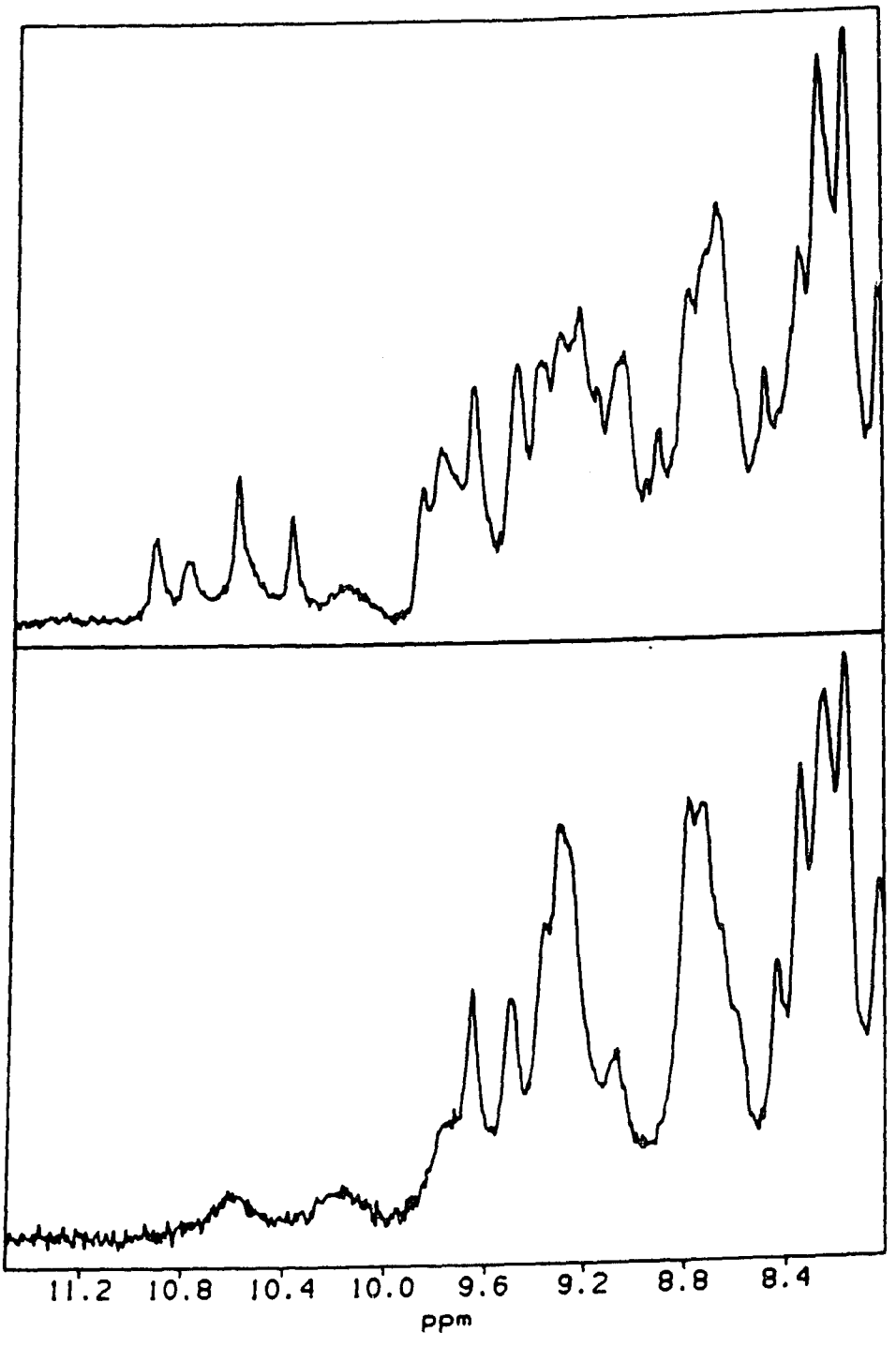
11.2
10.8
10.4
10.0
9.6
9.2
8.8
8.4
ppm

proteins (2), and the 2.2-7.5 ms found for reduced high potential iron protein (3).

No loss of intensity was observed for resonances F' and F'' after incorporation of either α- or β-deuterium cysteine (Figure 5.4, 5.5, and 5.6), demonstrating that they are neither cysteinyl α- nor β-protons. That peak F is not a cysteinyl α-proton is confirmed by the short T_1 values seen (5.6 ms for F' and 5.8 for F'') when comparing the >25 ms T_1 observed for the cysteinyl α-protons in oxidized high potential iron proteins (2). Resonances F' and F'' have been assigned to protons near to the 3Fe center based on the previously reported results (1 and 4-6). F' is Curie temperature dependent and F'' is anti-Curie temperature dependent.

1D Steady State NOE: The results of the NOE experiments on *A. vinelandii* ferredoxin I are given in Table 5.6. Distances calculated from symmetric experiments were in good agreement. For instance, irradiation of peak E yielded an Overhauser effect in peak C corresponding to a distance of 2.8 Å, while irradiation of peak C and observation of peak E indicated a distance of 2.9 Å (Table 5.6 and Figure 5.11). Due to the spin diffusion effects that were observed, these distances represent upper limit bounds to the true internuclear separations.

The calculated upper limit separation of 1.9 Å between the protons giving rise to resonances A and B is consistent with the ~1.75 Å separation expected for a geminal pair of cysteinyl β-protons (Table 5.8). Thus, peaks A and B are single proton resonances arising from protons on the same cysteinyl β-carbon. Since the five most downfield peaks (A-E) exhibit approximately equal intensity, this implies that these peaks arise from individual protons, confirming the earlier work (1).

Table 5.8 Proton-Proton Distances Between Two β-Protons on the Cysteinyl Residues Bound with the [3Fe-4S] Center in Å

[3Fe-4S]		Cys8		Cys16		Cys49	
		β1	β2	β1	β2	β1	β2
Cys8	β1	0	1.75	8.29	7.35	6.32	6.95
	β2		0	9.62	8.84	8.05	8.68
Cys16	β1			0	1.75	4.78	6.46
	β2				0	3.40	5.10
Cys49	β1					0	1.76

a. All distances are measured from the X-ray structure of *A. vinelandii* ferredoxin I (14)

Table 5.9 Proton-Proton Distances Between Two β-Protons on the Cysteinyl Residues Bound with the [4Fe-4S] Center in Å

[4Fe-4S]		Cys20		Cys39		Cys42		Cys45	
		β1	β2	β1	β2	β1	β2	β1	β2
Cys20	β1	0	1.76	7.97	9.50	8.96	8.42	5.39	4.00
	β2		0	8.67	10.2	9.53	8.91	7.13	5.72
Cys39	β1			0	1.75	9.79	8.30	9.13	8.42
	β2				0	9.90	8.36	10.4	9.71
Cys42	β1					0	1.75	9.80	8.42
	β2						0	9.74	8.30
Cys45	β1							0	1.75

a. All distances are measured from the X-ray structure of *A. vinelandii* ferredoxin I (14)

The upper limit separation of 2.9 Å (Table 5.6) found between the hydrogens giving rise to peaks C and E is inconsistent with a geminal pair of hydrogen atoms (Table 5.8 and 5.9). Peak C has been assigned as a proton associated with the 3Fe center in the previous studies (1 and 4-6). However, the smallest separation between two nongeminal pair of β-cysteinyl protons is 3.4 Å for cysteines associated with the 3Fe center, and 4.0 Å for cysteines associated with the 4Fe center (Table 5.8). These distances are significantly longer than the upper limit separation of 2.9 Å found. Thus the resonances C and E cannot arise from two β-cysteinyl protons on cysteinyl residues associated with same iron-sulfur center, and the resonance E must arise from a β-proton, on the cysteinyl residue associated with the [4Fe-4S] center. If the calculation of the distance is scaled using the observed NOE between the geminal pair of protons (peaks A and B) to correct for spin diffusion and error in the rotational correlation time, the separation calculated is 2.6 Å (1.75Å x 2.8 Å /1.9 Å). A β-proton of Cys45 is only 2.5 Å away from a β-proton on Cys16 in the X-ray structure (Table 5.10), in close agreement with the Overhauser result. The next closest 4Fe center cysteinyl β-proton to a 3Fe center cysteinyl β-proton is 3.2 Å; too far to be a possibility. Therefore, resonance C can be assigned to a β-proton on Cys16, while resonance E must arise from a β-proton on Cys45.

Peak E was originally assigned as a 4Fe cysteinyl resonance (1). However, later work suggested that it arose from a hydrogen atom near the 3Fe center (4 and 5). In reviewing their experimental results, Nagayama *et al.* (6) proposed that the proton giving rise to peak E may be near both the 3Fe and 4Fe centers. The present NOE results confirm this hypothesis, while assigning it as a β-proton on the cysteine associated with the 4Fe center.

Table 5.10 Proton-Proton Distances Between β-Protons on the Cysteinyl Residues Associated with [3Fe-4S] and [4Fe-4S] Center and in Å

[3Fe-4S]		Cys8		Cys16		Cys49	
[4Fe-4S]		β1	β2	β1	β2	β1	β2
Cys20	β1	12.8	13.9	5.05	6.71	9.60	11.1
	β2	14.2	15.2	6.57	8.18	11.2	12.8
Cys39	β1	13.9	14.4	9.73	11.3	12.7	13.9
	β2	15.1	15.6	11.3	12.7	13.9	15.0
Cys42	β1	18.6	19.9	11.6	12.8	13.9	14.6
	β2	18.3	19.4	11.4	12.8	14.1	14.9
Cys45	β1	9.26	10.7	2.47	3.22	4.64	5.95
	β2	10.8	12.2	3.24	4.49	6.35	7.63

a. All distances are measured from the X-ray structure of *A. vinelandii* ferredoxin I (14)

b. The closest distance of between the two β-protons on cysteinyl residues bound with [3Fe-4S] cluster and bound with [4Fe-4S] cluster is indicated by a box.

When peak D was irradiated, two NOE peaks were found at 9.8 ppm (H) and 9.2 ppm (I). The spin diffusion and error in the rotational correlation time were minimized by calculating the interproton distances from NOE buildup curves. The calculated interproton distances indicate that peak I and D (1.8 Å separation) arise from a geminal pair of β-protons on the cysteine liganded with the [4Fe-4S] cluster. The proton which gives rise to peak H is 2.5 Å away from the proton which gives peak D, and the chemical shift of peak H is similar to that one of the difference peaks in the difference ^{1}H NMR spectrum of α-^{2}H-cysteine labeled *P. putida* ferredoxin (Figure 5.6). The X-ray structure of *A. vinelandii* ferredoxin I shows that interproton distances between α- and β-cysteinyl proton on the same cysteinyl residue liganded with iron-sulfur center are from 2.39 to 3.02 Å (Table 5.11 and 5.12). Therefore, peak H can be assigned to the α-proton on the cysteinyl residue which gives rise to peak D. The T_1 value of peak H is 25 ms for *P. putida* obtained from the inversion-recovery experiment, and 21 ms for *A. vinelandii* estimated from the NOE buildup curve (Table 5.1), consistenting with the > 25 ms T_1 values observed for the α-cysteinyl protons in oxidized high potential iron proteins (2).

SM-NOESY: With a large spectral window and a very short mixing time, the standard NOESY experiment can be used to obtain nuclear Overhauser information between protons near a paramagnetic center. As discused in Chapter 2, the intensity for NOE cross-peak arising from paramagnetically shifted resonances is a sharp function of the mixing time. The spectrum recorded with a mixing time of 5 ms gave maximum NOE cross-peak intensity for the five most downfield resonances, A-E (Figure 5.14). The auto-cross-peaks of peaks A and C-E are seen in the

Table 5.11 The Proton-Proton Distances Between the α-protons and β-protons on the Cysteines Coordinated with the [3Fe-4S] Center (in Å)

[3Fe-4S]	Cys8 β1	Cys8 β2	Cys16 β1	Cys16 β2	Cys49 β1	Cys49 β2
Cys8 α	2.43	3.01	9.55	8.31	7.13	7.51
Cys16 α	9.72	11.2	2.44	2.39	5.00	6.41
Cys49 α	7.32	9.01	5.41	3.71	2.44	3.03

a. All distances are measured from the X-ray structure of *A. vinelandii* ferredoxin I (14)

Table 5.12 The Proton-Proton Distances Between the α- protons and β-protons on the Cysteines Liganded with the [4Fe-4S] Cluster (in Å)

[4Fe-4S]	20 β1	20 β2	39 β1	39 β2	42 β1	42 β2	45 β1	45 β2
20 α	2.52	3.02	8.25	9.48	6.66	6.28	6.16	4.43
39 α	7.32	7.68	2.43	3.02	8.31	6.69	9.58	8.46
42 α	10.2	11.0	9.40	9.16	2.28	2.52	10.4	9.22
45 α	5.76	7.30	10.6	11.8	8.85	9.20	2.48	2.38

a. All distances are measured from the X-ray structure of *A. vinelandii* ferredoxin I (14)

diagonal. Peak B is unobservable due to its very short T_1 relaxation time (1.6 ms for *A. vinelandii* ferredoxin I (Table 5.1)). For those nuclear Overhauser effects observed in the 1D steady state NOE experiments, NOE cross-peaks are also seen in the NOESY spectrum, i.e., NOE cross-peaks are seen between peaks A and B (cross-peak #10), peaks C and E (cross-peak #8), and peaks D, H and I (cross-peaks #3 and #4). Further, more NOE cross-peaks correlated to the five most downfield resonances are observed in the spectrum (cross-peaks #1, #2, #5, #6, #7, and #9) (Figure 5.14, 5.15 and Table 5.7).

Since for paramagnetically shifted resonances, the cross relaxation through the nucleus and the paramagnetic center is much more efficient than through other dipolar coupled nuclei, the NOE between two paramagnetically shifted resonances are very week, the NOE cross-peaks observed in the SM-NOESY must arise from closed nuclei. Therefore, based on the X-ray structure of *A. vinelandii* ferredoxin I, the cross-peaks observed in the downfield region of the SM-NOESY spectrum (Figure 5.14) should from cysteinyl protons. Peaks A and B have been assigned to two geminative β-protons of Cys8 (or 49) in the 1D steady state NOE ecperiments, thus cross-peak #9 can be assigned to the Cys8 (or 49) α-β cross-peak based on its chemical shift. Cross-peaks #6 and #7 have been assigned to α-β and β-β cross-peaks of Cys16 respectively based on the facts: a α-cysteinyl proton peak is observed at 7.3 ppm in the 1D ^{1}H NMR difference spectrum obtained from subtracting from the spectrum of native *P. putida* ferredoxin and the one of α-^{2}H-cysteine labeled ferredoxin (Figure 5.6); the chemical shift dispersion of the resonances from the iron-bound cysteines in the NMR spectrum of *A. vinelandii* ferredoxinI should be similar to the NMR spectrum of *P. putida* ferredoxin, because the spin

states of the iron-sulfur clusters in these two 7Fe ferredoxins are the same, the chemical shift ratio of cross-peak #7 is essentially in accord with the ratios of their temperature dependence coefficients (see section 5.4). Based on the similar reasons, cross-peaks #1 and #2 are assigned to α-β and β-β NOE cross-peaks of Cys45 respectively (see section 5.4).

One NOE cross-peak (#5) is observed along the β-cysteinyl proton peak D (16.9 ppm in ω1 dimension) at 0.93 ppm/16.9 ppm (Figure 5.15). The chemical shift of this cross-peak indicates that it arises from the dipole correlation between a β-cysteinyl proton and a methyl group proton. Peak D has been assigned to a β-proton on one cysteine associated with the 4Fe center. The X-ray structure shows that Cys20, 39, 42 and 45 are four cysteines liganded with the irons on the 4Fe center. There are not any experiments which shows that peaks E (which has already been assigned to a β-proton on Cys45) and D arise from β-protons on the same residue. Thus peak D can not arise from a β-proton on Cys45. The distances between the nearest methyl protons and the other three 3Fe center iron-bound cysteines, Cys20, Cys39 and Cys42, are examined by using the X-ray structure of *A. vinelandii* ferredoxin I. This distance examination shows that the shortest distance between the closest methyl proton from γ-CH_3 of Val19 to a β-proton of Cys20 is 3.96 Å. This distance is too large to give a NOE cross-peak in the SM-NOESY spectrum. Since the closest methyl protons from δ-CH_3 of Leu44 is 2.8 Å away from a β-proton of Cys42, and the closest methyl protons from γ-CH_3 of Ile34 are about 2.5 Å away from a β-proton of Cys39, the NOE cross-peak may arise from a nuclear Overhauser effect between these protons. Therefore, based on the NOE cross-peak at 16.9 ppm/0.93 ppm, the β-proton peak D is tentatively assigned to either Cys39 or 42. Neither of these two possibilities can be excluded.

Reduction: An overall spectral line width broadening was seen in the ferredoxin reduction experiments. Line-width broadening can be explained by an intermolecular electron transfer at a rate near the NMR time scale or by protein aggregation. When the 3Fe center was reduced by zinc-reduced methyl viologen or the mixture of zinc reduced methyl viologen and sodium dithionite, the line-widths of the resonances A, B, and C became broader. Meanwhile a intensity decrease with a slightly line broadening was seen for peak E. The degree of these changes are greater than concurrent changes of other resonances, i.e., a broadening seen for the resonances in aliphatic and aromatic regions. It indicates that the broadening in the line-widths of the resonances A-C and E and the intensity loss of peak E are caused by a mechanism related to the reduction of the 3Fe center. A slow intermolecular electron transfer may exist between [3Fe-4S] centers in different molecules. This could explain why a line-width broadening rather than diminishing in intensity is observed for these resonances when the 3Fe center is partially reduced. The rate of this electron transfer must be near the NMR time scale (7). The degree of changes in the intensity and line width of resonance E was not linearly proportional to the line broadening of the resonances A, B, and C. The reason for this is not known.

The ^{1}H NMR spectra, presented here, of the partially reduced ferredoxin, reduced by various reductants are different from the spectrum of methyl viologen partially reduced *A. vinelandii* ferredoxin I reported by Sweeney (1). After the protein was reduced by methyl viologen, Sweeney reported that the ^{1}H NMR spectrum showed no intensity change in

resonance E and the resonances A, B, and C all disappeared. The reason for the different spectrum obtained is not known.

After ferredoxin was reduced by sodium borohydride, no new peaks were found in the downfield region, while the resonances A, B, C and E vanished from the ^1H NMR spectrum. This is in accord with that reported by T. Antony Malikayil in his Ph.D dissertation (8), but it is in contrast to a report by K. Nagayama (4). Previously, K. Nagayama had reported that some new peaks were seen in the downfield region of the ^1H NMR spectrum after *P. putida* ferredoxin was reduced by sodium borohydride (4). The new peaks reported by Nagayama may be from protein denaturation caused by a pH change. No significant pD change was observed in my progressive reduction experiment, where a 1 M phosphate buffer was used. It was noted that the buffer used by Nagayama was 1/15M (67 mM) phosphate. This buffer is not strong enough to keep the pH from changing after the addition of sodium borohydride. A large pH change, from pH 7.4 to about pH 10, was observed when a 50 mM phosphate buffer was used in my experiments.

pH Dependence: For both ferredoxins, the chemical shifts of resonances A-E, and G-H were pH dependent, but resonances F' and F'' were not (Table 5.2, 5.3, 5.4 and 5.5). The resonances assigned as 3Fe cysteinyl β-protons (A-C) all exhibited pK values between 5.3 and 5.7 (Tables 5.2, 5.3, 5.4, and 5.5). It was possible to obtain a reasonable fit corresponding to the titration curves of all three resonances with a pK of 5.6 (27 °C) for *P. putida* ferredoxin and with a pK of 5.4 (27 °C) for *A. vinelandii* ferredoxin I. Since His103 is not existed in *P. putida* ferredoxin, and the imidazole ring of His35 is more closed to the 4Fe center than the 3Fe center,

and it is about 14 Å away from the nearest β-proton on the cysteine associated with the 3Fe center. The contribution from the imidazole ring of His35 is considered very small to the pH titrations of the 3Fe center iron-bound cysteinyl protons. Thus, these pK_a values suggest may represent the influence of one or more aspartic or glutamic acid residues. The closest acidic oxygen is from Asp15, which is 4.9 Å from a sulfide in the 3Fe center. Titration of Asp15 may cause a less specific alternation in conformation near the 3Fe center. No other acidic residue was found within 6 Å of the 3Fe center or a β-proton on a cysteine coordinated with the 3Fe center.

Resonances D, E and G (see later) arise from β-cysteinyl protons on residues bound to the 4Fe center. Peak D exhibits a pK_a near 4.8 (27 °C) for both proteins (Table 5.3 and 5.5). One possible origin of this pH dependence is Asp41, which is hydrogen bonded to the sulfur of Cys39.

The weak pH dependence observed for resonance E (Figure 5.7 and 5.8) is more difficult to explain. The nuclear Overhauser experiments lead to the assignment of this peak as the β-proton of Cys45. Its pK is 6.2 (27 °C) in *P.putida* ferredoxin (Table 5.5) and 6.0 in *A. vinelandii* ferredoxin I (Table 5.3). Although the pK suggests a histidine, there are none nearby. Only His35 is common to both proteins, and its closest ring nitrogen is over 14 Å away from the Cys45 β-proton giving rise to peak E. Indeed, there appear to be no titratable residues in the vicinity of the Cys45 β-proton.

The pH titration shows that peak G has a pK of 5.7 (27 °C) for *A. vinelandii* ferredoxin I (Table 5.3) and 5.5 (27 °C) for *P. putida* ferredoxin (Table 5.5). Although the result from the heteronuclear correlated experiment on *P. putida* ferredoxin indicates that peak G can be assigned to a β-cysteinyl proton. The pK of peak G can not be explained because the origin of this peak is not known.

Resonance H arises from an α-proton of Cys39 or Cys42. The pH titrations show pK_as of 5.1 (27 °C) for *A. vinelandii* ferredoxin I (Table 5.3) and 5.2 (27 °C) for *P. putida* ferredoxin (Table 5.5). These pK values suggest there are acidic-charged groups near to these two α-cysteinyl protons. But no acidic groups are found adjacent to the α-proton on either Cys39 or Cys42 in the X-ray structure. The nearest carboxyl group to the α-proton of Cys39 is Oε1 of Glu38, and it is about 6.6 Å away. For Cys42, the nearest carboxyl group to the α-proton of Cys42 is 6.53 Å away from Oδ2 of Asp41. Thus, presently the origin of the pK for the pH titration of peak H is unknown.

In the pH titration, the appropriate titration data has been fitted to a modified Henderson-Hasselbalch equilibrium (equation 3.1) and also a Hill plot (equation 3.2). The pK_as calculated from these two methods were essentially the same. The Hill coefficient generally has been used to determine protein-ligand binding. In my research, it was found that the Hill coefficient can be used as a reference to keep from peak-mis-monitoring. Generally, the Hill coefficient should be unit. If a far off Hill coefficient is obtained, the peak may be mis-assigned.

5.2 Ring Protons of Aromatic Amino Acids and Histidine

5.2.1 Ring Proton Partial Assignment

P.putida ferredoxin and *A. vinelandii* ferredoxin I each has nine aromatic amino acids (five phenylalanines: Phe2, 25, 31, 55, and 67; two tyrosines: Tyr13 and 26; two tryptophanes: Try78 and 94) (Table 1.2). Two histidines, His35 and 105, are found in the amino acid sequence of *A. vinelandii* ferredoxin I, whereas, only one histidine, His35, is contained in the amino acid sequence of *P. putida* ferredoxin. These resonances were

partially assigned based on their characteristic patterns of spin systems in two-dimensional NMR spectra and the X-ray structure of *A. vinelandii* ferredoxin I, keeping in mind the difference in amino acid sequences between these two ferredoxins.

Figure 5.21A is the D_2O DQF-COSY spectrum of the aromatic region of *A. vinelandii* ferredoxin I in D_2O 50 mM phosphate buffer containing 50 mM NaCl at pH 7.4. Figure 5.22A and Figure 5.23 are the D_2O NOESY and D_2O TOCSY spectra of *A. vinelandii* ferredoxin I under the same condition. Figure 5.21B and 5.22B are the D_2O DQF-COSY and D_2O NOESY spectra of *P.putida* ferredoxin. The aromatic ring proton resonances are usually distributed between the 6 ppm and 8 ppm region. Inspecting D_2O COSY spectra of these two ferredoxins, a number of spin coupled cross-peaks were seen in this aromatic region. They are listed in Table 5.13. These resonances were carefully analyzed by comparing D_2O NOESY and TOCSY spectra. For *A. vinelandii* ferredoxin I, the imidazole ring -CH protons of all of both histidines, His35 and His103, were assigned; the indole ring -CH and -NH protons of both trptophanes were assigned; for two tyrosines and five phenylalanines, the phenyl ring -CH protons of Phe25 and Tyr26 were assigned. For *P. putida* ferredoxin, the imidazole ring -CH protons of His35 were assigned. Furthermore, the ring protons of Try78, Phe25 and Tyr26 were assigned. These partial assignments are summarized in Table 5.13 and the basis for the assignment is given in the discussion section.

The resonances arising from the imidazole ring -CH protons of histidines in both ferredoxins were pH titratable (Figures 5.24, 5.25 and 5.26). After nonlinear least square fit with a Henderson-Hasselbalch equation and Hill plot, the pK_a values of histidinyl ring proton resonances were calculated and presented in Table 5.14. The pK_a values for the pH

Figure 5.21 The D_2O DQF-COSY Spectra of Two 7Fe Ferredoxins in the Aromatic Ring System Proton Region

A: *A. vinelandii* Ferredoxin I

B: *P. putida* Ferredoxin

3.5 mM proteins in a 50 mM Tris-DCl buffer containing 50 mM NaCl with a pH of 7.4

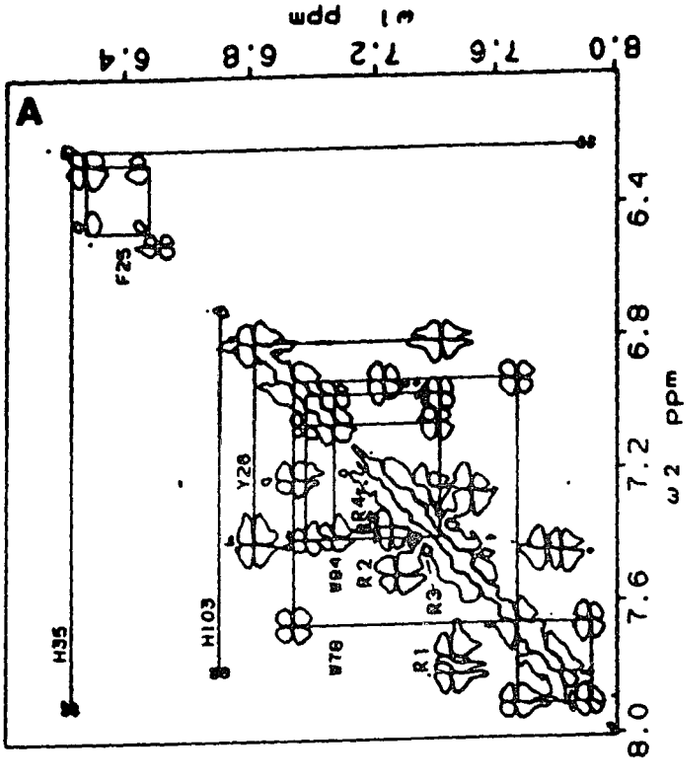
A
ω1 ppm
8.0
7.6
7.2
6.8
6.4
ω2 ppm
F25
Y26
R4
R2
R3
R1
W84
W78
H103
H35

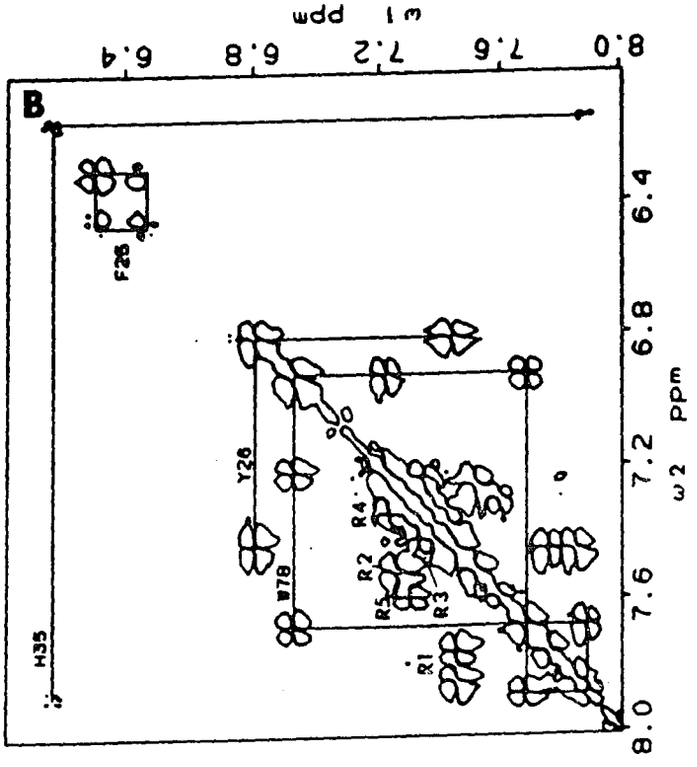
B
ω1 ppm
8.0
7.6
7.2
6.8
6.4
ω2 ppm
F25
Y26
R4
R2
R5
R3
R1
W78
H35

Figure 5.22 The D_2O NOESY Spectra of Two 7Fe Ferredoxins in the Aromatic Ring System Proton Region

A: *A. vinelandii* Ferredoxin I

B: *P. putida* Ferredoxin

3.5 mM proteins in a 50 mM Tris-DCl buffer containing 50 mM NaCl with a pH of 7.4

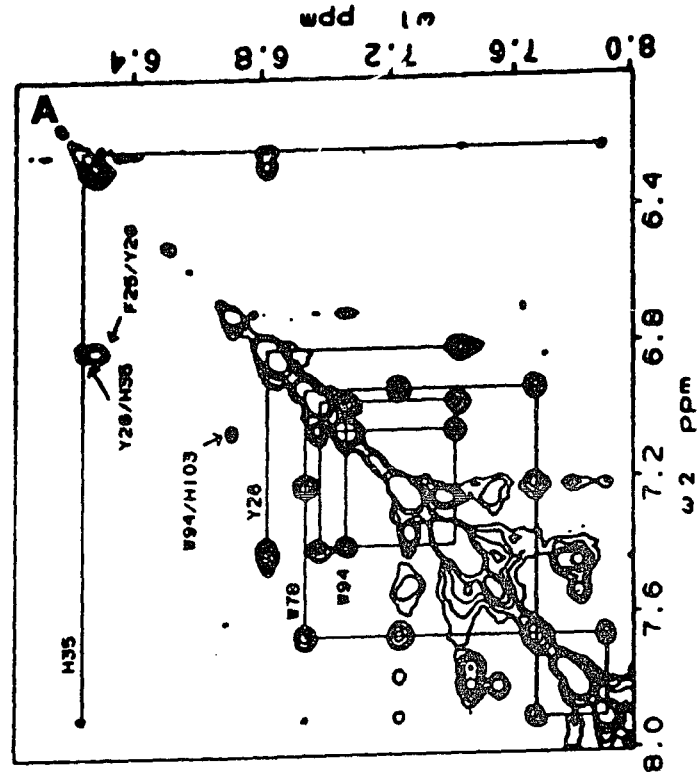
A
F25/Y26
Y26/H35
B94/H103
Y26
B94
B78
H35
ω1 ppm
ω2 ppm
8.0
7.6
7.2
6.8
6.4

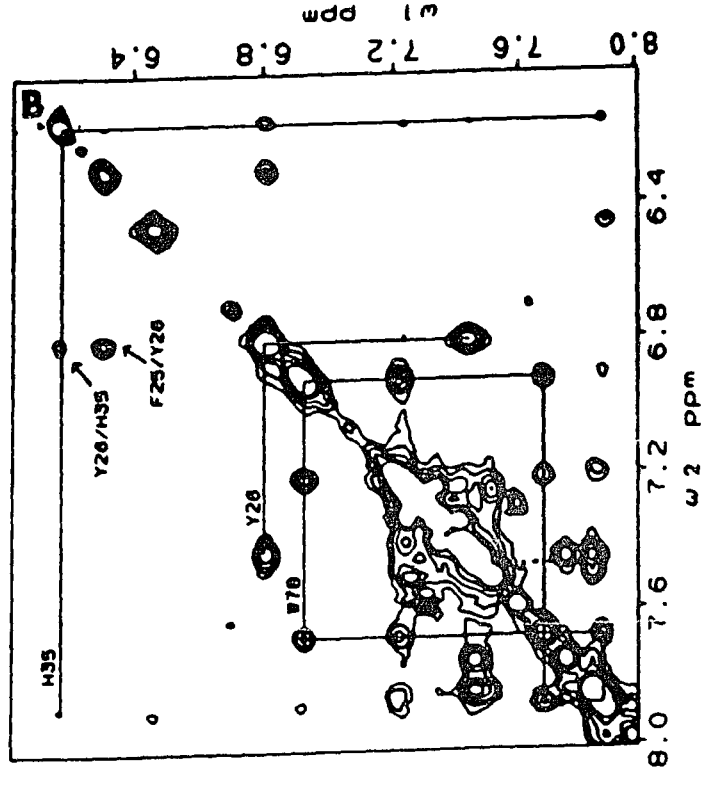
B
F25/Y26
Y26/H35
Y26
B78
H35
ω1 ppm
ω2 ppm
8.0
7.6
7.2
6.8
6.4

Figure 5.23 The D_2O TOCSY Spectrum of *A. vinelandii* Ferredoxin I in the Aromatic Ring System Proton Region

3.5 mM proteins in a 50 mM Tris-DCl buffer containing 50 mM NaCl with a pH of 7.4

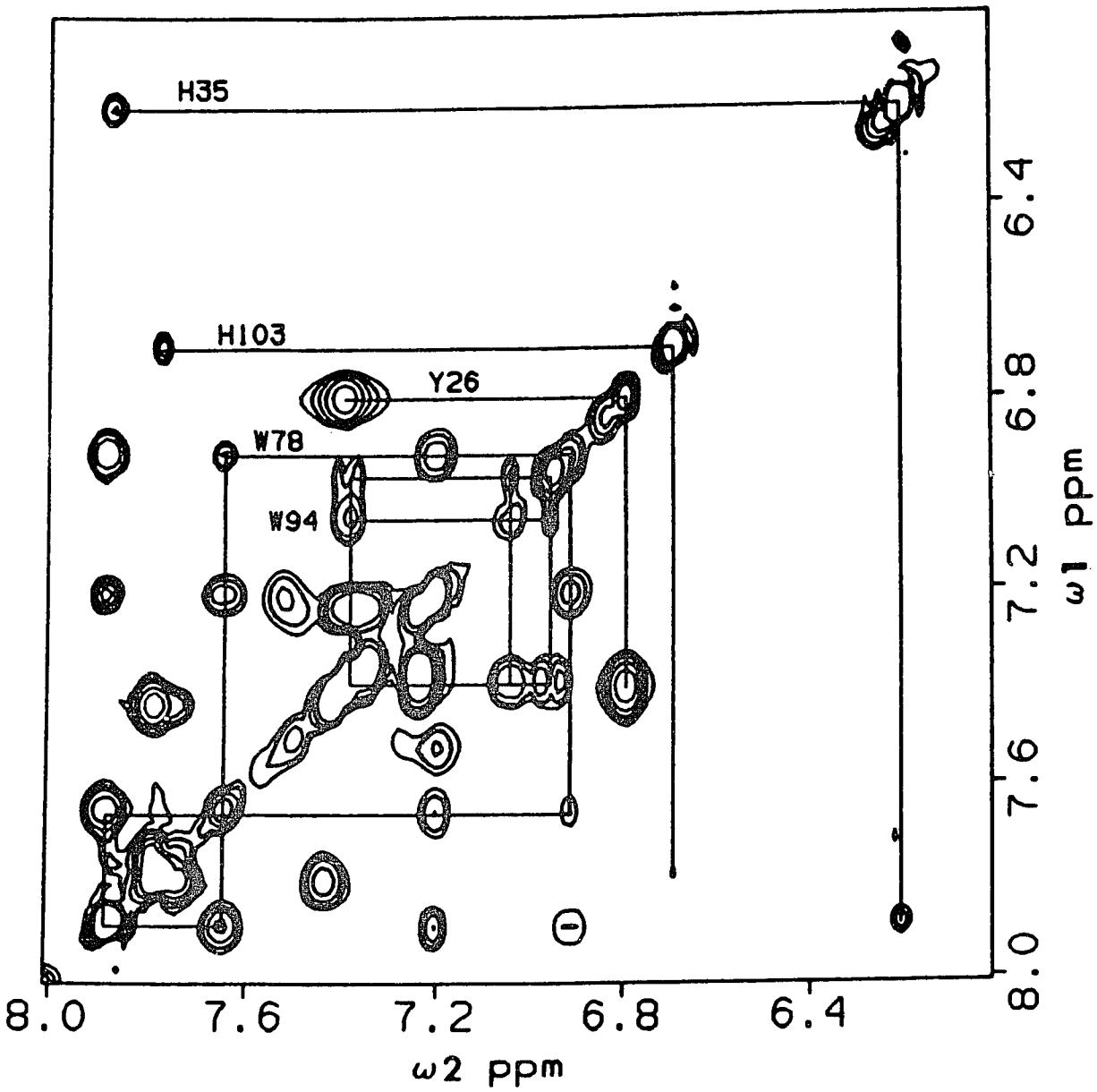
H35
H103
Y26
W78
W94
8.0
7.6
7.2
6.8
6.4
ω2 ppm
ω1 ppm

Table 5.13 Ring System Resonances and Assignments (27 °C)

Spin System	Chemical Shift (ppm)		Assign-ment
	A. vinelandii Fd I	*P. putida* 7Fe Fd	
H1	C2-H: 7.90, C4-H: 6.23	C2-H: 7.88; C4-H: 6.16	His35
H2	C2-H: 7.79, C4-H: 6.71		His103
W1	2H: 7.23, 4H: 7.22, 5H: 6.94, 6H: 7.66, 7H: 7.90, NH: 10.51	4H: 7.21, 5H: 6.93, 6H: 7.68, 7H: 7.89	Trp78
W2	7.39, 7.06, 6.97, 7.40		Trp94
Y1	2,6H: 7.41, 3,5H: 6.81	2,6H: 7.43, 3,5H: 6.81	Tyr26
F1	6.47 ppm/6.27 ppm	6.46 ppm/6.30 ppm	Phe25
R1	7.81/7.45, 7.76/7.45	7.85/7.45, 7.75/7.45	Phe
R2	7.51 ppm/7.27 ppm	7.51 ppm/7.26 ppm	
R3	7.42 ppm/7.35 ppm	7.41 ppm/7.33 ppm	
R4	7.37 ppm/7.26 ppm	7.34 ppm/7.23 ppm	
R5		7.59 ppm/7.30 ppm	

a. All chemical shifts are referenced to water peak at 4.78 ppm.

Figure 5.24 pH Titration for His35 Imidozle Ring -CH Protons of *P. putida* 7 Fe Ferredoxin

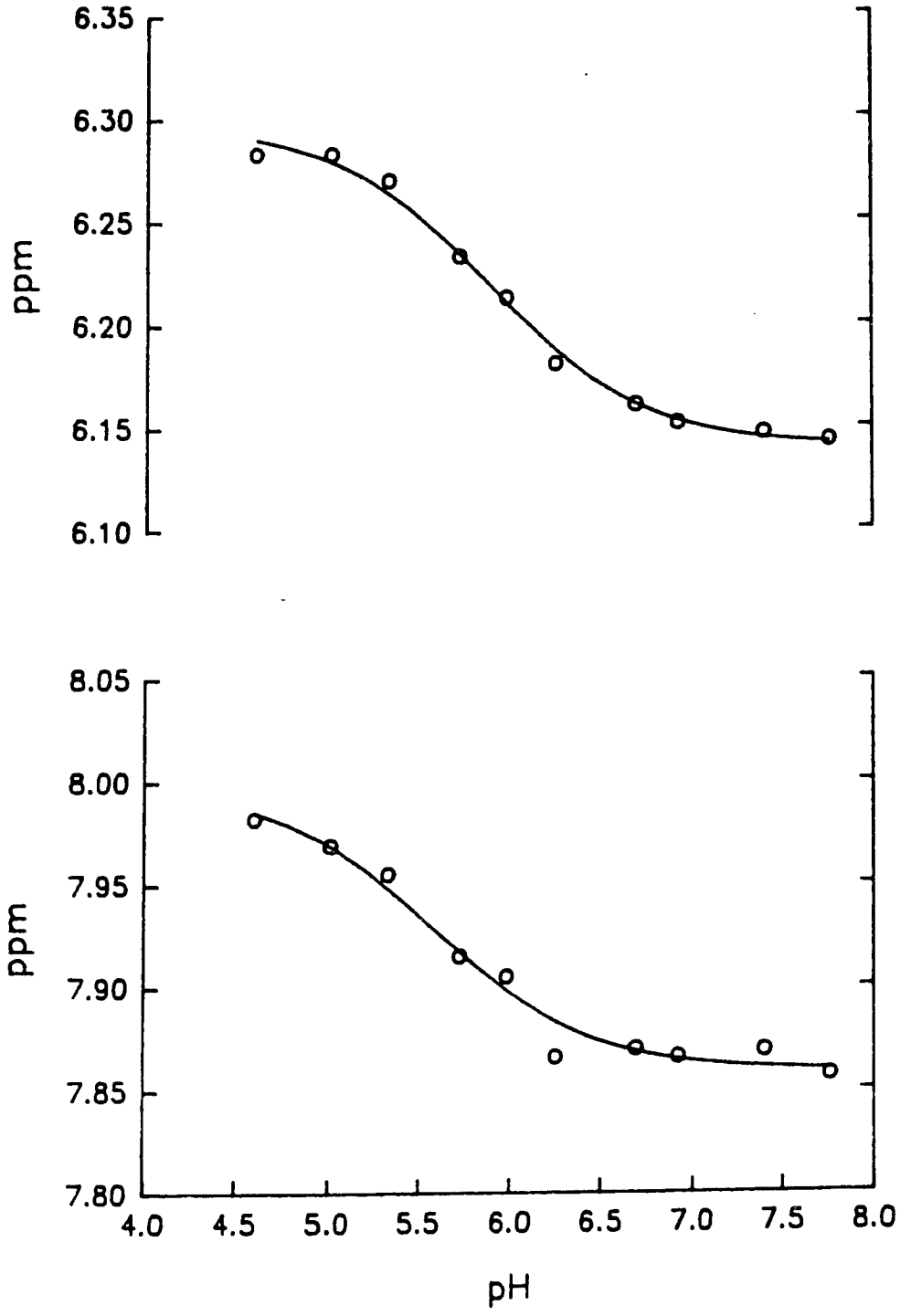
6.35
6.30
6.25
6.20
6.15
6.10
ppm
8.05
8.00
7.95
7.90
7.85
7.80
ppm
4.0
4.5
5.0
5.5
6.0
6.5
7.0
7.5
8.0
pH

Figure 5.25 pH Titration for His35 Imidozle Ring -CH Protons of *A. vinelandii* 7 Fe Ferredoxin

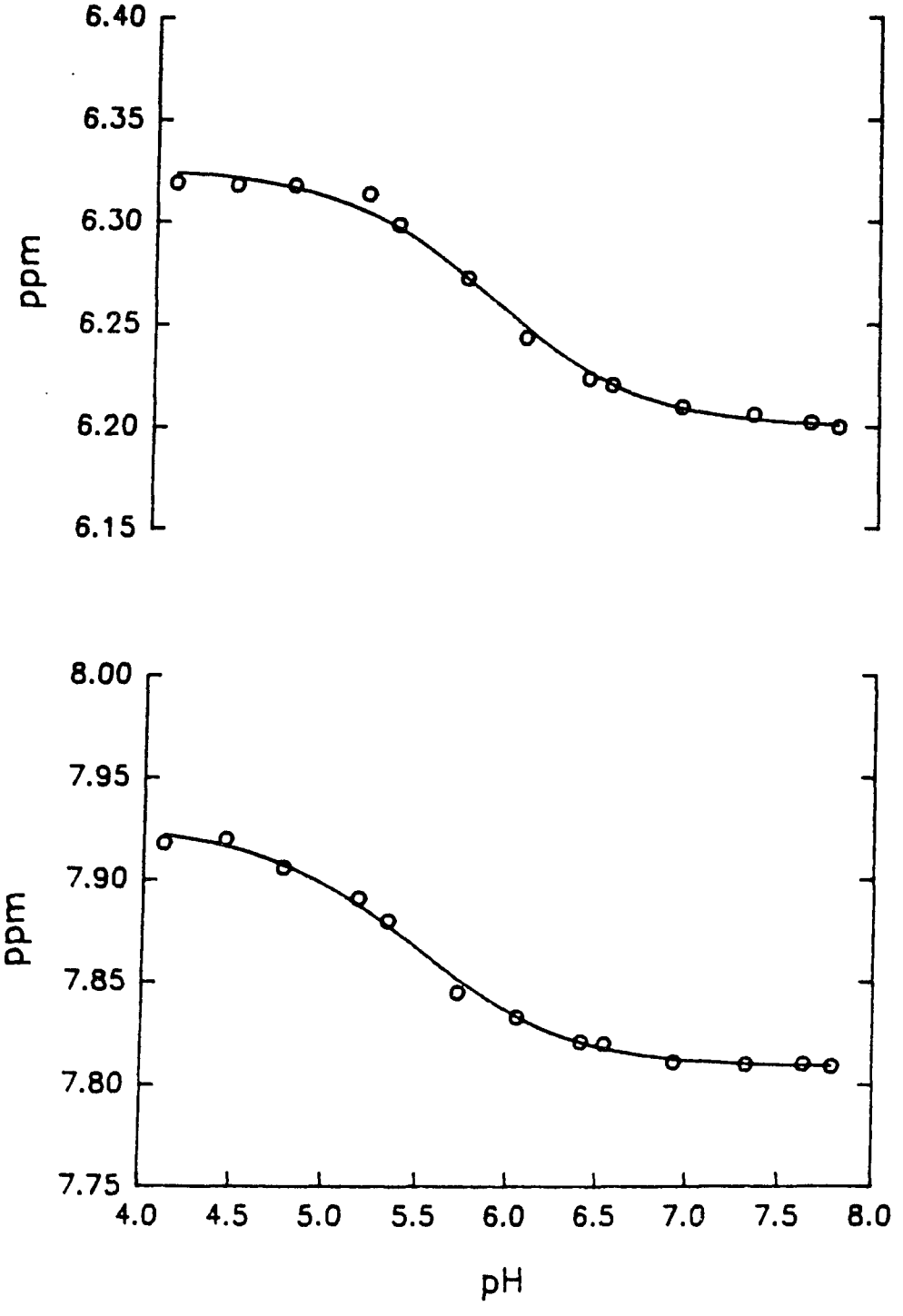
6.40
6.35
6.30
6.25
6.20
6.15
ppm
8.00
7.95
7.90
7.85
7.80
7.75
ppm
4.0
4.5
5.0
5.5
6.0
6.5
7.0
7.5
8.0
pH

Figure 5.26 pH Titration for His103 Imidozle Ring -CH Protons of *A. vinelandii* 7 Fe Ferredoxin

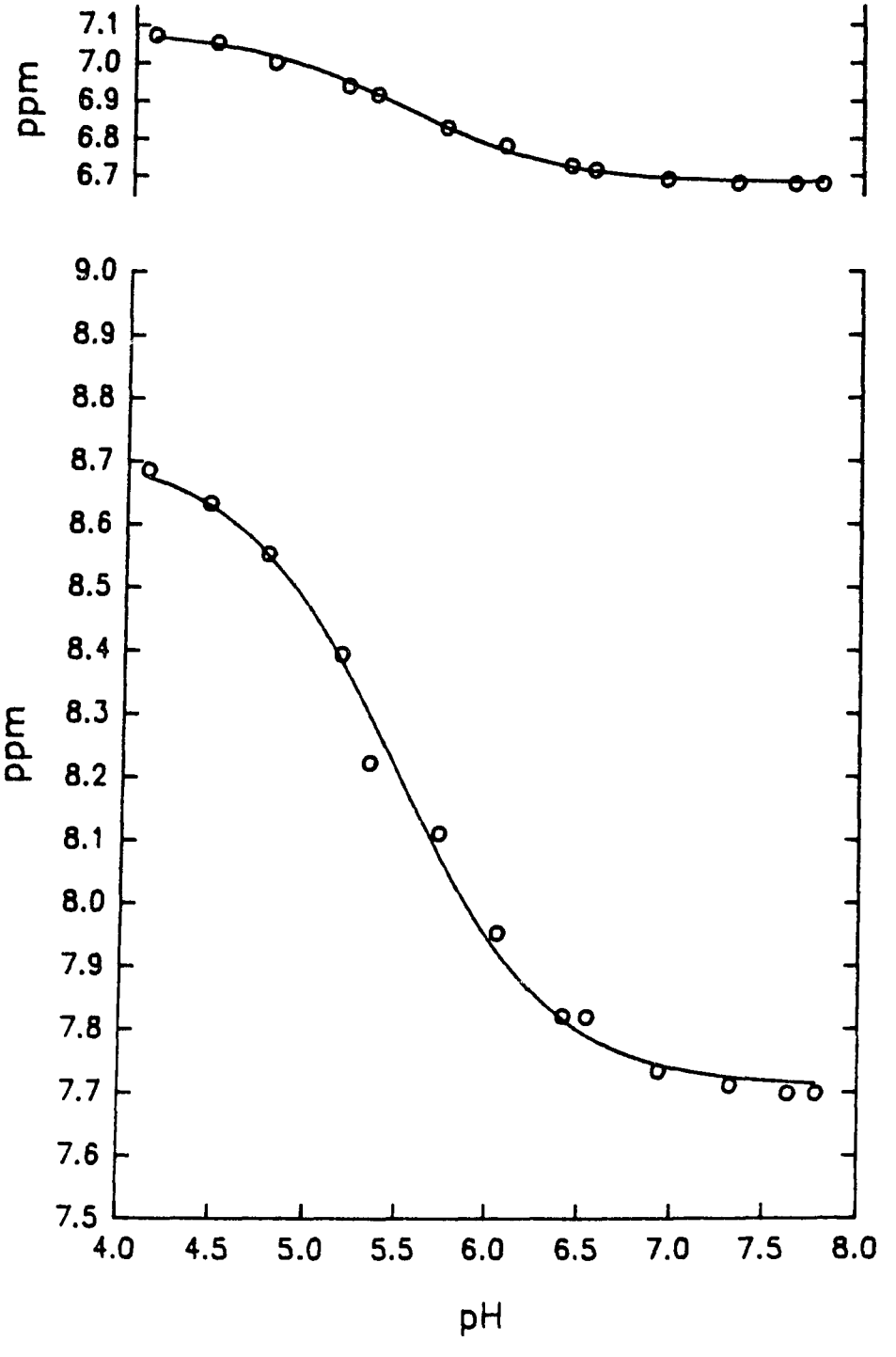
ppm
7.1
7.0
6.9
6.8
6.7
ppm
9.0
8.9
8.8
8.7
8.6
8.5
8.4
8.3
8.2
8.1
8.0
7.9
7.8
7.7
7.6
7.5
4.0
4.5
5.0
5.5
6.0
6.5
7.0
7.5
8.0
pH

Table 5.14 Titration Parameters of the Histidinyl Residues of Two 7Fe Ferredoxins at 28 °C

				Henderson-Hasselbalch Equation			Hill Plot	
Ferredoxin	Histidine	Proton	pK_a	δ_{AH}(ppm)	δ_A-(ppm)	$\Delta\delta_{AH,A}$-(ppm)	pK_a	Hill Coefficient
A. vinelandii	H35	C2-H	5.5	7.93	7.81	0.12	5.5	0.91
		C4-H	5.9	6.33	6.20	0.13	5.8	1.10
	H103	C2-H	5.5	8.71	7.71	1.00	5.5	0.95
		C4-H	5.5	7.08	6.68	0.40	5.5	0.90
P. putida	H35	C2-H	5.6	8.00	7.86	0.14	5.6	0.97
		C4-H	5.9	6.30	6.14	0.16	5.9	1.09

1. δ_{AH}, δ_A- and $\Delta\delta_{AH,A}$- are the results of a nonlinear least-square fit to a modified Henderson-Hasselbalch equation and the chemical shifts are referenced to DSS at 0 ppm.

2. pK_a are the results of a nonlinear least-square fit to a modified Henderson-Hasselbalch equation or a Hill plot.

titrations of two histidinyl ring proton resonances, both arising from His35, are different for both ferredoxins. Whereas, the pK_as are essentially the same for the resonances arising from the analogous protons in different ferredoxin. For example, the pK_a value of His35 C4-H in *A. vinelandii* ferredoxin I was 5.9, which was the same as that in *P. putida* ferredoxin (Table 5.14). The pK_a value of C2-H of His35 in *A. vinelandii* ferredoxin I was 5.5, which was close to the pK_a of 5.6 for the resonance arising from the C2-H of His35 in *P. putida* ferredoxin. It implies that the local ionization states of His35 for these two ferredoxins are similar. Furthermore, the titration steps of His35 are from 0.12 to 0.16 ppm for these two ferredoxins, which are lower than the values, 0.95 ppm of C2-H and 0.42 ppm of C4-H, for the model peptide studies (9, 10).

The pH titration curves of two resonances arising from two His103 imidazole -CH ring protons, C2-H and C4-H, of *A. vinelandii* ferredoxin can be fit with a single pK_a of 5.5. This is lower than the pK_a of 6.8 reported in model peptide studies (9, 10). The titration step was 0.4 ppm for C4-H and 1.0 ppm for C2-H; these values are very similar as that of the model peptides (9,10).

5.2.2 Discussion

Histidine: The two long range scalar coupled imidazole ring protons, C2-H and C4-H, give rise to characteristic patterns of symmetric cross-peaks in the aromatic ring system proton region of D_2O COSY spectra (Figure 5.21). Two such long rang scalar coupling cross-peaks were seen in the D_2O DQF-COSY spectrum of *A.vinelandii* ferredoxin I (Figure 5.21 top), while only one of this type cross-peak was seen in the spectrum of *P. putida* ferredoxin (Figure 5.21 bottom). This is expected, as *A. vinelandii*

ferredoxin I has two histidines, His35 and His103, but *P. putida* ferredoxin has only one histidine, His35 (Table 1.2). Thus comparing the DQF-COSY spectra of these two ferredoxins in the aromatic region, the resonances of C2-H and C4-H of His35 in these two ferredoxins are assigned, and at the same time the assignment of ring protons of His103 in *A. vinelandii* ferredoxin I is also given (Table 5.13).

The pK_a values of His35 imidazole ring -CH protons in the two ferredoxins are between 5.5 and 5.9. They are lower than the values of 6.8 and 7.0 obtained from the model peptides, Gly-His-Gly by Markley (9) and Gly-Gly-His-Ala by Bundi & Wüthrich (10). Furthermore, the titration steps $\Delta\delta_{AH,A^-}$ for His35 residues in *A. vinelandii* ferredoxin I were 0.12 and 0.13 ppm for C2-H and C4-H, and in *P. putida* ferredoxin were 0.14 and 0.16 ppm for C2-H and C4-H respectively (Table 5.14). These values are lower than 0.95 and 0.42 for C2-H and C4-H respectively in the model peptides (9 and 10). No single pK_a value can fit the titrations of both the C2-H and C4-H resonances from His35. This implies that these pK_a values do not originate from the pH perturbation of histidinyl ring current. The X-ray structure of *A. vinelandii* ferredoxin I shows that there is a hydrogen bond between the imidazole ring N1 of His35 and Oε2 of Glu76 (11), and Oδ2 of Asp37 is only 1.92 Å away from C2-H of His35. Thus, the pK_a value of C2-H of His35, 5.5, for *A. vinelandii* ferredoxin I, and 5.6 for *P. putida* ferredoxin, may reflect the pH titration of the carboxyl side group of Asp37. The origin of the pK_a of C4-H of His35, 5.9, for both ferredoxins, is from Glu76.

Although the pK_a value of His103 is also lower compared with the model peptides (9 and 10), the titration steps, $\Delta\delta_{AH,A^-}$, are comparable to the model peptides (9 and 10), and the pK_a of the C2-H proton is the same as for the C4-H proton. Thus, the pK_a of His103, 5.9, is due to the pH perturbation

of the imidazole ring current. A low pK_a observed may be because the ε-amino group of Lys10, which is right on top of the imidazole ring of His103 and about 5 Å away. The unfavorable interaction between two positive charged side chain groups is eliminated when the imidazole ring of His103 is deprotonated at neutral pH.

Tyrosine: The ring protons of tyrosine can be assigned by the fact that only one cross-peak is expected in the aromatic ring proton region of the D_2O DQF-COSY, which arises from the 2,6H and 3,5H ring protons. However, this kind of cross-peak may also arise from the 2,6H and 3,5H of phenylalanine ring protons when the chemical shifts of 4H and 3,5H ring protons are very close to each other. In that case, the cross-peak from phenylalanine 4H and 3,5H ring protons is near the diagonal and can not be identified. The ring protons of tyrosine herein are assigned using observed cross-peak in the NOESY spectrum based on distance information from the X-ray structure of *A. vinelandii* ferredoxin I. Tyr26 is the only aromatic amino acid which is within 5 Å of His35. The distance between the ring protons H5 of Tyr26 and C4-H of His35 is only 3.77 Å (Table 5.15). It gives rise to a symmetric NOE cross-peak at 6.23 ppm/6.81 ppm (*A. vinelandii*) in the D_2O NOESY spectrum (Figure 5.22). An average distance was calculated based on the intensities of the NOE cross-peaks in the NOESY of *P. putida* ferredoxin scaled on the distance of 2.44 Å for two vicinal ring protons of Tyr26. A 3.6 Å distance between 4H of His35 and H3,5 of Tyr26 was obtained, in good agreement with the X-ray structure. A similar calculation was also performed for the NOESY of *A. vinelandii* ferredoxin I. Because of peak overlap, the distance obtained from the *A. vinelandii*

calculation is not reliable. Thus, the cross-peak at 7.41 ppm/6.81 ppm is assigned to the ring protons, 2,6H and 3,5H of Tyr26.

Tryptophan: The four spin coupled indole ring protons, H4, H5, H6, and H7 of a Tryptophan give a characteristic patterns in D_2O COSY (Figure 5.21) and D_2O TOCSY spectra (Figure 5.23) (12). However, an examination of these two spectra only allows the cross-peaks between *ortho*-coupled nuclei to be assigned. A specific assignment is carried out by examining the NOESY spectrum in H_2O, where it is possible to identify cross-peaks between the Trp indole-NH proton and the neighboring C2-H and C7-H protons. Two such NOE cross-peaks are seen in the H_2O NOESY spectrum of *A. vinelandii* ferredoxin I at 7.23 ppm/10.51 ppm and 7.90 ppm/10.51 ppm (the spectrum is not shown here). Comparing with the H_2O COSY spectrum (the spectrum is not shown here), the cross-peak 7.23 ppm/10.51 ppm is assigned to the Trp78 indole-NH and C2-H proton cross-peak. The ring protons of Trp94 of *A.vinelandii* Fd I are assigned because Trp94 is the only aromatic amino acid which is close to the His103 (Table 5.15). A symmetric NOE cross-peak at 6.71 ppm/7.05 ppm is seen in the D_2O NOESY spectrum (Figure 5.20 top). This NOE cross-peak has been considered from the ring protons of His103 C4-H and one of the indole ring protons on Trp94. A 3.4 Å distance is obtained from the distance calculation. This distance does not agree with that observed in the X-ray structure (Table 5.15). Although the imidazole ring proton C2-H of His103 is close to two indole ring protons, H5 (3.0 Å) and H6 (3.3 Å), no NOE cross-peak arising from these resonances is observed in the NOESY spectrum. The X-ray structure shows that both His103 and Try94 are on the surface of the protein. Therefore, the side chain groups of these two amino acids have

Table 5.15 The Proton-Proton Distances Between the Closest Aromatic Ring Protons and the Ring Protons of Histidinyl Residues in *A. vinelandii* Ferredoxin I

Histidine	Proton	Tyr 26			Trp 94	
		H3	H5	H6	H5	H6
His35	C4-H	4.76 Å	3.77 Å	4.41 Å		
His103	C2-H				3.00 Å	3.26
	C4-H				4.72 Å	

All distances are measured from the revised X-ray structure of *A. vinelandii* ferredoxin I (14)

higher rotation freedom than the side chain groups on the residues buried inside the protein, the orientation of the imidazole ring of His103 to the indole ring of Trp94 in solution may be somewhat different from in the crystal structure. The specific assignment for indole ring protons can not be given at this step, because no cross-peaks arising from Trp indole-NH proton and C2-H or C4-H protons is seen in the H_2O spectra. This is presumably because that the Trp94 is on the surface of the protein, and so the indole-NH proton of Trp94 may be much more rapidly exchangeable.

The chemical shifts of resonances from indole ring protons of Trp94 in *P. putida* ferredoxin are different from those in *A. vinelandii* ferredoxin I. The indole ring protons of Trp94 can not be assigned. A comparison of the amino acid sequences of these two ferredoxins shows that there is significant amino acid variation in these region, e.g., His103 in *A. vinelandii* ferredoxin I is substituted by a Asp103 in *P. putida* ferredoxin (Table 1.2). Thus, a considerable alteration in local structure between these two 7Fe ferredoxins is not surprising, resulting from the primary amino acid sequence difference.

Phenylalanine: *A. vinelandii* ferredoxin I and *P. putida* ferredoxin each contains five phenylalanines. A symmetric NOE cross-peak at 6.23 ppm/6.81 ppm is seen in the D_2O NOESY spectrum (Figure 5.22), which arises from Tyr26 2,6H and another aromatic amino acid ring proton. In the X-ray structure of *A. vinelandii* ferredoxin I, Phe25 is the only aromatic amino acid close to Tyr26. However, the X-ray structure shows that the distances between any two ring protons on these two residues are more than 5 Å away. A rotation along either one or both Cβ-Cγ bonds of these two aromatic amino acids does not result in a distance of less than 5 Å between

any two ring protons on these two residues. It may reflect that a local difference between the crystal and solution structure.

5.3 β-Cysteinyl Carbon Resonances and Their Correlated β-Cysteinyl Proton Assignments

The β-carbons of cysteines in *P. putida* 7Fe ferredoxin have been ^{13}C enriched by growing *P. putida* cystine auxotroph cells in the presence of d,l-[3,3'-^{13}C]-cystine (2 g in 50 l medium). The magnetogyric ratio of carbon (γ_{13C}: 1070.3 Hz/G) is four times smaller than proton (γ_{13H}: 4257.7 Hz/G), and the chemical shift dispersion in the ^{13}C NMR spectrum is larger than in the ^{1}H NMR spectrum. Therefore, the line-widths of paramagnetically shifted carbon resonances should be smller than that of the proton resonances, and peak overlap in ^{13}C NMR spectrum should be less than in ^{1}H NMR spectrum. Further, since the natural abundance of ^{13}C is only 1.1%, the resonances arising from ^{13}C labeled carbons should have much larger intensities than for unlabeled carbons.

Figure 5.27 is the 100.4 MHz ^{13}C NMR spectrum β-^{13}C-cysteine labeled *P. putida* ferredoxin. Eight peaks were distinct from the natural abundant resonances. They were lying near 174.4, 152.0, 112.2, 110.8, 94.7, 88.3, 39.9, and 32.7 ppm at 28 °C and were labeled as 1, 2, 3, 4, 5, 6, 7, and 8 respectively. From the previous deuteration studies and HPLC amino acid analysis of β-^{14}C-cystine labeled ferredoxin, these eight peaks must arise from the β-carbons on cysteinyl residues. Temperature dependence studies showed that peaks 2-6 were anti-Curie temperature dependent, whereas peak 1 was Curie temperature dependent (Figure 5.28). Peak 7, and peak 8 were nearly temperature independent. The chemical shifts for these two β-cysteinyl carbon resonances (39.9 and 32.7 ppm at 28 °C) are comparable to

Figure 5.27 100.4 MHz ^{13}C NMR Spectrum of *P. putida* 7Fe Ferredoxin Isolated form the Cells Grown in the Presence of β',β''-^{13}C-Cystine (7 °C)

0.2 mM protein dissolved in a 50 mM Tris-DCl and 50 mM NaCl buffer with a pH of 7.4

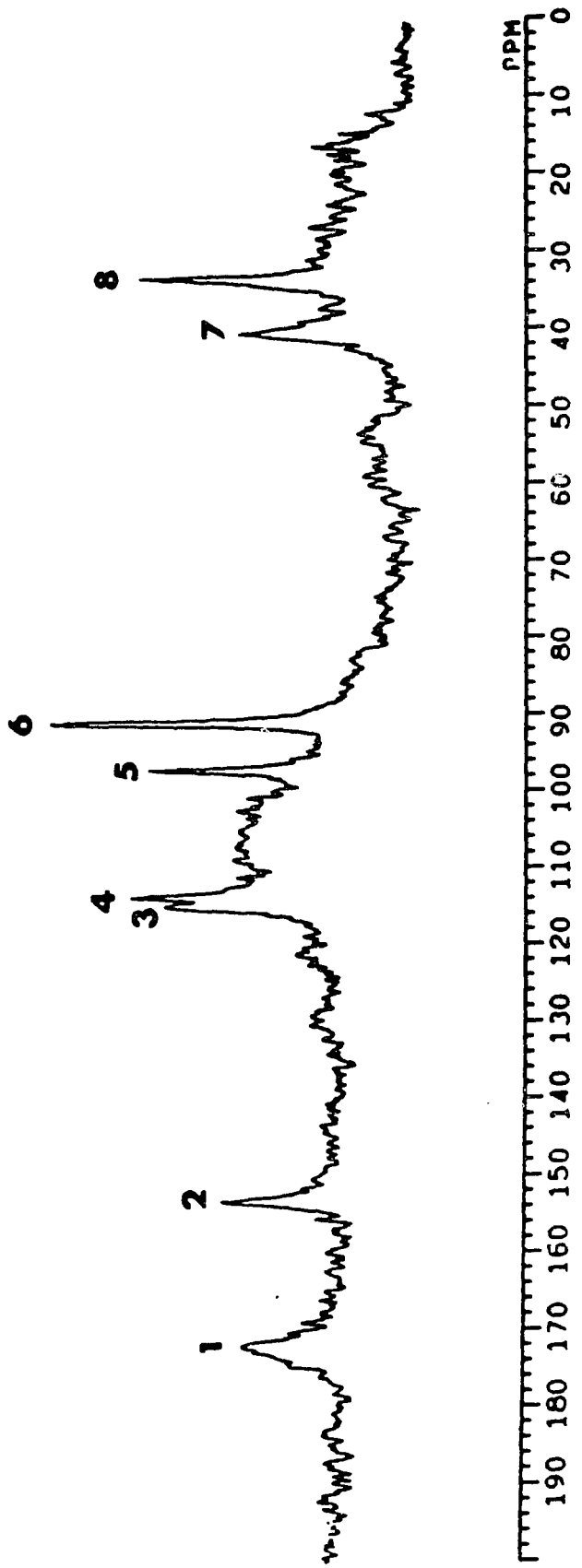
1
2
3
4
5
6
7
8
PPM
0
10
20
30
40
50
60
70
80
90
100
110
120
130
140
150
160
170
180
190

Figure 5.28 Temperature Dependences of β-Cysteinyl Carbon Resonances in the NMR Spectrum of *P. putida* 7Fe Ferredoxin

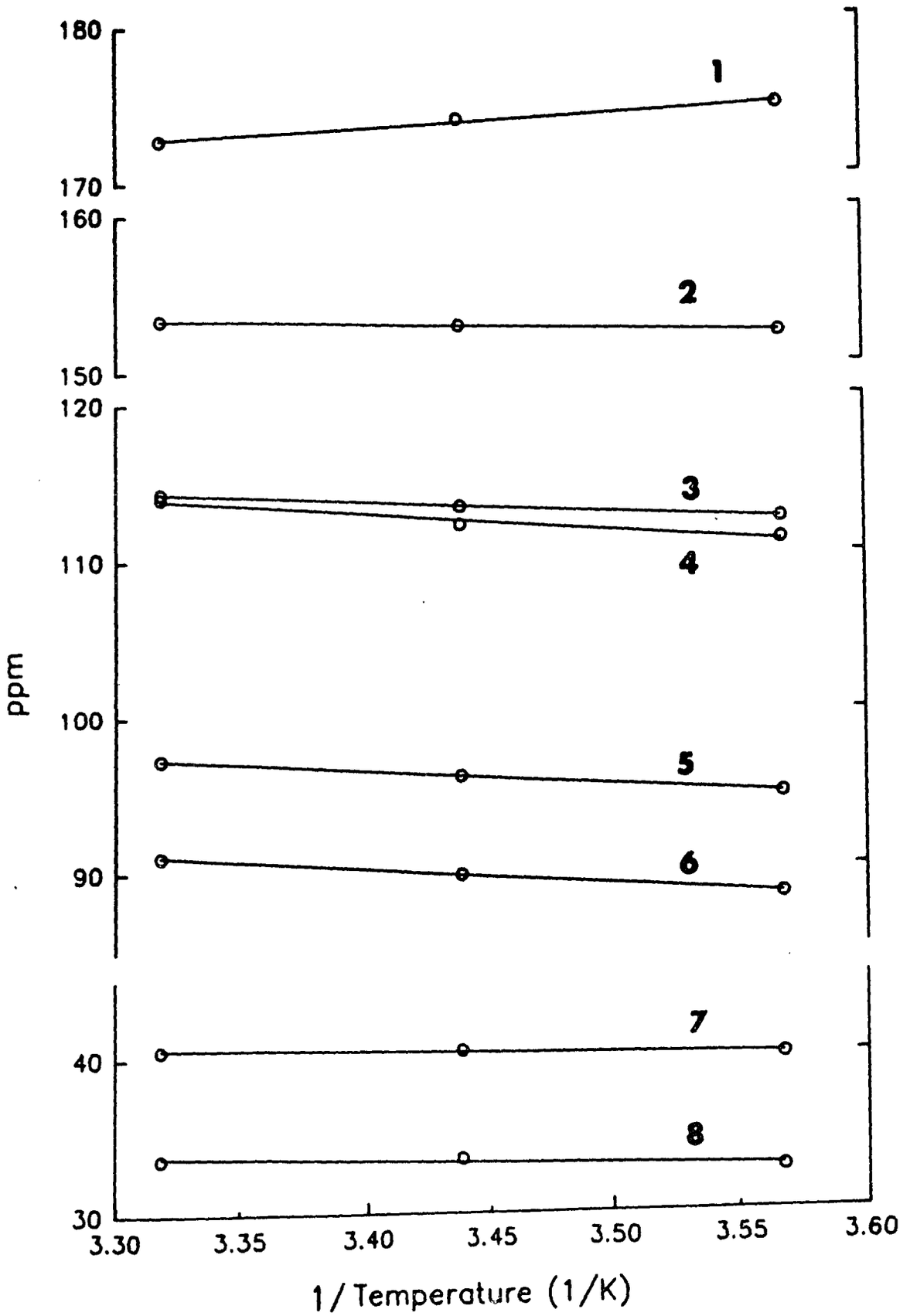
180
170
160
150
120
110
100
90
40
30
ppm
1
2
3
4
5
6
7
8
3.30
3.35
3.40
3.45
3.50
3.55
3.60
1/ Temperature (1/K)

the expected chemical shift of a free amino acid β-carbon resonance. Thus peak 7 and 8 arise from the β-carbons on the cysteinyl residues with free sulfhydryl groups, Cys11 and Cys24. The remaining six peaks, 1-6, are assigned to β-carbons on the iron-bound cysteines. Their chemical shifts are in the region between 80 ppm and 180 ppm, consistent with what have been seen in ^{13}C NMR spectroscopy studies of three 2[4Fe-4S] ferredoxins (13).

Since proton-proton one bond *J* coupling constant is very small ($^1J_{HH} \leq 10$ Hz), the time required for coherence transfer between two protons is relatively longer. During this relatively long time period, the fast relaxed paramagnetic protons have decayed away. Therefore, the correlation transfer between two paramagnetically shifted protons is difficult to be seen in normal 2D homonuclear *J*-correlated experiments. However, since ^{13}C-^1H has a relative large one-bond *J* coupling ($^1J_{CH} \sim 125$ Hz), coherence transfers can be effected in a short period of time in a heteronuclear correlated experiment. This allows the fast relaxed β-protons on the iron-bound cysteine to be assigned, through the correlation between these protons and their scalar coupled (through chemical bond) β-cysteinyl carbon.

The correlation between these eight β-cysteinyl carbon resonances and previously assigned β-cysteinyl protons was studied by carbon on resonance decoupling during FID accumulation and proton detected heteronuclear correlated spectroscopy, HMQC (heteronuclear multiple quantum correlated spectroscopy). Figure 5.29 (top) shows the ^1H NMR spectrum of β-^{13}C-cysteine labeled *P. putida* ferredoxin with carbon on-resonance decoupling at carbon peak 5 (95 ppm). Figure 5.29 (middle) is the

Figure 5.29 Downfield Region of the 400 MHz ^{1}H NMR Spectrum of *P. putida* 7Fe ferredxoin with Carbon On-Resonance Decoupling

0.05 mM protein in 50 mM Tris-DCl buffer containing 50 mM NaCl with a pH of 7.4

A: a carbon on resonance decoupling is set on carbon peak 5 (95 ppm)

B: a carbon on resonance decoupling is set on carbon peak 6 (88 ppm)

C: the difference spectrum obtained from subtracting spectrum A from spectrum B

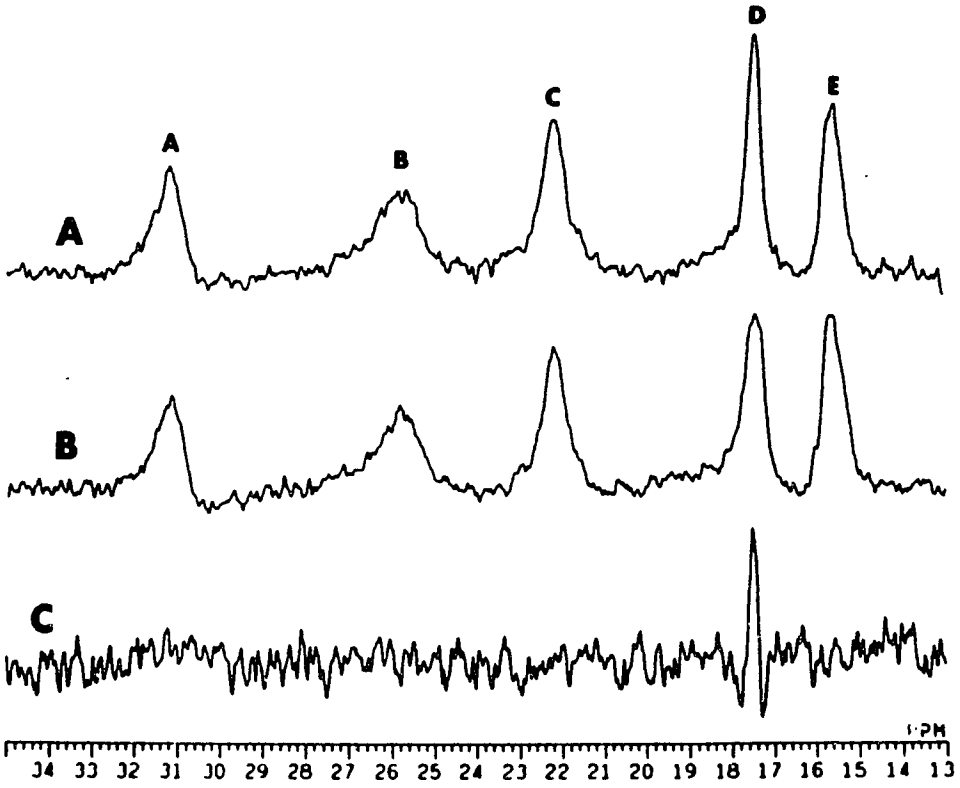
A
B
C
D
E
A
B
C
δ PPM
34 33 32 31 30 29 28 27 26 25 24 23 22 21 20 19 18 17 16 15 14 13

^{1}H NMR spectrum of β-^{13}C-cysteine labeled *P. putida* ferredoxin with carbon on resonance decoupling at the carbon peak 6 (88 ppm). The difference spectrum (Figure 5.29 bottom) indicated that the intensity of proton peak D was changed when a decoupling carbon frequency was setting on peak 5. Therefore, the β-cysteinyl proton resonance, peak D, was correlated to the β-cysteinyl carbon resonance, peak 5. Thus they arise from the same cysteinyl residue, Cys39 or 42. Similarly, the intensity of the proton peak E was changed when a carbon decoupling frequency was set between peak 3 and 4 (111.5 ppm) (Figure 5.30). Thus, proton peak E and the carbon peak 3 or 4 are assigned to β-proton and β-carbon on the same cysteinyl residue, Cys45 respectively.

The correlation between β-cysteinyl proton resonances and β-cysteinyl carbon resonances was also studied by proton detected heteronuclear correlated spectroscopy, HMQC. Figure 5.31 shows the HMQC spectrum of β-^{13}C cysteinyl carbon enriched *P. putida* ferredoxin. The correlated β-cysteinyl proton resonances for five β-cysteinyl carbon resonances were seen in the spectrum. The cross-peaks are splited by β-^{13}C-cysteinyl carbon about 125 Hz along the proton frequency. These peaks are assigned and summarized in Table 5.16. The two β-cysteinyl proton resonances which correlated to the carbon peak 7 were at 5.8 and 2.1 ppm, and the correlated β-proton resonances of carbon peak 8 were at 2.7 and 2.3 ppm. The carbon peaks 7 and 8 have been assigned to β-cysteinyl carbons on two cysteines with free sulfhydryl groups. The random coil ^{1}H chemical shifts for two geminal pair β-cysteinyl proton resonances are 3.28 and 2.96 ppm (12). Thus, the chemical shifts of the correlated β-proton resonances consistent the previous assignment. The reason for the one of the correlated β-cysteinyl proton resonance with a unusually large chemical

Figure 5.30 Downfield Region of the 400 MHz ^{1}H NMR Spectrum of *P. putida* 7Fe ferredxoin with Carbon On-Resonance Decoupling

A: a carbon on resonance decoupling is set between carbon peaks 3 and 4 (111.5 ppm)

B: a carbon on resonance decoupling is set on carbon peak 6 (88 ppm)

C: the difference spectrum obtained from subtracting spectrum A from spectrum B

0.05 mM protein in 50 mM Tris-DCl buffer containing 50 mM NaCl with a pH of 7.4

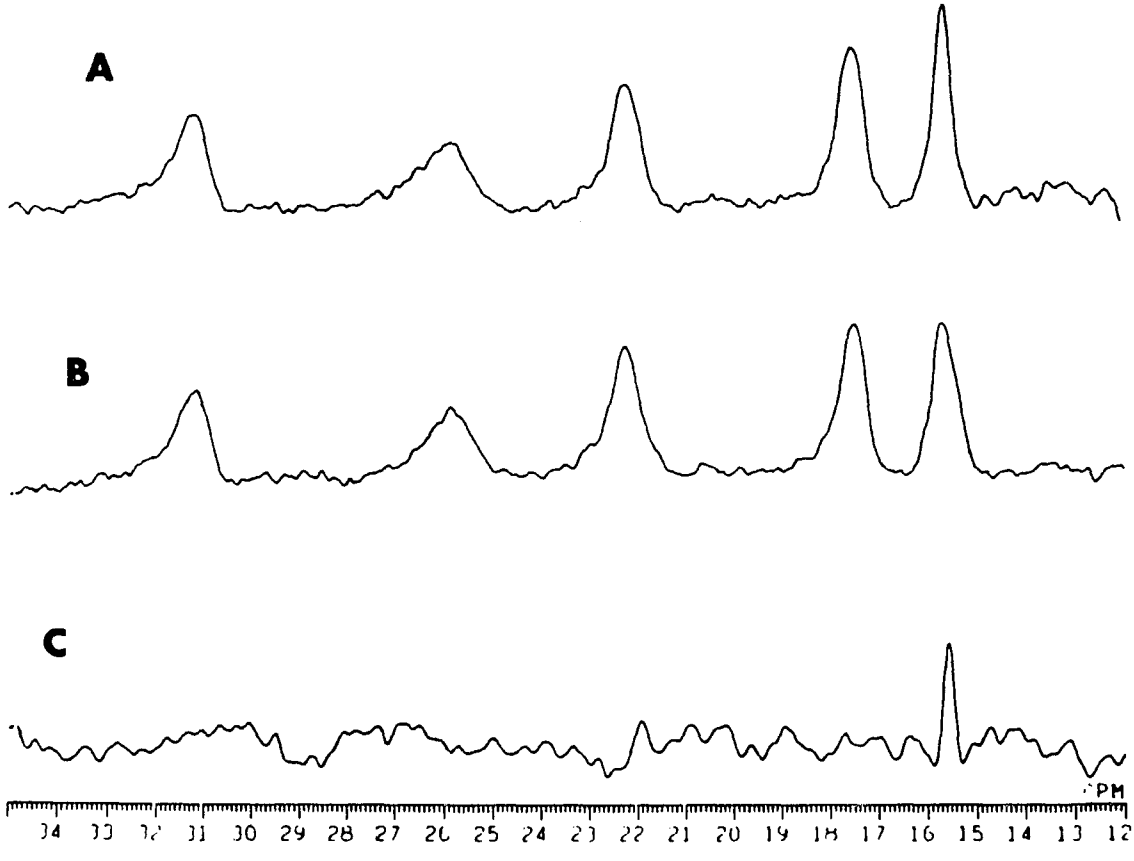
A
B
C
PPM
34 33 32 31 30 29 28 27 26 25 24 23 22 21 20 19 18 17 16 15 14 13 12

Figure 5.31 HMQC Spectrum of *P. putida* 7Fe Ferredoxin (7 °C)

0.02 mM Protein in a 50 mM Tris-DCl buffer containing 50 mM NaCl with a pH of 7.4

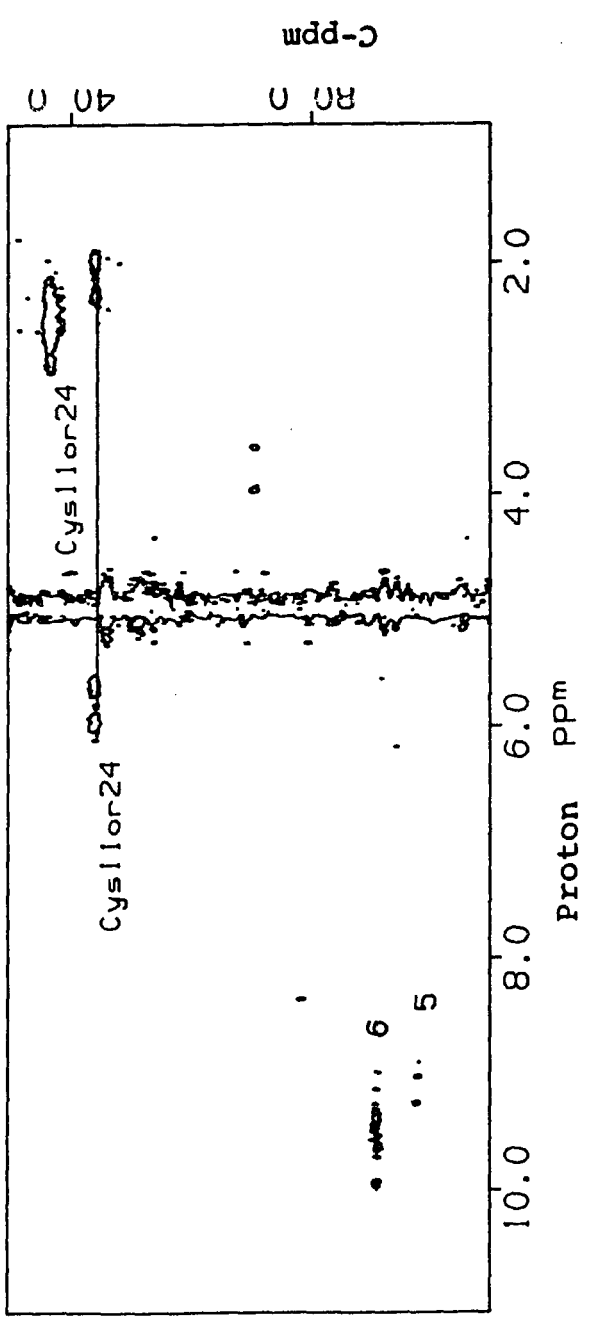
C-ppm
40
80
Cys11or24
Cys11or24
6
5
2.0
4.0
6.0
8.0
10.0
Proton ppm

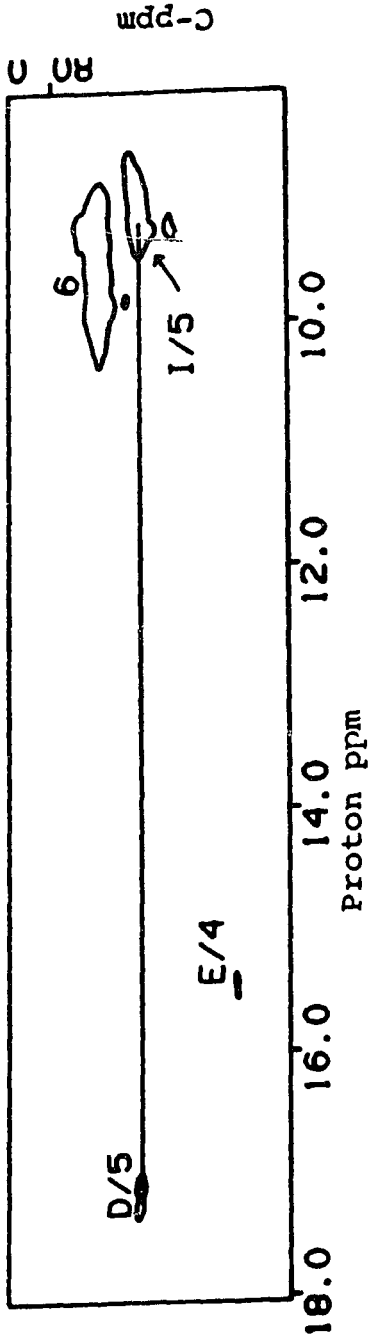
C-ppm
80
6
I/5
D/5
E/4
10.0
12.0
14.0
16.0
18.0
Proton ppm

Table 5.16 β-^{13}C-Cysteinyl Carbon Resonance Assignments for the ^{13}C NMR Spectrum of *P. putida* 7Fe Ferredoxin

Peak	ppm (7°C)	Temperature Dependence	Assignment	Correlated β-H protons
1	174	Curie	-	-
2	152	Anti-C	-	-
3	112	Anti-C	4Fe-4S Cys (Cys45)?	15.2 (E)?
4	111	Anti-C	4Fe-4S Cys (Cys45)?	15.2 (E)?
5	95	Anti-C	4Fe-4S Cys (Cys39 or 42)	17.3 (D), 9.2 (I)
6	88	Anti-C	-	9.8, 9.2
7	40	none	Free Cys (Cys11 or 24)	5.8, 2.1
8	33	none	Free Cys (Cys11 or 24)	2.73, 2.32

? these proton resonances their correlated carbon resonances are tentatively assigned.

Table 5.17 Cysteinyl Resonance Assignment (7 °C)

Assign-ment	*P. putida* Fd			*A. vinelandii* Fd	
	β-H (ppm)	α-H (ppm)	β-C (ppm)	β-H (ppm)	α-H (ppm)
	31.8, 26.3		-	32.8, 26.5	6.5
Cys16	21.8	7.3[a]	-	21.1,8.6	7.2
Cys39 or 42	17.3, 9.2[a]	9.8[a]	95	17.1, 9.1	9.6
Cys45	15.3	-	111/112	15.5, 7.3	5.6
	9.8, 9.2	-	88	-	-
Cys11 or 24	5.8, 2.1	-	40	-	-
Cys11 or 24	2.73, 2.32	-	33	-	-

a. these chemical shifts were recorded at 17 °C

shift, 5.8 ppm, is not known.

The assignments of cysteinyl β-carbon, and α- or β-proton for two ferredoxins are summarized in Table 5.17. Four of nine cysteinyl residues in *A. vinelandii* ferredoxin I their α- and two β-cysteinyl protons are completely assigned. In *P. putida* ferredoxin, eight β-cysteinyl carbon resonances are assigned, the β-protons of seven cysteines are partially assigned. Two α-cysteinyl protons are assigned in these seven cysteines.

P. putida 7Fe ferredoxin contains nine cysteines, and only eight β-cysteinyl carbon peaks were observed in the ^{13}C NMR spectrum of β-^{13}C-cysteine enriched ferredoxin. Peak 1 has more intensity than the other seven peaks. Therefore, the ninth β-cysteinyl resonance may overlap with carbon peak 1 or it may be too broad to be seen from the natural abundance carbon envelope.

Two of the nine cysteines in the ferredoxin are not liganded with any iron-sulfur centers. Peaks 7 and 8 have relatively smaller temperature dependencies and their chemical shifts in the methylene carbon region. As for the remaining seven cysteines, four of them should be associated with the 4Fe center. Thus, only three cysteines are liganded with the 3Fe center. This result supports the view that the correct structure of the 3Fe center is $Fe_3S_4(S^{Cys})_3$, as reported in the revised X-ray structure of *Azotobacter vinelandii* ferredoxin I (14 and 15).

5.4 Chemical Shift, Temperature Dependence, and Dihedral Angle

As mentioned in Chapter 2, based on the Poe, et al., hyperconjugation model (16), the chemical shifts of two geminal β-CH_2 protons on an iron bound cysteine are expected to depend on dihedral angles θ between the Fe-Sγ-Cβ and the Sγ-Cβ-H according to the following

equation (17):

$$A_c = \beta_o + B_2\cos^2\theta \qquad (2.2)$$

where A_c is the proton-unpaired electron hyperfine coupling constant, B_2 is related to the spin density on the proton resulting from hyperconjugation, and β_o is related to spin density resulting from other delocalization mechanisms.

Since the chemical shift of a paramagnetically shifted resonance is proportional to the proton-unpaired electron hyperfine coupling constant, A_c, Ivano Bertini, et. al. (18) used equation 2.2 to analyze the separation of resonances arising from β-CH_2 protons on iron-bound cysteines in the ^1H NMR spectrum of *Clostridium pasteurianum* 2[4Fe-4S] ferredoxin.

The proton resonances of four of seven iron-bound cysteines in *A. vinelandii* ferredoxin I have been assigned; geminal pair β-CH_2 protons from Cys16 and Cys45 have been further stereo specifically assigned. Their temperature dependencies have been studied. The dihedral angles θ between the Fe-Sγ-Cβ and the Sγ-Cβ-H for iron-bound cysteines are obtained from the X-ray structure of *A. vinelandii* ferredoxin I at 1.9 Å. Table 5.18 shows the chemical shifts, temperature dependence intercepts and temperature coefficients for four assigned iron-bound cysteinyl proton resonances and one histidinyl indole ring proton resonance. The temperature dependence intercepts (the chemical shifts at 1/T = 0) and the temperature coefficients (the slopes of the temperature dependence curve) are the results from a plot of chemical shifts with the temperature. Their ratios of chemical shifts, temperature dependence intercepts, and temperature coefficients between a geminal pair β-CH_2 protons are presented in Table 5.19. Table 5.20 lists the dihedral angles θ between the

Table 5.18 Chemical Shifts and Temperature Dependence Parameters

Spin System		*A. vinelandii* Ferredoxin I			*P. putida* 7Fe Ferredoxin		
		δ (ppm)[1]	δ∞ (ppm)[2]	Δδ (ppm°K)[3]	δ (ppm)[1]	δ∞ (ppm)[2]	Δδ (ppm°K)[3]
Cys 8 or 49	β1	32.3 (A)	18.0	3977	31.8 (A)	17.9 (ppm)	3843
	β2	26.5 (B)	16.2	2923	26.3 (B)	16.1	2816
	α	6.5					
Cys16	β1	21.1 (C)	31.8	-2974	21.8 (C)	31.8	-2832
	β2	8.6	12.4	-1051			
	α	7.2			7.3		
Cys39 or 42	β1	17.1 (D)	25.0	-2214	17.2 (D)	24.9	-2159
	β2	9.1 (I)	13.6	-1245	9.2 (I)		
	α	9.6 (H)	12.9	-921	9.6 (H)		
Cys45	β1	15.5 (E)	22.2	-1893	15.3 (E)	22.4	-1982
	β2	7.3	10.0	-743			
	α	5.6	9.4	-1063			
His35	C2-H	7.8	7.7	40.8	7.9	7.7	52.3
	C4-H	6.1	6.5	-98.5	6.1	6.3	-51.0

1. chemical shift; 2. the temperature dependence intercept; 3. the temperature dependence coefficient

Table 5.19 Ratios of Temperature Dependence Parameters of β-Cysteinyl Proton Resonances in the ^{1}H NMR Spectrum of *A. vinelandii* Ferredoxin I

Cys	Chemical Shifts (ppm) of Geminal Pair β-Cysteinyl Protons	δ1/δ2	$(\delta_\infty)_1/(\delta_\infty)_2$	$(\Delta\delta)_1/(\Delta\delta)_2$
Cys8 or 49	32.3 ppm (A)/ 26.5 ppm (B)	1.22	1.11	1.36
Cys16	21.1 ppm (C)/8.6 ppm	2.45	2.56	2.83
Cys39 or 42	17.1 ppm (D)/ 9.1 ppm (I)	1.88	1.84	1.78
Cys45	15.5 ppm (E) /7.3 ppm	2.12	2.22	2.31

Table 5.20 Dihedral Angles (θ) Between the Fe-Sγ-Cβ and the Sγ-Cβ-H Planes of Two Geminal β-Cysteinyl Protons and Their Cosine Square Ratios

	Cysteine	θ (β1/β2)	$(\cos\theta_1/\cos\theta_2)^2$	$(\cos\theta_2/\cos\theta_1)^2$
3Fe-4S	Cys8	-36/-153	0.824	1.21
	Cys16	124/7	0.317	3.15
	Cys49	-43/-164	0.579	1.73
4Fe-4S	Cys20	-52/-171	0.389	2.57
	Cys39	-58/-176	0.282	3.54
	Cys42	175/57	3.35	0.30
	Cys45	130/13	0.435	2.30

Fe-Sγ-Cβ and the Sγ-Cβ-H for all iron-bound cysteines in *A. vinelandii* ferredoxin I. The ratios of $\cos^2\theta$s are also listed in Table 5.20.

Our results indicate that the equation 2.2 is not applicable to the question of ferredoxins, although it is successful for the organic compounds (19-21). For example, the resonance at 21.1 ppm is assigned to one β-CH_2 proton of Cys16, it has a θ of 124.3°. The chemical shift for another β-CH_2 proton of Cys16 is 8.6, and its dihedral angle is 6.5°. Their ratio of $\cos^2\theta$ is 0.32 (Table 5.20). This value is far away from the ratio of their respected chemical shifts ($\delta 1/\delta 2 = 2.45$) (Table 5.19), but it nearly equals to the reciprocal of the ratio of their respected temperature coefficients ($(\Delta\delta)_2/(\Delta\delta)_1 = 0.35$) (Table 5.19). A similar thing has happened for geminal pair β-CH_2 protons of Cys45. Furthermore, for other assigned geminal pair β-CH_2 protons of iron-bound cysteines, their ratios of the dihedral angles are not in accord with other ratios, i.e., the ratios of chemical shifts, the ratios of temperature coefficients and the ratios of temperature dependence intercepts, even when their reciprocals are considered (Table 5.19 and 5.20). Since the spin density sensed by the β-CH_2 protons through hyperconjugative mechanisms is the one transferred from an iron of the iron-sulfur center to a non-bound p orbital of the cysteinyl sulfur, the angle θ used in the equation 2.2 should be the dihedral angle between the H-Cβ-Sγ and the Cβ-Sγ-p(empty) planes. The dihedral angle between the H-Cβ-Sγ and the Cβ-Sγ-Fe planes can be far off from the dihedral angle between the H-Cβ-Sγ and the Cβ-Sγ-p(empty) planes. Therefore, any efforts to use equation 2.2 to predicate the dispersion of the chemical shifts of the iron-bound cysteinyl β-proton resonances should be done cautiously.

However, a study of the chemical shifts, temperature dependence intercepts and temperature coefficients for the assigned β-CH_2 proton

resonances arising from the iron-bound cysteines shows that they are essentially in accord with each other for a geminal pair β-cysteinyl protons. For example, the chemical shift ratio (δ1/δ2) for a geminal β-protons on Cys16 is 2.45 (Table 5.19), their temperature dependence intercept ratio $((\delta\infty)_1/(\delta\infty)_2)$ is 2.56 (Table 5.19), they are essentially in accord with the temperature coefficient ratio, $((\Delta\delta)_1/(\Delta\delta)_2)$, which is 2.83 (Table 5.19). It is also valid for other assigned geminal pair β-cysteinyl protons (Table 5.19). This can be understood as they are all dependent on the proton-unpaired electron hyperfine coupling. This correlation has been used as a guide to assign geminal pair β-CH_2 cysteinyl protons in our research. For example, two NOE cross-peaks at 15.5 ppm/7.3 ppm and 15.5 ppm/5.6 ppm are seen in the NOESY spectrum of *A. vinelandii* ferredoxin I. An examination of the ratios of their chemical shifts, temperature dependence intercepts and temperature coefficients shows that the ratios calculated for the resonance at 15.5 ppm are in more accord with the ratios for the one at 7.3 ppm (Table 5.19). Thus the resonances at 15.5 ppm and 7.3 ppm have been assigned to a pair geminal pair β-CH_2 protons on Cys45, the resonance at 5.6 should be its α-CH proton.

5.5 References

(1) Sweeney, W. V. (1981) *J. Biol. Chem.* **256**, 12222-12227

(2) Krishnamoorthi, R., Markley, J. L.., Cusanovich, M. A., Przysiecki, C. T., and Meyer, T. E. (1986) *Biochemistry* **25**, 60-67

(3) Sola, M., Cowan, T. A., and Gray, G. (1989) *Biochemistry* **28**, 5261-5268

(4) Nagayama, K., Ohmori, D., Imai, T., and Oshima, T. (1983) *FEBS Lett.* **158**, 208-212

(5) Nagayama, K., Imai, T, Ohmori, D., and Oshima, T. (1984) *FEBS Lett.* **169**, 79-84

(6) Nagayama, K., and Ohmori, D. (1984) *FEBS Lett.* **173**, 15-18

(7)Bertini, I., and Luchinat, C. (1986) "NMR of Paramagnetic Molecules in Biological Systems" The Benjamin/Cummings Publishing Company, Inc. pp. 86-91

(8) Malikayil, J. A. (1986) Ph.D dissertation:"A Chemical and Spectroscopic Study of Ferredoxin I from *Azotobacter vinelandii*". City University of New York, New York

(9) Markley, J. L (1973) *Biochemistry* **12**, 2245-2250

(10). Bundi, A. and Wüthrich, K. (1979) *Biopolymers* **18**, 285-297

(11) Stout, C. D. (1989) *J. Mol. Biol.* **205**, 545-555

(12) Wüthrich, K. (1986) in *NMR of Proteins and Nucleic Acids*, John Wiley & Sons, New York

(13)Packer, E. L., and Rabinowitz, J. C. (1978) *J. Biol. Chem.* **253**, 7722-7730

(14) Stout, C. D. (1988) *J. Biol. Chem.* **263**, 9256-9260

(15) Stout, G. H.; Turley, S.; Sieker, L. C. and Jensen, L. H. (1988) *Proc. Nat. Acad. Sci., U. S. A.* **85**, 1020-1022

(16) Poe, M., Philips, W. D., Mcdonald, C. C., and Lovenberg, W. (1970) Proc. Natl. Acad. Sci. **65**, 797-804

(17) Cowan J. A. and Sola, M. (1990) *Biochemstry* **29**, 5633-5637

(18) Bertini, I., Briganti, F., Luchinat, C., and Sozzafava, A. (1990) *Inorg. Chem.* **29**, 1874-1880

(19) Heller, C. and McConnell, H. M. (1960) *J. Chem. Phys.* **32**, 1575-1539

(20) Ho, F. F.-L. and Reilley, C. N. (1969) *Anal. Chem.* **41**, 1835-1841

(21) Stone, E. W.; Maki, A. H. (1962) *J. Chem. Phys.* **37**, 1326-1333

SUMMARY

This dissertation presented practical assignment strategies for the paramagnetically shifted resonances in the NMR spectra of 7Fe ferredoxins. 2D NMR spectroscopy has been adapted to assign the paramagnetically shifted resonances. The paramagnetically shifted resonances arise from the nuclei near the iron-sulfur centers. Thus, the events and geometry changes in the vicinity of the iron-sulfur centers as a result of electron transfer can be studied through the specifically assigned paramagnetically shifted resonances. Furthermore, the assignment strategies presented in this dissertation potentially could provide a way to completely assign the NMR spectra of paramagnetic proteins.

The results from the isotopic labeling (including deuterium and carbon-13 labeling), SM-NOESY (standard NOESY with a short mixing time), and heteronuclear correlation experiments have been carefully studied in conjunction with other results. This study leads to the assignment of the five most downfield resonances and their paired β-cysteinyl proton and correlated α-proton resonances for two 7Fe ferredoxins, *A. vinelandii* ferredoxin I and *P. putida* ferredoxin.

Eight β-cysteinyl carbon resonances were observed in the ^{13}C NMR spectrum of *P. putida* ferredoxin isolated from cells grown in the presence of β, β'-^{13}C-cystine. Their chemical shifts and temperature dependencies supported the view that the correct structure of the 3Fe center is $Fe_3S_4(S^{Cys})_3$, as reported in the revised X-ray structure of *Azotobacter vinelandii* ferredoxin I. For the two cysteines with a free sulfhydryl group, assignment of their β-cysteinyl proton and β-carbon resonances has been made.

Ring system proton resonances are partially assigned after a examination of 2D ^{1}H NMR spectra of two 7Fe ferredoxins. Alterations in local conformation between the solution structure and crystal structure of *A. vinelandii* ferredoxin I are observed when the results from NOESY experiments are compared with the X-ray structure.

The chemical shifts of iron-bound cysteinyl β-proton resonances are not related to the dihedral angles between the Fe-Sγ-Cβ and the Sγ-Cβ-H planes, as contrary to expectations. However, both the temperature dependence slope and intercept at 1/T = 0 depend on the contact interaction constant for these β-proton resonances. The chemical shift also has this same dependence. Thus, the ratio of any of these parameters for a given geminal pair of paramagnetically shifted β-cysteinyl protons would be expected to be approximately the same. For example, the ratio of chemical shifts fro a geminal pair would be expected to be approximately equal to the ratio of slopes in a plot of chemical shift vs. 1/T. This relationship was observed to hold for all the geminal pairs that were assigned.

Appendix 1 Distances Between the Nearest Aromatic Ring Protons to The Atoms of Iron-Sulfur Centers in *A. vinelandii* Ferredoxin I (Å)

Amino Acid		Tyr13		Phe2		Phe25			
Proton		H5	H6	H2	H3	H2	H3	H4	H5
	Fe1								4.56
	Fe2		3.77 Å						
3Fe	Fe3		4.54 Å						
I	S1		4.29 Å						
4S	S2								4.26 Å
	S3								
	S4	4.27 Å	2.39 Å						
	Fe1			4.27 Å					
	Fe2								
4Fe	Fe3						3.94 Å	3.87 Å	
I	Fe4						3.45 Å	4.87 Å	
4S	S1								
	S2			3.36 Å	4.35 Å				
	S3					4.76 Å	3.40 Å	3.69 Å	
	S4					4.74 Å	3.79 Å	4.81 Å	

All distances are measured from the revised X-ray structure of *A. vinelandii* (Stout, C. D. (1988) *J. Biol. Chem.* 263, 9256-9260)

Appendix 2 The Proton-Proton Distances Between Two Adjacent Aromatic Ring Protons in *A. vinelandii* Ferredoxin I

Phe 31	Phe67		Tyr78			
	H2	H3	H4	H5	H6	H7
H3	4.13 Å	3.74 Å				
H4	2.20 Å	3.01 Å				
H5	3.63 Å	4.05 Å		3,98 Å	4.25 Å	
H6			4.83 Å	2.42 Å	2.02 Å	4.44 Å

a. All distances are measured from the revised X-ray structure of *A. vinelandii* (Stout, C. D. (1988) *J. Biol. Chem.* 263, 9256-9260)

Appendix 3 The Proton-Proton Distances Between Protons on the Cysteines Coordinated with the [3Fe-4S] Center and Iron and Sulfur Atoms in the 3Fe Center in Å for *A. vinelandii* Ferredoxin I (Å)

3Fe-4S		Fe1	Fe2	Fe3	S1	S2	S3	S4
Cys8	α	5.980	4.419	3.416	6.339	4.819	5.446	2.735
	β1	5.315	4.226	3.030	6.305	3.458	5.267	3.736
	β2	6.596	5.851	4.118	7.801	4.915	6.064	4.990
	NH	7.689	6.117	5.304	8.329	5.808	7.547	5.221
Cys16	α	5.014	6.217	7.673	4.654	6.312	7.011	8.238
	β1	3.994	5.649	6.504	4.746	4.861	6.007	7.663
	β2	2.962	4.124	5.459	3.134	3.928	5.207	6.222
	NH	3.241	4.561	5.782	2.465	5.187	4.814	6.128
Cys49	α	4.469	3.260	5.802	2.651	4.907	6.280	5.077
	β1	4.485	3.284	5.591	3.819	3.884	6.580	5.466
	β2	6.055	4.281	6.719	5.070	5.235	7.977	6.106
	NH	6.516	5.512	8.012	5.246	6.453	8.661	7.562

All distances are measured from the X-ray structure of *A. vinelandii* ferredoxin I (Stout, C. D. (1988) *J. Biol. Chem.* 263, 9256-9260)

Appendix 4 The Proton-Proton Distances Between the Protons on the Cysteine Liganded with the [4Fe-4S] Cluster and the Iron and Sulfur Atoms in the 4Fe Center in Å

[4Fe-4S]		Fe1	Fe2	Fe3	Fe4	S1	S2	S3	S4
Cys20	α	5.552	3.995	4.615	3.056	4.397	5.938	5.102	2.504
	β1	5.950	5.449	4.821	3.336	5.461	6.782	4.515	3.607
	β2	6.986	6.436	6.320	4.284	6.008	8.067	5.766	4.900
	NH	7.902	6.660	6.453	5.280	7.100	8.264	6.749	4.654
Cys39	α	3.289	5.149	5.739	4.401	3.136	5.426	4.419	6.377
	β1	3.502	6.130	5.685	5.234	4.728	5.522	4.049	7.080
	β2	4.361	6.825	6.751	6.523	5.490	6.001	5.509	8.182
	NH	5.569	7.852	7.976	6.949	5.968	7.633	6.304	8.999
Cys42	α	6.696	5.020	7.180	7.681	6.181	5.348	8.651	6.895
	β1	6.783	4.453	6.903	6.909	5.686	5.687	8.396	5.896
	β2	5.588	3.653	6.295	5.946	4.305	4.975	7.403	5.512
	NH	4.030	3.018	5.186	5.351	3.591	3.361	6.160	5.266
Cys45	α	7.659	6.428	5.084	6.508	8.185	6.622	6.727	4.595
	β1	6.684	6.389	4.161	5.862	7.757	6.056	5.274	4.667
	β2	5.665	4.975	3.160	4.410	6.328	5.184	4.423	3.017
	NH	5.566	4.049	3.258	5.118	6.145	4.043	5.456	3.039

All distances are measured from the X-ray structure of *A. vinelandii* ferredoxin I (Stout, C. D. (1988) *J. Biol. Chem.* 263, 9256-9260)

BIBLIOGRAPHY

Following papers have been used as references in this manuscript:

Antonio, M. A., Averill, B. A., Moura, I., Moura, J. J. G., Orme-Johnson, W. H., Teo, B. K. and Xavier, A. V. (1982) *J. Biol. Chem.* **257**, 6646-6649.

Averill, B. A., Bale, J. R., and Orme-Johnson, W. H. (1978) *J. Amer. Chem. Soc.* **100**, 3034-3043.

Bax, A., Griffey, R. H., and Hawkins, B. L. (1983) *J. Am. Chem. Soc.* **105**, 7188-7190

Bax, A., Griffey, R. H., and Hawkins, B. L. (1983) *J. Magn. Reson.* **55**. 301-315

Bax, A., and Davis, D. G. (1985) *J. Magn. Reson.* **63**, 207-213

Bax, A., and Davis, D. G. (1985) *J. Magn. Reson.* **65**, 355-360

Beinert, H., Emptage, M. H., Dreyer, J-L., Scott, R. A., Hahn, J. E., Hodgson, K. O. and Thomson, A. J. (1983) *Proc. Natl Acad. Sci. USA* **80**, 393-396.

Beinert, H. and Thomson, A. J. (1983) *Arch. Biochem. Biophys.* **222**, 333-361.

Bendall, M. R., Pegg, D. T., and Doddrell, D. M. (1983) *J. Magn. Reson.* **52**, 81-117

Bertini, I., and Luchinat, C. (1986) "NMR of Paramagnetic Molecules in Bertini, I., Briganti, F., Luchinat, C., and Sozzafava, A. (1990) *Inorg. Chem.* **29**, 1874-1880

Biological Systems" The Benjamin/Cummings Publishing Company, Inc. pp. 86-91

Bloembergen, N. (1957) *J. Chem. Phys.* **27**, 595-596

Braunschweiler, L. and Ernst, R. R. (1983) *J. Magn. Reson.* **53**, 521-528

Bruschi, M., and Guerlesquin, F. (1988) *FEMS Microbiol. Rev.* **54**, 155-176

Buchauan, R. E. and Gibbons, N. E. (1974) "Bergey's Manual of Determinative Bacteriology", 8th Edison. The Williams & Wilkins Company, Baltimore

Bundi, A. and Wüthrich, K. (1979) *Biopolymers* **18**, 285-297

Calhoun, D. H. and Feary, T. W. (1969) *J. Bacteriol.* **97**, 210-216

Cammack, R., Krishna, K. K. and Hall, D. O. (1985) Physiol. Vèg. **23** (5)

Capetanaki, Semi (1979) Master Thesis, Hunter College, CUNY

Cowan, J. A. and Sola, M. (1990) *Biochem* **29**, 5633-5637

Dugad, L. B., La Mar, G. N., Banci, L., and Bertini, I. (1990) *Biochemistry* **29**, 2263-2271

Duport, C., Jounanequ, Y. and Vignais, P. M. (1990) *Nucleic Acids Research* **18**, 4618

Dwek, R. A. (1973) "Nuclear Magnetic Resonance in Biochemistry: Applications to Enzyme System" Oxford Univ. Press (Clarendon), London and New York

Emptage, M. H., Kent, T. A., Huynh, B. H., Rawlings, J., Orme-Johnson, W. H. and Munck, E. (1980) *J. Biol. Chem.* **255**, 1793-1796.

George, S. J., Richards, A. J. M., Thomson, A. J. and Yates, M. G. (1984) *Biochem. J.* **224**, 247-251.

Ghosh, D., O'Donnell, S., Furey, W.,Jr., Robbins, A. H., and Stout, C. D., (1982) *J. Mol. Biol.*, **158**, 73-109.

Gluck, M. R. (1989) Ph.D dissertation, The City University of New York, New York

Hase, T., Wakabayashi, S. Matsubara, H., Ohmori, D., and Suzuki, K. (1977) *FEBS Lett.* **91**, 315-319.

Hase, T., Wakabayashi, S., Matsubara, H., Imai, T., Matsumoto, T., and Tobari, J. (1979) *FEBS lett.* **103**, 224-228.

Heinrikso, R.L. and Meredith, C.S. (1984) *Anal. Biochem.* **136**, 65-74

Heller, C. and McConnell, H. M. (1960) *J. Chem. Phys.* **32**, 1575-1539

Hirs, C.H.W., *Meth. Enz.* **11**, 197-199

Ho, F. F.-L. and Reilley, C. N. (1969) *Anal. Chem.* **41**, 1835-1841

Howard, J. B., Lorsbach, T. W., and Que, L. (1976) *Biochem. Biophys. Res. Commun.* **70**, 582-588.

Howard, J. B., Lorsback, T. W., Ghosh, D., Melis, K., and Stout, C. D. (1983) *J. Biol. Chem* **258**, 508-522.

Imai, T., Matsumoto, T., Ohta, S., Ohmori, D., Suzuki, K., Tanaka, J., Tsukihara, M., and Tobari, J. (1983) *Biochim. Biophys. Acta 743*, 91-97.

Imai, T., Saito, H., Tobari, J., Ohmori, D. and Suzuki, K. (1984) *FEBS*, **165**, 227-230

Jardetzky, O., & Roberts, G. C. K. (1981) in "NMR in Molecular Biology", Academic Press, New York

Johnson, M. K., Hare, J. W., Spiro, T. G., Moura, J. J. G., Xavier, A. V. and LeGall, J. (1981) *J. Biol. Chem.* **256**, 9806-9808

Johnson, M. K., Czernuszewicz, R. S., Spiro, T. G., Fea, J. A. and Sweeney, W. V. (1983) *J. Am. Chem. Soc.* **105**, 6671-6678

Jouanneau, Y., Meyer, C., Gaillard, J. and Vignais, P. M. (1990) *Biochem. Biophys. Res. Comm.* **171**, 273-279

Kalk, A; Berendsen, H. J. C. (1976) *J. Magn. Reson.* **24**, 343-366

Krishnamoorthi, R., Markley, J. L., Cusanovich, M. A., and Przysiecki, C. T. (1986) *Biochemistry*, **25**, 50-54

Lecomte, J. T. J., and La Mar, G. N. (1986) *Eur. Biophys. J.* **13**, 373-381

Lutz, M., Moulis, J-L., and Meyer, J.,(1983) *FEBS* **153**, 212-216

Macura, S., and Ernst, R. R. (1980) *Mol. Phys.* **41**, 95-117

Malikayil, J. A., Sweeney, W. V., McCracken, J., and Peisach, J., (1985) *Biochem. Biophys. Research Communication* **133**, 1119-1124.

Malikayil, J. A. (1986) Ph.D dissertation, The City University of New York. New York

Malthouse, J. P. G. (1986) *Prog. NMR Spec.* **18**, 1-59

Markley, J. L (1973) *Biochemistry* **12**, 2245-2250

Marshall, A. G., Lee, K. M., and Martin, P. W. (1980) *J. Am. Chem. Soc.* **102**, 1460-1462

Martin, A. E., Burgess, B. K., Stout, C. D., Cash, V. L., Dean, D. R., and Jensen, G. M. (1990) *Proc. Natl. Acad. Sci. USA* **87**, 598-602.

Matsumoto, T., Tobari, J., Suzuki, K., Kimura, T., and Tchen, T. T. (1976) *J. Biochem* **79**, 937-943.

McConnell, H. M. and Robertson, R. E. (1958) *J. Chem. Phys.* **29**, 1361-1365
Moore, S. (1962) *J. Biol. Chem.* **238**, 235-237

Morgan, T. V., Stephens, P. J., Burgess, B. K., and Stout, C. D. (1984) *FEBS* **167**, 137-141.

Morgan, T. V., Stephens, P. J., Devlin, F., Stout, C. D., Melis, K. A, and Burgess, B. K. (1984) *Proc. Natl. Acad. Sci. USA* **81**, 1931-1935

Mortenson, L. E., Valentine, R. C. and Carnahan, J. E., (1962) *Biochem. Biophys. Res. Commun.*, **7**, 448-454

Müller, L. (1979) *J. Am. Chem. Soc.* **101**, 4481-4484

Müller, L., and Ernst, R. R. (1979) *Mol. Phys.* **38**, 963-992

Nagayama, K., Ohmori, D., Imai, T., and Oshima, T. (1983) *FEBS Lett.* **158**, 208-212

Nagayama, K., Imai, T, Ohmori, D., and Oshima, T. (1984) *FEBS Lett.* **169**, 79-84

Nagayama, K., and Ohmori, D. (1984) *FEBS Lett.* **173**, 15-18

Nagayama, K., Ohmori, D., Imai, T., and Oshima, T., (1986) in "Iron-Sulfur Protein Research", eds. H. Matsubara et al., pp. 125-138. Japan Sci. Soc. Press, Tokyo/Springer-Verlag, Berlin

Nauhans, D. and williamson, M. (1989) in " The Nuclear Overhauser Effect in Structural and Conformational Analysis" VCH publisher, New York

Noggle, J. H., Sirmer, R. E. (1971) *The Nuclear Overhauser Effect*; Academic; New York

Oh, Byung-Ha and Markley, J. (1990) *Biochemistry* **29**, 3993-4004

Ohmori, D. (1976) *Biochem. Biophys. Res. Commun.*, **72**, 566-574

Ohmori, D. (1984) *Biochim. Biophys. Acta* **790**, 15-21

Ohmori, D., Yamakura, F., Suzuki, K., Imai, T., and Nagayama, K., (1986) in "Iron-Sulfur Protein Research", eds. H. Matsubara et al., pp. 116-124. Japan Sci. Soc. Press, Tokyo/Springer-Verlag, Berlin

Otting, G., Widmer, H., Wagner, G., and Wüthrich, K. (1986) *J. Magn. Reson.* **66**, 187-193

Packer, E. L., and Rabinowitz, J. C. (1978) *J. Biol. Chem.* **253**, 7722-7730
Packer, E. L. (1979) Ph.D dissertation, University of california, Berkeley. Berkeley, California

Piantini, U., Sorensen, O. W., and Ernst, R. R. (1982) *J. Am. Chem. Soc.* **104**, 6800-6801

Poe, M., Philips, W. D., Mcdonald, C. C., and Lovenberg, W. (1970) Proc. Natl. Acad. Sci. **65**, 797-804

Rossomand, Edward F. (1990) *Meth. Enzy.* **182**, 309-343
Rudner, R. (1981) *Mutation Res.* **83**, 339-347

Saeki, K., Wakabayashi, S., Zumft, W. G., and Matsubara, H. (1988) *J. Biochem.* **104**, 242-246.

Sato, S., Nakazawa, K., Hon-nami, K., and Oshima, T. (1981) *Biochim. Biophys. Acta* **668**, 277-289.

Schlatter, D., Waldvogel, S., Zülli, F., Suter, F., Portmann, W. and Zuber, H. (1985) *Biol. Chem. Hoppe-Seyler* **366**, 223-231

Schwinghamer, E. A. (1980) *FEMS Microbio. Lett.* **7**, 157-162

Scott, R. A., Kazmi, S. A., Beinert, H., Emptage, M. H., Hahn, J. E., Hodgson, K. O., Stout, C. D. and Thomson, A. J. (1983) *Inorg. Chim. Acta.* **79**, 142

Scott, R. A., Penner-Hahn, J. E., Hodgson, K. O., Beinert, H. and Stout, C. D. (1984) in EXAFS and Near Edge Structure III (Hodgson, K. O., Hedmann, B. and Penner-Hann, J. E., eds), pp 105-110, Springer-Verlag

Shaka, A. J., and Freeman, R. (1983) *J. Magn. Reson.* **51**, 169-173

Shethna, Y. I. (1970) *Biochim. Biophys. Acta* **205**, 58-62

Sola, M., Cowan, T. A., and Gray, G. (1989) *Biochemistry* **28**, 5261-5268

Soloman, I. (1955) *Phys. Rev.* **99**, 559-565

Solomon, I. and Bloembergen, N. (1956) *J. Chem. Phys.* **25**, 261-266

States, D. J., Harberkorn, R. A., and Reuben, D. J. (1982) *J. Magn. Reson.* **48**, 286-292

Stephens, P. J., Morgan, T. V., Devlin, F., Penner-Hahn, J. E., Hodgson, K. O., Scoot, R. A., Stout, C. D. and Burgess, B. K. (1985) *Proc. Natl. Acad. Sci. USA* **82**, 5661-5665

Stephens, P. J., Morgan, T. V., Stout, C. D., and Burgess, B. K., (1986) Frontiers of Bioinorganic Chemistry (Xlvier, A. V. ed) VCH Publisher, Weisheir

Stone, E. W.; Maki, A. H. (1962) *J. Chem. Phys.* **37**, 1326-1333

Stout, C. D. (1979) *J. Biol. Chem.* **254**, 3598-3599

Stout, C. D. (1979) *Nature* **279**, 83-84

Stout, C. D., Ghosh, D., Pattabhi, V., and Robbins, A. H. (1980) *J. Biol. Chem.* **255**, 1797-1800

Stout, C. D. (1988) *J. Biol. Chem.* **263**, 9256-9260

Stout, C. D. (1989) *J. Mol. Biol.* **205**, 545-555

Stout, G. H., Turley, S., Sieker, L. C. and Jensen, L. H. (1988) *Proc. Natl Acad. Sci. USA* **85**, 1020-1022

Sweeney, W. V., Rabinowitz, J. C., and Yoch, D. C. (1975) *J. Biol. Chen. 250*, 7842-7847.

Sweeney, W. V. (1981) *J. Biol. Chem.* **256**, 12222-12227

Trower, M. K., Marshall, J. E., Doleman, M. S., Emptage, M. H., and Sariaslani, F. S. (1990) *Biochim. Biophys. Atca.* **1037**, 290-296

Yates, M. G. (1970) *FEBS Lett.* **8**, 281-285

Yates, M. G., O'Donnell, M. J., Lowe, D. J., and Bothe, H. (1978) *Eur. J. Biochem.* **85**, 291-299.

Yoch, D. C., Benneman, J. R., Valentine R. C., and Arnon, D. I. (1969) *Proc. Natl. Acad. Sci. USA* **64**, 1404-1410.

Yoch, D. C. and Arnon, D. I. (1972) *J. Biol. Chem.* **247**, 4514-4520.

Yoch, D. C., Carithers, R. P., and Arnon, D. I. (1977) *J. Biol. Chem.* **252**, 7453-7460.

Wagner, G. and Wüthrich, K. (1979) *J. Magn. Reson.* **33**, 675-680

Wood, J. L., and Du Vigneaud, V. (1939) *J. Biol. Chem.* **131**, 267-274

Wüthrich, K. (1986) in *NMR of Proteins and Nucleic Acids*, Wiley, New York